549443

AP-125 Analysis Report:
Evaluation of Culebra Brine Chemistry

(AP-125: Analysis Plan for the Evaluation of Culebra Brine Compositions)

Task Number 1.4.2.3

Report Date: July 28, 2008

Authors:

Paul S. Domski
S.M. Stoller Corporation

7/29/08
Date

Richard L. Beauheim, 6712
Repository Performance Department

7/29/08
Date

Technical Review:

Gregory T. Roselle, 6712
Repository Performance Department

7/29/2008
Date

QA Review:

Shelly R. Johnsen, 6710
Carlsbad Programs Group

7-29-08
Date

Management Review:

C.D. Leigh, 6712
Repository Performance Department

7/29/08
Date

WIPP:1.4.2.3:TD:QA-L:RECERT:549336

Information Only

CONTENTS

1. Introduction 5
   1.1 Geologic Setting 5
   1.2 Previous Studies 9
   1.3 Data Sources 10
   1.4 Data Uncertainty 12
2. Methods 17
   2.1 Computer Codes 17
   2.2 Classifications 18
      2.2.1 Hydrochemical Facies 18
      2.2.2 Salt Norm Classification 20
      2.2.3 Normative Excess Classifications 21
      2.2.4 Ionic Strength and Mineral Saturation Index 22
3. Results 23
   3.1 Hydrochemical Facies 24
   3.2 Salt Norm Types 28
      3.2.1 Sulfatic Weathering Solutions 28
      3.2.2 Sulfatic Weathering Solutions with a Marine Component 31
      3.2.3 Marine-type Waters 33
      3.2.4 Diagenetic-type Waters 34
   3.3 Excess Normative Halite and Anhydrite 37
4. Chemical Evolution of the Culebra Groundwater 41
   4.1 Ionic Strength Effect and Partial Equilibrium 41
   4.2 Mineral Phases Contributing to the Evolution of Culebra Waters 45
   4.3 Forward Geochemical Modeling with PHREEQCI 54
      4.3.1 The Run 10 Model 54
      4.3.2 Alternate Conceptual Model 56
   4.4 Large-Scale Groundwater Mixing 63
      4.4.1 Mixing of SNL-16 and H-8 Waters 63
      4.4.2 Mixing of SNL-15 and WQSP-4 Waters 64
      4.4.3 Mixing of H-2c and H-3b2 Waters 65
      4.4.4 Conclusions from Mixing Calculations 67
5. Summary 68
6. References 71

Appendix 1 – Computer Files 75

Information Only

FIGURES

Figure 1. General stratigraphy at the WIPP site. 6
Figure 2. Detailed stratigraphy of the Rustler Formation. 7
Figure 3. Mudstone-Halite (M-H) margins in the Rustler Formation. 7
Figure 4. WIPP site and surrounding area with the Culebra wells considered in this report. 8
Figure 5. Probability distribution for the %CBE for the Culebra water analyses. 14
Figure 6. Quantile-normal plot for the %CBE for the Culebra water analyses. 14
Figure 7. Probability distribution for the %CBE for the PHREEQCI output water analyses. 15
Figure 8. Quantile-normal plot for the %CBE for the PHREEQCI output water analyses. 16
Figure 9. Hydrochemical facies zones of Siegel et al. (1991b). 19
Figure 10. Piper plot of the Culebra wells symbol-coded to reflect their hydrochemical facies and color-coded to reflect their SNORM type. 25
Figure 11. Culebra wells color-coded on the basis of hydrochemical facies. 26
Figure 12. Culebra wells color-coded to water type based on SNORM output with corresponding ionic strength values. 29
Figure 13. Sodium versus chloride for the Culebra waters coded by SNORM type. 37
Figure 14. Culebra wells color-coded based on the abundance of normative halite and anhydrite. 38
Figure 15. Culebra waters' ion concentrations versus ionic strength. 41
Figure 16. Halite saturation index versus ionic strength color coded by hydrochemical facies. 42
Figure 17. Ion activity coefficients for the Culebra waters versus ionic strength. 44
Figure 18. Gamma product values for phases of interest for the Culebra waters. 44
Figure 19. Gypsum saturation index versus ionic strength for the Culebra waters. 47
Figure 20. Calcium concentration versus gypsum saturation index for the Culebra waters. 48
Figure 21. Dolomite saturation index versus ionic strength for the Culebra waters. 49
Figure 22. Calcium and magnesium concentrations versus dolomite saturation index for the Culebra waters. 49
Figure 23. Calcite saturation index versus ionic strength for the Culebra waters. 50
Figure 24. Calcium concentration versus calcite saturation index for the Culebra waters. 50
Figure 25. Polyhalite saturation index versus ionic strength for the Culebra waters. 51
Figure 26. Calcium, magnesium, and potassium concentrations versus polyhalite saturation index for the Culebra waters. 52
Figure 27. Carnallite saturation index versus ionic strength for the Culebra waters. 52
Figure 28. Magnesium and potassium concentrations versus carnallite saturation index for the Culebra waters 53
Figure 29. Calcium, magnesium, potassium, and sulfate concentrations versus ionic strength for the Culebra waters 53
Figure 30. Potassium:chloride ratio versus ionic strength. 55
Figure 31. Magnesium:chloride ratio versus ionic strength. 55
Figure 32. Measured and simulated magnesium concentration versus ionic strength. 57
Figure 33. Measured and simulated potassium concentration versus ionic strength. 58
Figure 34. Measured and simulated calcium concentration versus ionic strength. 58
Figure 35. Measured and simulated sulfate concentration versus ionic strength. 59
Figure 36. Measured and simulated sodium concentration versus ionic strength. 59
Figure 37. Measured and simulated chloride concentration versus ionic strength. 60

Information Only

Figure 38. Measured and simulated calcite saturation versus ionic strength. 60
Figure 39. Measured and simulated dolomite saturation versus ionic strength. 61
Figure 40. Normative phases resulting from mixing SNL-16 and H-8b waters. Also plotted is the H-7b1 salt norm. 64
Figure 41. Normative phases resulting from mixing SNL-15 and WQSP-4 waters. Also plotted is the DOE-1 salt norm. 65
Figure 42. Normative phases resulting from mixing H-2c and H-3b2 waters. Also plotted are the WIPP-30 and H-18 salt norms. 66

TABLES

Table 1. Summary of the data-based studies on the Culebra groundwater chemistry. 9
Table 2. Culebra wells, sample dates, and analysis %CBE for the wells used in this report. 11
Table 3. Summary statistics for the %CBE for the Culebra and PHREEQCI data. 15
Table 4. Hydrochemical facies descriptions. 20
Table 5. Classification of the Culebra waters sorted by hydrochemical facies (zone) and ionic strength (μ). 23
Table 6. Ionic strength (μ) and SNORM results for the northern cluster of sulfatic weathering solution wells. 30
Table 7. Ionic strength (μ) and SNORM results for the southern cluster of sulfatic weathering solution wells. 31
Table 8. Ionic strength (μ) and SNORM results for the sulfatic weathering solution with marine component waters. 32
Table 9. Ionic strength (μ) and SNORM results for the Culebra waters with marine-type normative assemblages. 33
Table 10. Ionic strength (μ) and SNORM results for the Culebra waters with diagenetic-type normative assemblages. 34
Table 11. Excess normative halite and anhydrite for the wells along the M2-H2 margin. 39
Table 12. Comparison of H-10b water to H-10b water with three moles of halite added. 39
Table 13. Ionic strength (IS) and mineral saturation index values for the Culebra waters 45
Table 14. Summary of the Run 10 and alternate model constraints. 57

Information Only

1. Introduction

This analysis report discusses the aqueous geochemistry of the waters from the Culebra Dolomite Member of the Rustler Formation, and functions as a point of reference for the wells installed and samples collected since 1987. The purpose of examining the aqueous geochemistry of the Culebra is twofold: First, to classify the samples which have been collected since the publication of Siegel and Lambert (1991); and second, to gain a better understanding of flow in the Culebra and how the groundwater geochemistry might be related to observed patterns in the transmissivity of the Culebra. This analysis report has been prepared to meet the requirements of Tasks 1 – 4 of AP-125 (Domski and Beauheim, 2005).

Inasmuch as understanding the aqueous geochemistry of the Culebra requires consideration of vertical flow to the Culebra, a knowledge of the aqueous geochemistry of the overlying Magenta Member of the Rustler Formation is also pertinent. However, the water-chemistry data available for the Magenta are limited. Additional sampling of Magenta wells will take place in FY09, after which a follow-on report will consider the Magenta brine chemistry and its relationship to the Culebra.

Trends in the aqueous geochemistry of the Culebra waters were identified by organizing the waters into groups based on several criteria. These criteria included the hydrochemical facies designations first proposed by Ramey (1985) and expanded by Siegel et al. (1991b), normative salt assemblages as calculated with the code SNORM (Bodine and Jones, 1986), and solution concentration as represented by ionic strength calculated using PHREEQCI (Parkhurst and Appelo, 1999).

1.1 Geologic Setting

The Waste Isolation Pilot Plant (WIPP) is the U.S. Department of Energy's deep geologic repository for transuranic and mixed waste. The WIPP repository has been excavated 655 m below ground surface in Permian halite beds of the Salado Formation (Figure 1) in the Delaware Basin in southeastern New Mexico. The Salado Formation is overlain by the Permian Rustler Formation, which consists of five members. The Culebra is the lower of two dolomite members of the Rustler. The other three members of the Rustler consist principally of beds of anhydrite (locally altered to gypsum) and mudstone (or other fine-grained clastics). Figure 2 shows the stratigraphic subdivisions of the Rustler, including the informal stratigraphy of Holt and Powers (1988). Halite beds are found in association with the mudstones east of the WIPP site, and halite beds and/or cements are found over much of the WIPP site in the lower Los Medaños mudstone and clastics. Using data from borehole geophysical logs, Powers (2007) has mapped the margins of halite in the mudstone units of the Rustler (Figure 3).

The Culebra is a locally argillaceous and arenaceous, well- to poorly indurated dolomicrite approximately 7-8 m thick. It exhibits significant spatial heterogeneity in the types of porosity, the amount of fracturing, and the amount of porosity-filling cements (primarily gypsum, with some halite) that are present. Hydraulic testing at individual well locations has shown that the transmissivity (T) of the Culebra varies over more than ten orders of magnitude. Lower transmissivities are associated with low degrees of fracturing and pervasive porosity-filling cements and higher transmissivities are associated with extensive fracturing and little porosity-filling cements (Holt et al., 2005). Fractures in the Culebra are significant to WIPP because of

Information Only

their potential to act as "fast paths" for radionuclide transport. The Culebra is the most transmissive member of the Rustler and would accordingly provide the most significant groundwater pathway for radionuclides released from the WIPP repository by inadvertent human intrusion. Extensive characterization of the geologic, hydrologic, and hydrogeochemical properties of the Culebra has been performed to allow development of groundwater flow and transport models.

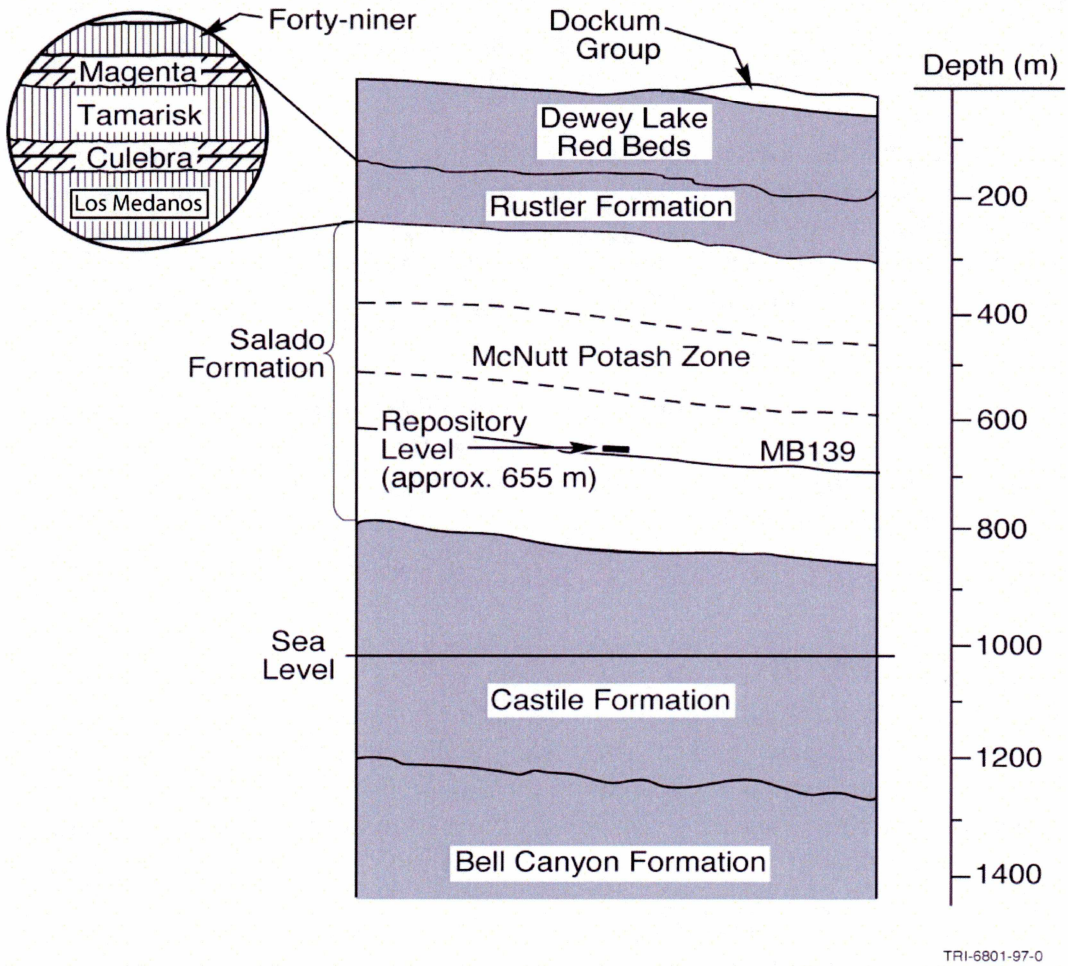

Figure 1. General stratigraphy at the WIPP site.

Dissolution of the upper Salado Formation has created a large subsidence trough, known as Nash Draw, to the west of the WIPP site (Figure 4). Within Nash Draw, evaporite karst is present in the sulfatic members of the Rustler Formation, and the Culebra is collapsed and broken. East of the WIPP site where the Culebra is deeply buried, few fractures are observed and both the fractures and varying amounts of the primary porosity of the Culebra are filled with sulfatic and/or halite cements. In the area between Nash Draw and the eastern boundary of the WIPP site, the presence and continuity of fracturing and sulfatic fracture fillings are hard to predict.

Information Only

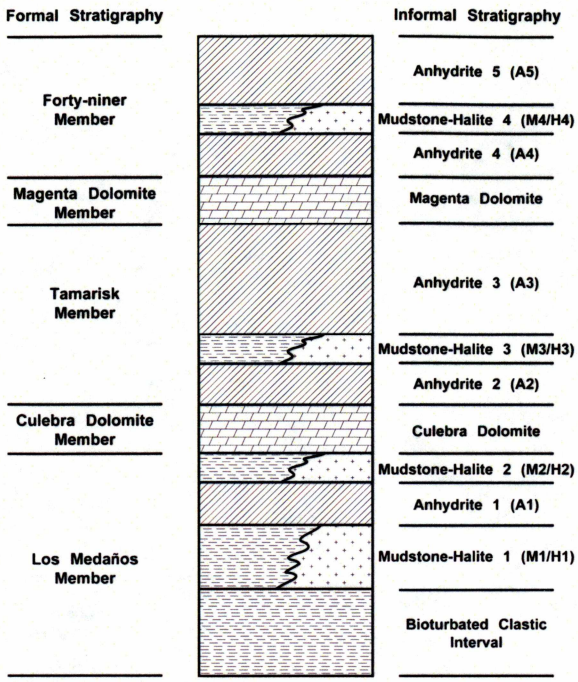

Figure 2. Detailed stratigraphy of the Rustler Formation.

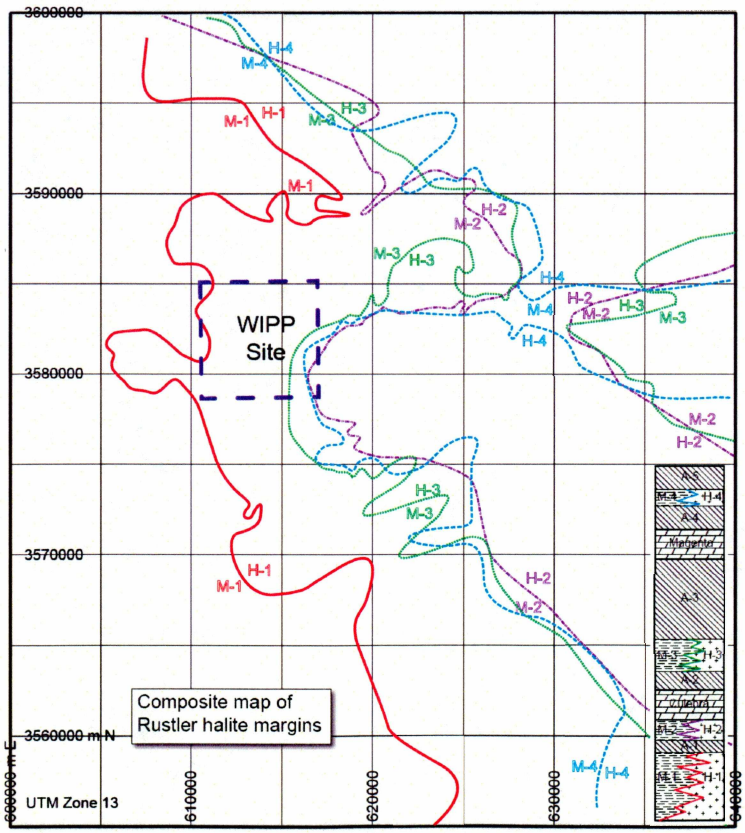

Figure 3. Mudstone-Halite (M-H) margins in the Rustler Formation.

Information Only

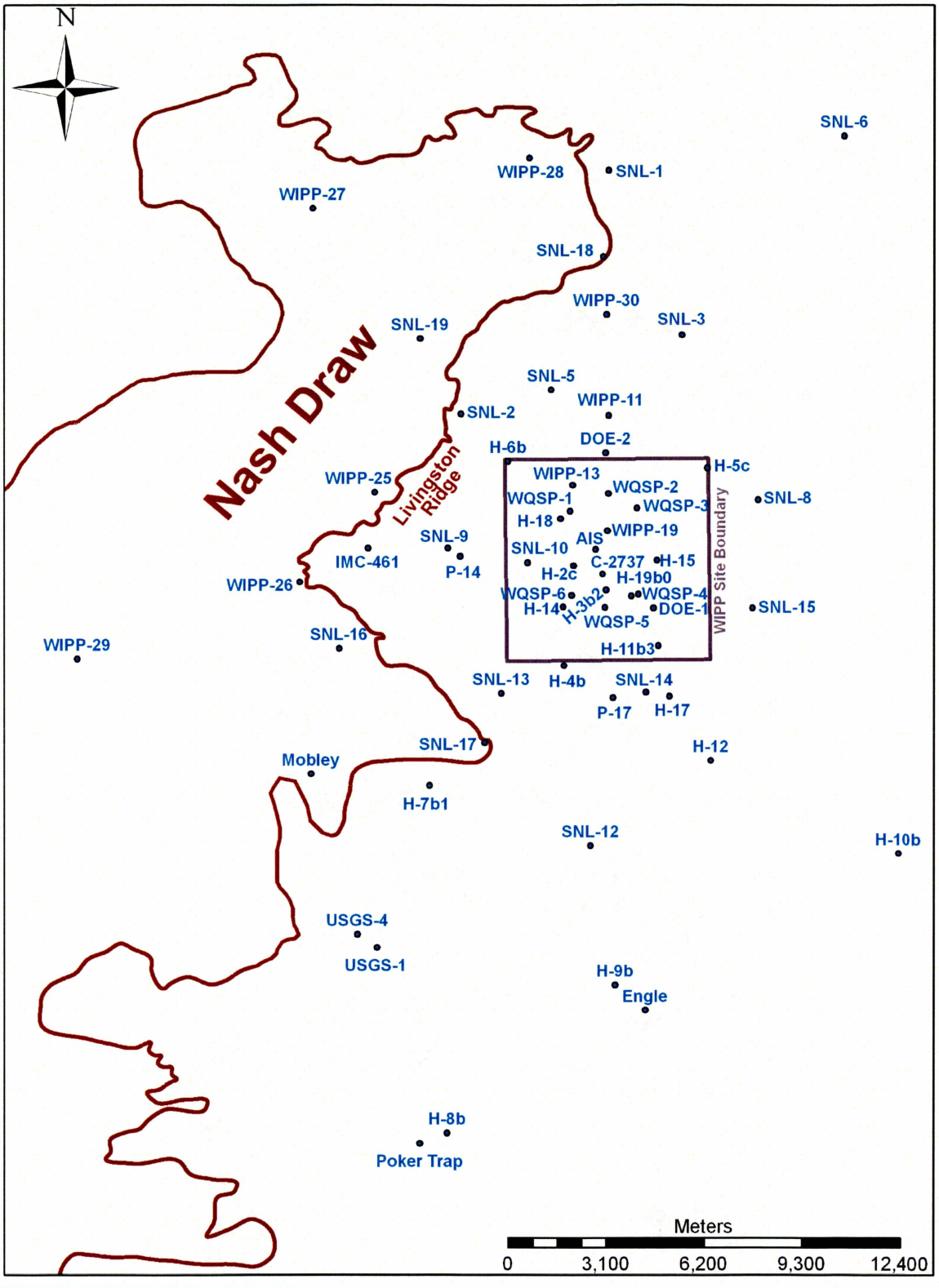

Figure 4. WIPP site and surrounding area with the Culebra wells considered in this report.

Information Only

1.2 Previous Studies

Previous studies of the chemistry of the Culebra groundwater fall into two groups, data-based studies which examine the chemistry of water samples (Ramey, 1985; Lambert, 1991; Lambert and Carter, 1987; Chapman, 1988; Myers et al., 1991; Siegel and Lambert, 1991; Siegel et al., 1991b), and flow-modeling-based studies which seek to explain the distribution of the Culebra water types (Corbet and Knupp, 1996; Kröhn and Schelkes, 1996; Corbet, 1998). Siegel et al. (1991a) provide a comprehensive summary of the previous data-based studies, and only a brief overview is provided in this report.

Ramey (1985) recognized three hydrochemical facies within the Culebra and, based on the two-dimensional flow model in use at that time, concluded that flow was from regions of high total dissolved solids concentration to regions of lower concentration. Table 1 provides specific information on the hydrochemical facies identified by Ramey (1985). Subsequent studies sought to explain the compositional variations in the Culebra brines citing reasons such as climate change (Lambert, 1991; Lambert and Carter, 1987) and dilution and/or recharge (Chapman, 1988; Myers et al., 1991). Some of these later studies (Lambert, 1991; Lambert and Carter, 1987) supported the conceptual model of confined groundwater flow in the Culebra, and used several lines of argument against vertical flow into the Culebra. Among these were the prevalence of anhydrite over gypsum in the Rustler members above the Culebra (Siegel and Lambert, 1991), hydrogen and strontium isotope signatures of gypsum and sulfate and carbonate minerals (Lambert, 1991; Brookins and Lambert, 1988), and radiocarbon dates of Culebra waters (Lambert, 1987).

Table 1. Summary of the data-based studies on the Culebra groundwater chemistry.

Author	Facies	Location (relative to the WIPP site)	Predominant Ions	TDS/Ionic Strength Range	Culebra Transmissivity Condition
Ramey (1985)	A	East	Na – Cl (high K & Mg)	>60,000 mg/L	Low
	B	South	Ca – SO_4	Typically < 9,000 mg/L	High
	C	North and west	Na – Cl (low K & Mg)	9,000 – 239,000 mg/L (increases W to E)	Variable
Siegel et al. (1991b)	A	East	Na – Cl Mg:Ca molar ratios 1.2 - 2	2 – 3 molal	Low
	B	South	Ca - SO_4	<0.1 molal	High
	C	West, east side of Nash Draw	Variable	0.3 – 1.6 molal	Generally high
	D	North and West, west side of Nash Draw	Possible contamination from potash mining	3 – 7 molal	High

Siegel et al. (1991b) used statistical techniques to classify the brines and delineate four regions within the Culebra, each with its own hydrochemical signature (see Table 1). Bodine and Jones' (1990) analyses supported the hydrochemical facies of Siegel et al. (1991b), and explained the

Information Only

complex chemistry of the Culebra brines as mixtures of connate brines with meteoric waters that had reacted with the overlying Rustler members.

Later groundwater modeling studies (Corbet and Knupp, 1996; Kröhn and Schelkes, 1996; Corbet, 1998) sought to develop alternate conceptual models of flow in the Culebra that included vertical flow (leakage) from other Rustler members. The studies of Kröhn and Schelkes (1996) and Corbet (1998) concluded that the observed compositional variations of the Culebra brines were consistent with limited vertical flow from the members of the Rustler overlying the Culebra. Additionally, these studies concluded that flow and groundwater compositional variations in the Culebra are determined by a combination of large-scale heterogeneities in Culebra permeability and the contribution of vertical flow to the Culebra.

1.3 Data Sources

Analyses of Culebra groundwater samples have been performed and reported by a variety of laboratories and organizations over the course of the WIPP project. The analyses have been compiled into an Excel spreadsheet, *Culebra_Hydrochemical_Data.xls*, which provides the fundamental data source for the interpretations described in this Analysis Report.

Representative samples and accurate chemical analyses are necessary to provide a valid interpretation of the Culebra aqueous geochemistry. The water sample must be representative of the formation water and not influenced by the introduced materials used in completion of the well. Likewise, the percent charge-balance error (%CBE) should not exceed five percent to have confidence in analytical accuracy. When the percent error for an analysis is above this threshold, the salt norm (SNORM) calculations described in this analysis report may result in non-representative normative assemblages; this is particularly important for highly concentrated waters such as many of the Culebra brines. The %CBE is the difference in equivalents between the cations and anions divided by their sum and multiplied by 100.

Thus, each chemical analysis used in this report was screened to determine if it met the 5% charge-balance error criterion. The screening was performed using PHREEQCI by entering the most recent analysis for each well, running the code, and outputting the percent error to an Excel spreadsheet. For analyses not meeting the 5% criterion, the next most recent data were entered into PHREEQCI and the procedure was repeated until either a suitable analysis was identified or it was determined that no analysis meeting the criterion existed for a particular well. It should be noted that PHREEQCI uses the speciated water composition as opposed to the straight sum of the cations and anions to calculate the percent error. The speciated composition accounts for lower absolute ionic charge due to the association of cations and anions in solution, which more closely represents the natural state of the water. Table 2 provides the wells, sample dates, and percent error for each of the Culebra analyses used in this Analysis Report. Note that samples that exceeded the 5% threshold criterion, but for which higher accuracy analyses were unavailable, are footnoted.

Information Only

Table 2. Culebra wells, sample dates, and analysis %CBE for the wells used in this report.

Well	Sample Date	%CBE
AIS	10/28/1988	-3.9
C-2737	3/4/2004	0.1
DOE-1[2]	7/28/1987	-4.2
DOE-2[2]	5/19/1988	1.1
Engle	3/5/1985	1.9
H-10b	3/21/1980	-2.0
H-11b3[2]	8/30/1994	-1.7
H-12[2]	12/14/1988	-3.7
H-14	8/27/1992	-2.4
H-15[1]	11/7/1988	-6.6
H-17	10/27/1987	0.4
H-18	4/7/1988	1.8
H-19b0	8/31/2006	-2.3
H-2c	6/21/1994	0.4
H-3b2[2]	12/16/1985	-1.6
H-4b[2]	9/17/1992	-3.2
H-5c[2]	10/15/1981	-2.1
H-6b[2]	3/29/1994	1.3
H-7b1[2]	2/25/1987	1.4
H-8b[1,2]	1/22/1986	6.6
H-9b[2]	9/27/1994	0.0
IMC-461	8/4/2006	-3.2
Mobley	4/14/1988	-2.9
P-14[2]	3/16/1988	0.6
P-17[2]	10/21/1987	2.4
Poker Trap	12/19/1987	-3.0
SNL-1	5/29/2004	-3.4
SNL-2	1/17/2004	-2.0
SNL-3[1]	4/16/2004	-5.3
SNL-5[1]	7/24/2004	-8.8
SNL-6	1/16/2008	1.4
SNL-8	8/2/2007	2.8
SNL-9	11/19/2004	-0.4
SNL-10	11/3/2006	0.0
SNL-12	8/14/2004	-1.7
SNL-13	7/17/2006	-0.3
SNL-14	8/21/2007	0.5
SNL-15	3/30/2007	1.9
SNL-16	6/9/2006	1.3
SNL-17A	9/15/2006	3.2
SNL-18	8/18/2006	-1.6
SNL-19	7/28/2006	2.2
USGS-1[1]	4/12/1988	-6.7
USGS-4[1]	7/19/2006	-6.9
WIPP-11	2/20/2005	-3.4
WIPP-13[1,2]	2/16/1987	-5.7

Information Only

WIPP-19	5/2/1995	1.8
WIPP-25[1,2]	9/23/2004	6.2
WIPP-26[2]	4/14/1988	-1.0
WIPP-27[2]	9/3/1980	-1.6
WIPP-28[2]	9/11/1980	-1.4
WIPP-29[2]	3/4/1987	0.3
WIPP-30[2]	9/6/1980	-3.2
WQSP-1	3/5/2003	-2.1
WQSP-2	3/14/2001	-1.7
WQSP-3	3/27/2003	-0.9
WQSP-4	10/15/2003	1.2
WQSP-5	10/29/2003	-2.6
WQSP-6	5/10/2000	-2.4

1- Analyses with %CBE exceeding 5% threshold.
2- Wells included in Siegel et al. (1991b).

Siegel et al. (1991b) used analyses from only 24 wells on 22 well pads (see footnotes in Table 2), compared to the 59 well locations used in this report. Four wells from Siegel et al. (1991b), H-2a, H-3b3, H-4c, and H-5b, were not included in the current report because of the availability of higher quality data from another well on the same well pad. Figure 4 shows a map of the Culebra wells considered in this report.

1.4 Data Uncertainty

Addressing the issue of analytical error and its impact on the results of the implemented classification methods is a necessary component of a study such as this. Because waters must be electrically neutral, any %CBE calculated from a laboratory analysis represents analytical error or uncertainty. For waters that fell close to the chemical boundaries imposed by the hydrochemical facies or salt norm groups, we evaluated whether slight changes to the constituent concentrations necessary to bring the solutions to electroneutrality (%CBE = 0) would also change the classification of the sample. The problem was how to change an analysis in a way that both honored the data and eliminated the %CBE. Geochemical modeling tools such as PHREEQCI and EQ6 (Wolery, 1992) have the capacity to balance charges in an analysis by choosing a constituent which the code then either adds or subtracts from solution to achieve electroneutrality. While this approach is effective, without some *a priori* knowledge of a sampling or analytical shortcoming in the analysis, it is difficult to rationalize which ion should be chosen to balance charges. Furthermore, altering the concentration of an important charge-contributing species will change its ratio with all of the other major charge contributors and potentially compromise interpretation of the sample.

Two approaches to eliminate the %CBE were attempted, both with merits, but only one approach was finally used. The Culebra waters range from relatively dilute (0.01 molal) calcium-sulfate waters to concentrated (8 molal) sodium-chloride brines. Thus, depending on the salinity of a sample, the majority of charge is carried either by the calcium and sulfate ions or by the sodium and chloride ions. Adjusting the concentration of the dominant cation-anion pair is an effective means of eliminating CBE and spreads the balancing over two ions compared to the single ion approach of PHREEQCI. While superior to the single ion approach, this method still has the

Information Only

pitfall of altering the ratios of the dominant cation-anion pair with all of the other constituent ions.

To minimize the shortcomings of this approach, a logical alternative was to distribute the CBE equally over all of the ions in an analysis. Analytical uncertainties vary by component and are generally not well-established. The underlying assumption of this approach is that all of the ions are subject to only analytic uncertainty; i.e., no additional uncertainties were introduced through improper sampling, storage, or preservation techniques. In addition, it assumes that all of the major charge-contributing ions have been analyzed.

Aqueous solutions are composed of positively and negatively charged species, the net sum of which is equal to zero. Therefore, some degree of offsetting errors between the cations and anions is inherent in all analytical data from a water sample. Because the %CBE is an ensemble term, i.e., it represents a group of errors, and because of coupling in the offsetting errors, the standard deviation of the %CBE for a group of analyses will be less than the standard deviation of the measurement error of individual ions.

To investigate this theory, model output data from the PHREEQCI forward model (Section 4, Run 10 model), and all of the Culebra analyses were subjected to a basic statistical analysis. The PHREEQCI model data were used as a control because they have no CBE, making it possible to introduce individual ion error in a controlled manner, i.e., random normally distributed error with a known standard deviation. Fifty-nine raw PHREEQCI output water compositions, the same number as Culebra analyses, that covered a similar compositional range as the Culebra waters were used. Using simple techniques in Excel, randomly generated normally distributed synthetic error was added to each ion's concentration value and the %CBE was calculated for each of the modeled compositions. Statistics (maximum, minimum, mean, median, frequency, etc.) of %CBE for the synthetic waters were calculated in Excel for comparison with the %CBE statistics for the Culebra water samples. The goal was to vary the standard deviation of the error term on the ion concentrations until a similar %CBE standard deviation was achieved.

Figure 5 shows the probability distribution of the %CBE for the Culebra analyses, and Figure 6 shows the quantile-normal graph of the Culebra %CBE data compared to a theoretical normal distribution. Both Figures 5 and 6 are representations of the %CBE meant to illuminate how the %CBE data are distributed. Figure 5 is the classic manner in which distributions are often displayed, and it appears that the %CBE is normally distributed with a slight negative bias. A quantile-normal graph plots the quantiles of an observed distribution, %CBE in this case, versus the quantiles of the standard normal distribution, i.e., the normal distribution with a mean of 0 and standard deviation of 1. If the observed data have a normal distribution, then they should lie very close to a straight line with the slope equal to the standard deviation and the y-intercept (y value when x value is 0) representing the mean. The Culebra %CBE data all fall very close to the theoretical normal distribution on Figure 6, indicating that the data are close to being normally distributed. The negative y-intercept and mean indicate that there is some bias towards the anions, though it is not possible to determine the cause of the bias from the analysis.

Information Only

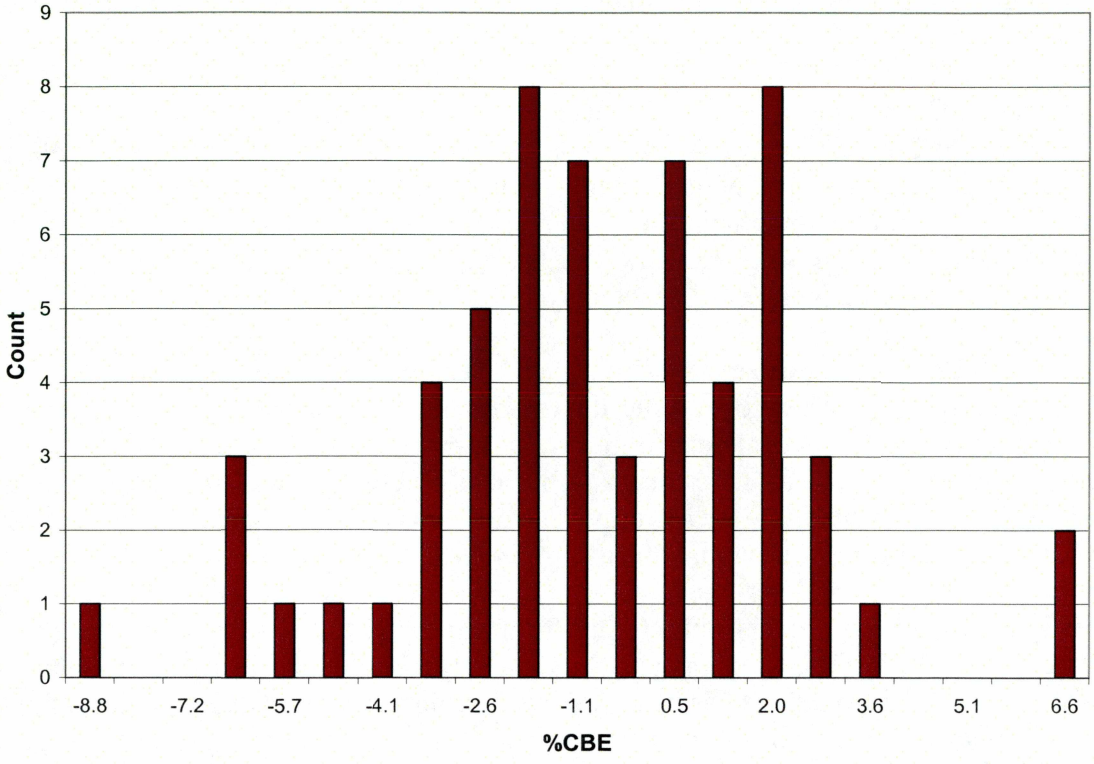

Figure 5. Probability distribution for the %CBE for the Culebra water analyses.

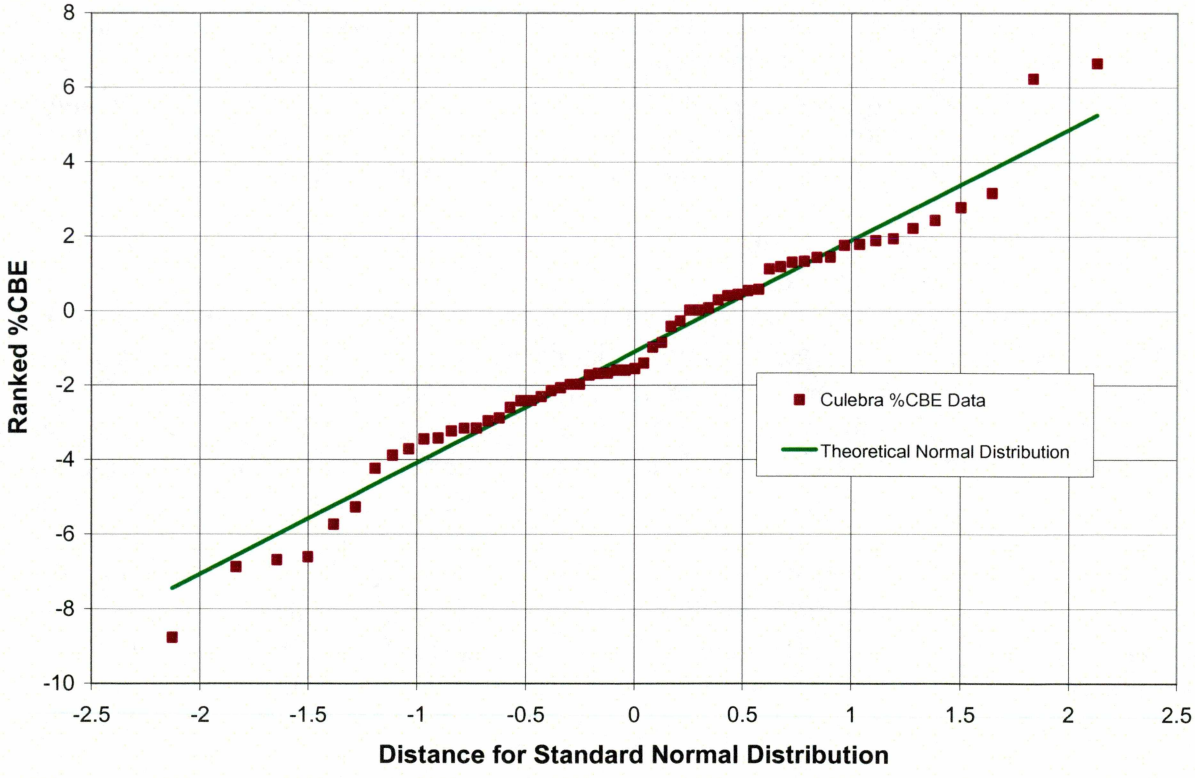

Figure 6. Quantile-normal plot for the %CBE for the Culebra water analyses.

Information Only

Figures 7 and 8 are the equivalent plots to Figures 5 and 6 for the PHREEQCI output data. As expected, both Figures 7 and 8 show that the data are normally distributed. Table 3 provides the summary statistics of the Culebra and PHREEQCI %CBE data. By manually changing the standard deviation of the individual ion error terms to 5% and recalculating the spreadsheet, the overall PHREEQCI %CBE standard deviation matched the 3% of the Culebra analyses. As predicted, %CBE standard deviation (3%) for a group of analyses is less than the standard deviation of the individual ion errors (5%). The lower standard deviation of the %CBE for a group of analyses is lower than the individual ion standard deviation because of offsetting errors in the cations versus anions. With respect to the Culebra data, this result can be interpreted as showing that the mean measurement error for the charge-contributing ions is approximately ±5%. Unfortunately, the origin of the negative bias in the mean of the Culebra %CBE cannot be discerned; any number of combinations of over- and under-estimating the cations and anions could lead to the observed bias.

Table 3. Summary statistics for the %CBE for the Culebra and PHREEQCI data.

	n	minimum	maximum	mean	median	std dev	skew
Culebra	59	-8.77	6.65	-1.09	-1.55	2.99	-0.02
PHREEQCI	59	-6.09	7.02	0.28	0.46	2.79	-0.08

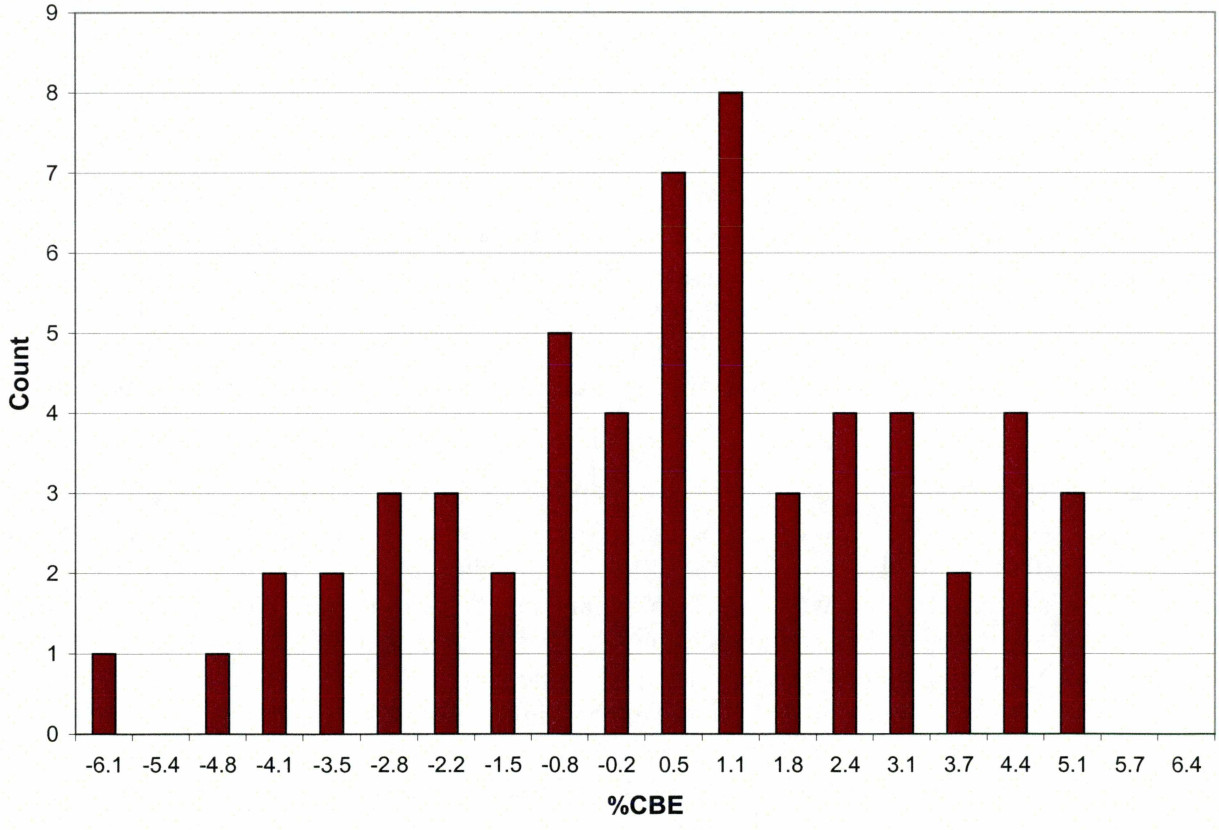

Figure 7. Probability distribution for the %CBE for the PHREEQCI output water analyses.

Information Only

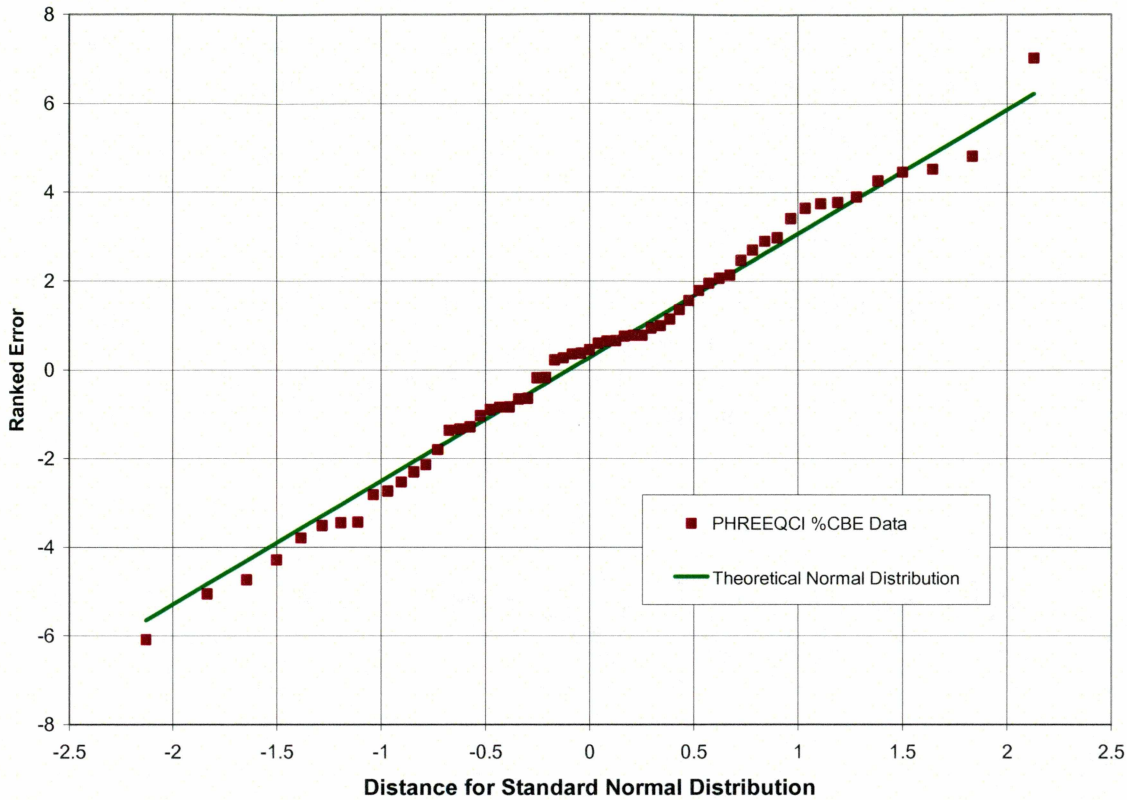

Figure 8. Quantile-normal plot for the %CBE for the PHREEQCI output water analyses.

Based on the results of this exercise, six Culebra analyses were identified for charge balancing: DOE-1, H-17, SNL-8, USGS-1, USGS-4, and WQSP-6. To determine the effect of the balancing technique on the salt norm classification, both methods, balancing on the major ion pair (sodium – chloride or calcium – sulfate) and balancing on all of the constituent ions, were used and the salt norms were calculated from the charge-balanced analyses. The new balanced salt norms were then compared to the original salt norms to ascertain if the norms changed enough to change their classification.

Wells DOE-1, H-17, SNL-8, and WQSP-6 were all balanced on sodium and chloride as well as all ions, and USGS-1 and USGS-4 were balanced on calcium and sulfate as well as all ions. The results showed that for DOE-1, H-17, and SNL-8, the method of balancing had an insignificant effect on their salt norms. For well WQSP-6, balancing on sodium and chloride alone changed the normative signature, while balancing on all of the ions did not change the signature. Balancing on calcium and sulfate only for the dilute USGS-1 and USGS-4 analyses had a dramatic impact on their salt norms because of the higher charge carried by these ions and the greater role they play in the total charge contribution of a dilute water. The result of balancing on all of the ions in the USGS-1 and USGS-4 analyses did not result in changes to their salt norms. We conclude from this exercise that balancing on all of the ions in the analysis is better than balancing on just the primary charge-contributing ions because, in the absence of some ion-specific error information, honoring the measured data as much as possible is the more prudent approach.

Information Only

2. Methods

2.1 Computer Codes

Two geochemical codes were used in the analyses of the Culebra groundwater chemical data, PHREEQCI version 2.12.5-669, (Parkhurst and Appelo, 1999) and SNORM version 2.1 (Bodine and Jones, 1986). PHREEQCI was used to perform basic speciation and saturation index calculations as well as theoretical reaction-path and mixing simulations. SNORM was used to calculate the normative salt assemblages (salt norms) for the Culebra waters and in some cases to calculate the salt norms from the PHREEQCI outputs. In addition, Microsoft Excel was used for data reduction and plotting.

PHREEQCI version 2.12.5-669 is a computer program written in the C programming language that is designed to perform a wide variety of low-temperature aqueous geochemical calculations. PHREEQCI is based on an ion-association aqueous model for dilute solutions, as well as the Pitzer virial-coefficient approach (expanded polynomial) for activity-coefficient corrections for high-ionic strength waters. PHREECQI has capabilities for (1) speciation and saturation-index calculations; (2) batch-reaction and one-dimensional (1D) transport calculations involving reversible reactions, which include aqueous, mineral, gas, solid-solution, surface-complexation, and ion-exchange equilibria, and irreversible reactions, which include specified mole transfers of reactants, kinetically controlled reactions, mixing of solutions, and temperature changes; and (3) inverse modeling, which finds sets of mineral and gas mole transfers that account for differences in composition between waters, within specified compositional uncertainty limits.

SNORM calculates an equilibrium normative salt assemblage (or salt norm) from the solute concentration data from a conventional water analysis. Although the salt norm can be visualized as the solid residuum that coexists with the small, last vestige of solution upon evaporation at 25°C and atmospheric carbon dioxide, the normative assemblage is computed directly from solute concentrations without proceeding along an evaporation path with its myriad succession of brine-solid interactions. Neither brine evolution nor character of the vestigial brine are considered; SNORM only distributes the solutes into the appropriate liquid-free salt assemblage. The program transforms 18 solutes into a normative salt assemblage (from a listing of 63 possible salts) and respective simple salts.

Quoting from the abstract for SNORM version 2.1 (Bodine and Jones, 1986):

> "The new computer program SNORM calculates the salt norm from the chemical composition of a natural water. The salt norm is the quantitative ideal equilibrium assemblage that would crystallize if the water evaporated to dryness at 25°C and 1 bar pressure under atmospheric partial pressure of CO_2. SNORM proportions solute concentrations to achieve charge balance. It quantitatively distributes the 18 acceptable solutes into normative salts that are assigned from 63 possible normative salts to allow only stable associations based on the Gibbs Phase Rule, available free energy values, and observed low-temperature mineral associations. Although most natural water compositions represent multiple solute origins, results from SNORM identify three major categories: meteoric or weathering waters that are characterized

Information Only

by normative alkali-bearing sulfate and carbonate salts; connate marine-like waters that are chloride-rich with a halite-bischofite-carnallite-kieserite-anhydrite association; and diagenetic waters that are frequently of marine origin but yield normative salts, such as Ca-bearing chlorides (antarcticite and tachyhydrite) and sylvite, which suggest solute alteration by secondary mineral reactions. The solute source or reaction process within each of the above categories is commonly indicated by the presence or absence of diagnostic normative salts and their relative abundance in the normative salt assemblage. For example, salt norms: (1) may identify lithologic source; (2) may identify the relative roles of carbonic and sulfuric acid hydrolysis in the evolution of weathering waters; (3) may identify the origin of connate water from normal marine, hypersaline, or evaporite salt resolution processes; and (4) may distinguish between dolomitization and silicate hydrolysis or exchange for the origin of diagenetic waters."

Chemical analyses from 59 Culebra wells were entered into the Excel file *Culebra_Hydrochemical_Data.xls* and then entered into PHREEQCI. The PHREEQCI code was used to calculate the aqueous speciation, mineral saturation index values, percent error values, ionic strength, and specific element ratios for each analysis. Based on the percent error, each analysis was screened and those meeting the 5% CBE criterion were entered into SNORM. The SNORM code calculated the normative mineral assemblages for each analysis.

The resulting outputs from SNORM and PHREEQCI were imported into Excel for interpretive analysis. Interpretation of the model results was aided by the generation of plots (ion and ion-ratio values, solution properties) and categorization of wells based on the presence and abundance of normative mineral phases, ionic strength, and hydrochemical facies (Siegel et al., 1991b). The various categories were then plotted areally as a function of well locations to examine the spatial distribution of the data. Based on the spatial distribution, reaction-path and mixing simulations were created in PHREEQCI to test the feasibility of the evolution of water along a flow path.

2.2 Classifications

As a means of distinguishing between different water types and for the purpose of gaining an understanding of their potential evolution and origins, three classification schemes were implemented: 1) hydrochemical facies; 2) normative mineral assemblages; and 3) the percentages of normative halite and anhydrite. In addition to the three classification schemes, mineral saturation index values and ionic strength values were also calculated as a further means of understanding the water chemistry of the samples.

2.2.1 Hydrochemical Facies

Siegel et al. (1991b) defined four hydrochemical facies, or hydrochemical zones, within the Culebra, as shown in Figure 9. The distinction between the facies was based on major element concentrations, concentration ratios, and ionic strength of the waters. In this report, we have adopted the facies conventions of Siegel et al. (1991b) and modified and expanded the facies to include two transitional facies and a new facies for waters not previously sampled. The original four facies of Siegel et al. (1991b) increased in salinity from B→C→A→D. In this report, we have added transitional facies B/C and A/C and the new facies E, such that salinity increases

Information Only

from B→B/C→C→A/C→A→D→E. These additional facies provide a more detailed illustration of the spatial variation and distribution of groundwater compositions.

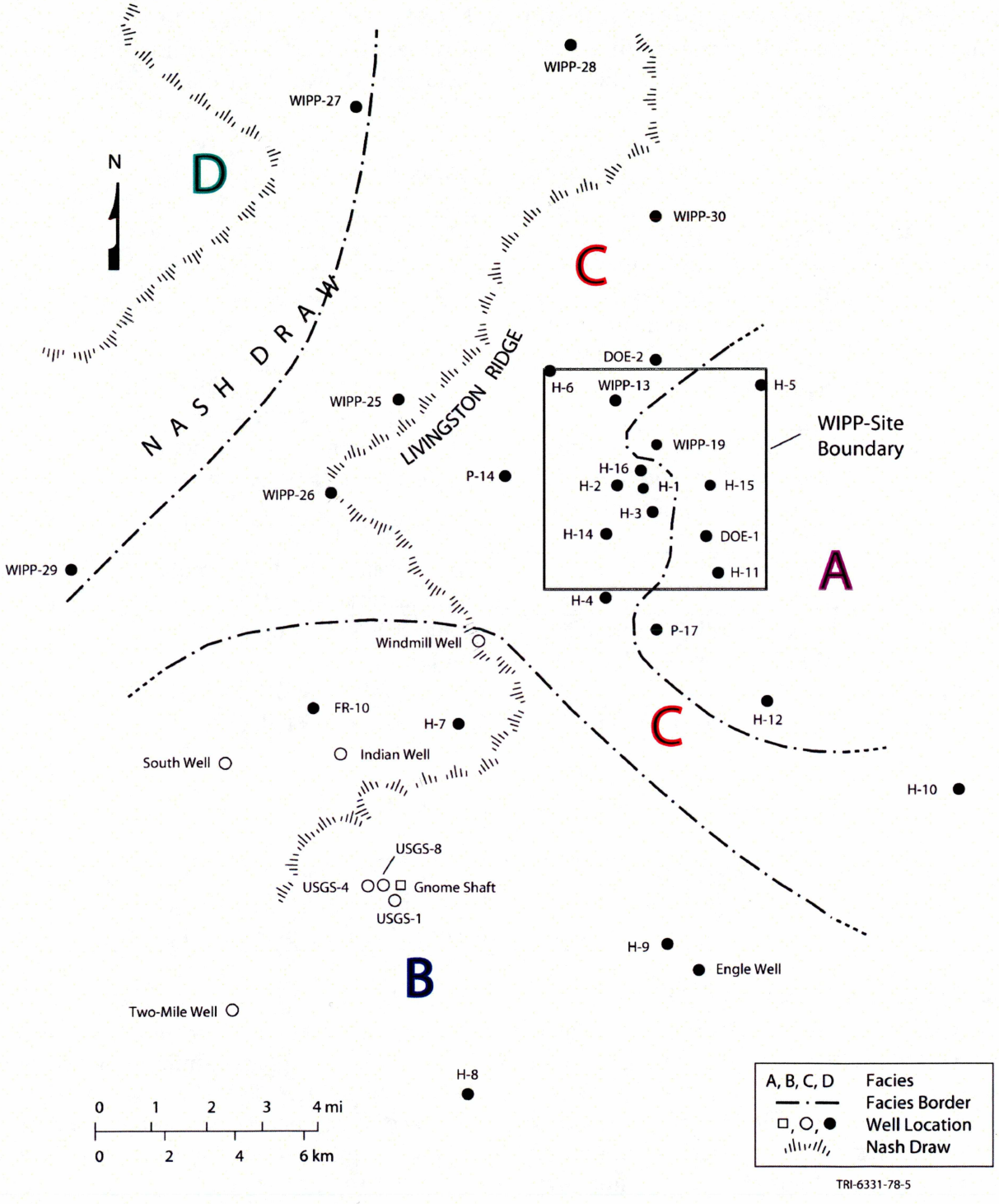

Figure 9. Hydrochemical facies zones of Siegel et al. (1991b).

Information Only

The definitions of the hydrochemical facies used by Siegel et al. (1991b) and those defined in this report are listed in Table 4. Note that the upper and lower limits of ionic strength and the Mg/Ca molar ratio often do not coincide exactly with the immediately adjacent facies because these limits were set by the data, i.e., compositional gaps exist in the data. Also note that the range of Mg/Ca ratios for facies B/C is wholly contained within the limits of the range for facies C; the ionic strength is the primary difference between these two facies. The classification of the Culebra waters into hydrochemical facies and conclusions drawn from that classification are discussed in Section 3.1.

Table 4. Hydrochemical facies descriptions.

	Facies	Siegel et al. (1991b)	This Report
Increasing Salinity ↓	B	Dilute (ionic strength <0.1 molal) $CaSO_4$ rich groundwater, from southern high transmissivity area	Same as Siegel et al. (1991b) Mg/Ca molar ratio: 0.32 to 0.52
	B/C	Not included.	Ionic strength 0.18 to 0.29 molal Mg/Ca molar ratio 0.4 to 0.6
	C	Variable composition waters, Mg/Ca molar ratio 0.3 to 1.2 for waters with ionic strength <1.25 molal	Ionic strength 0.3 to 1.0 molal Mg/Ca molar ratio 0.4 to 1.1
	A/C	Not included.	Ionic strength 1.1 to 1.6 molal Mg/Ca molar ratio 0.5 to 1.2
	A	Ionic strength ~2-3 molal, Mg/Ca molar ratio 1.2 to 2	Ionic strength >1.66 molal, up to 5.3 molal Mg/Ca molar ratio 1.2 to 2.4
	D	Defined based on inferred contamination related to potash refining operations. Ionic strength 3 molal, K/Na weight ratios of ~0.2	Same as Siegel et al. (1991b)
	E	Not included	Wells east of the mudstone-halite margins, ionic strength 6.4 – 8.6 molal, Mg/Ca molar ratio 4.1 – 6.6

2.2.2 Salt Norm Classification

The output data from the SNORM calculations were compiled in Excel for sorting, plotting, and analysis. Based on the presence and abundance of key normative phases, inferences regarding the origins of the solutes and potential flow paths can be made. The Culebra waters were subdivided into four primary groups based on the presence of key phases: 1) sulfatic weathering solutions; 2) sulfatic weathering solutions with a marine solute component; 3) waters with marine-derived solutes; and 4) solutions with a diagenetic (dolomitization) signature. During primary dolomitization in a salt pan type environment, fluids may be depleted in calcium and sulfate via gypsum precipitation, with the Mg/Ca ratio increasing up to 80 (Levy, 1977). Sodium will become depleted as halite precipitation advances. The remaining brine will be enriched in

Information Only

magnesium and give rise to salt norms characteristic of dolomitization. Based on the SNORM results and their high ionic strength, the waters sampled from wells SNL-15 and SNL-6 represent primitive diagenetic brine, i.e., synsedimentary brine that was present at the time of deposition of the Culebra. The remaining 57 Culebra waters appear to have infiltrated and reacted with the minerals along their flowpaths, as well as mixed with primitive waters of the Culebra. Discussion of the salt norms of the Culebra waters is presented in Section 3.2.

2.2.3 Normative Excess Classifications

In addition to the detailed interpretation of the normative mineral assemblage, a more general interpretation of the salt norm based on the abundance of halite and anhydrite can provide a simple model of the flow path that a water may have traveled to reach a well. Given the unique geologic environment of the Culebra with the Tamarisk sulfate beds above and the well-documented locations where halite is present in the surrounding members and formations (Holt et al., 2005), a simple model for flow can be deduced from the halite and anhydrite values of the norm.

1) Excess anhydrite ($CaSO_4$) in the salt norm (>4%, Bodine and Jones, 1986) suggests dissolution of calcium sulfate, either anhydrite or gypsum, along the flowpath. The greatest potential for dissolution of sulfate minerals in the Rustler Formation is through reaction with the Tamarisk Member, thus excess anhydrite could indicate that vertical flow through the Tamarisk Member occurred before water entered the Culebra.

2) Excess halite (NaCl) in the salt norm (>78%, Bodine and Jones, 1986) suggests *in situ* dissolution of halite cements or of bedded halite. Thus, the water may have flowed laterally through the Culebra with minimal reaction with sulfate beds, and either actively dissolved halite, for example in the area of the M2-H2 margin, or mixed with the synsedimentary brines which exist east of the M2-H2 margin, e.g., at SNL-6 and SNL-15. This scenario would involve a long flow path from the point of infiltration to the well.

3) Excess anhydrite (>4%) and halite (>78%) suggest potential vertical flow combined with lateral flow or mixing. Depending on whether this type of water dissolved halite or mixed with a halite-type water, this flow path could either be relatively long or relatively short.

4) Waters in which neither halite nor anhydrite exceed their threshold values could be either very old synsedimentary brines, e.g., SNL-15, or of relatively recent meteoric origin where dissolution reactions have not significantly altered their composition.

Four classifications were established based on this model: 1) *excess halite*; 2) *excess anhydrite*; 3) *excess anhydrite and halite*; and 4) *neither*. The *excess anhydrite* and *neither* classification schemes are potentially the quickest flow paths from the point of infiltration to the well, although truly primitive water samples, i.e., synsedimentary water, may also carry the *neither* classification. The classification for each well was plotted on a map to examine the spatial relationships of the classifications. These data will be discussed in Section 3.3.

Information Only

2.2.4 Ionic Strength and Mineral Saturation Index

The ionic strength and mineral saturation index values for each water sample were calculated in PHREEQCI. Ionic strength functions as a measure of concentration, and can be considered as reflecting the degree of interaction between water and rock. Ionic strength was used as a classification parameter in assigning waters to hydrochemical facies, as well as a standalone parameter used to observe concentration trends in the Culebra.

The mineral saturation index (*SI*) is calculated by PHREEQCI and is a measure of the degree of saturation of a mineral phase with respect to equilibrium. The saturation index is the log of the ratio of the ion activity product to the equilibrium constant for the phase of interest. Thus, as a log quantity, negative values of SI indicate undersaturation and positive values indicate supersaturation, while a value of zero indicates saturation conditions for the phase of interest. The PHREEQCI saturation index results are presented in Section 4.2.

Information Only

3. Results

The hydrochemical facies (zone), ionic strength (μ), SNORM type, and normative excess classifications for each well are compiled in Table 5 and discussed in the following subsections.

Table 5. Classification of the Culebra waters sorted by hydrochemical facies (zone) and ionic strength (μ).

Well	Zone	μ (molal)	SNORM Type	Normative Excess
SNL-14	A	1.68	Sulfatic weathering w/marine component	Excess anhydrite & halite
P-17	A	1.69	Marine	Excess anhydrite & halite
WQSP-4	A	1.71	Sulfatic weathering w/marine component	Excess anhydrite & halite
H-11b3	A	2.21	Marine	Excess anhydrite & halite
H-12	A	2.59	Marine	Excess anhydrite & halite
DOE-1	A	2.62	Marine	Excess halite
SNL-8	A	2.73	Marine	Excess anhydrite & halite
H-17	A	2.95	Sulfatic weathering w/marine component	Excess halite
H-5c	A	3.00	Marine	Excess halite
H-15	A	4.13	Marine	Excess halite
WQSP-3	A	4.50	Marine	Excess halite
DOE-2	A/C	1.07	Marine	Excess anhydrite & halite
H-3b2	A/C	1.09	Diagenetic	Excess anhydrite & halite
WIPP-13	A/C	1.19	Marine	Excess anhydrite & halite
WQSP-2	A/C	1.24	Marine	Excess anhydrite & halite
WQSP-1	A/C	1.24	Marine	Excess anhydrite & halite
H-6b	A/C	1.25	Diagenetic	Excess anhydrite & halite
H-10b	A/C	1.28	Marine	Excess anhydrite & halite
WIPP-19	A/C	1.37	Sulfatic weathering w/marine component	Excess anhydrite & halite
C-2737	A/C	1.53	Marine	Excess anhydrite & halite
H-19b0	A/C	1.55	Sulfatic weathering w/marine component	Excess anhydrite & halite
Poker Trap	B	0.06	Sulfatic weathering solution	Excess anhydrite
H-8b	B	0.08	Sulfatic weathering solution	Excess anhydrite
H-7b1	B	0.09	Sulfatic weathering w/marine component	Excess anhydrite
SNL-17A	B	0.09	Sulfatic weathering w/marine component	Excess anhydrite
Engle	B	0.09	Sulfatic weathering solution	Excess anhydrite
H-9b	B	0.09	Sulfatic weathering solution	Excess anhydrite
USGS-1	B	0.10	Sulfatic weathering solution	Excess anhydrite
Mobley	B	0.10	Sulfatic weathering w/marine component	Excess anhydrite
SNL-12	B	0.10	Sulfatic weathering w/marine component	Excess anhydrite
USGS-4	B	0.10	Sulfatic weathering w/marine component	Excess anhydrite
SNL-19	B/C	0.18	Marine	Excess anhydrite
SNL-10	B/C	0.19	Sulfatic weathering solution	Neither
IMC-461	B/C	0.21	Diagenetic	Excess anhydrite
H-2c	B/C	0.22	Sulfatic weathering solution	Excess anhydrite
SNL-2	B/C	0.24	Marine	Excess anhydrite
WIPP-26	B/C	0.28	Diagenetic	Excess anhydrite

Information Only

Well	Zone	μ (molal)	SNORM Type	Normative Excess
SNL-5	B/C	0.29	Diagenetic	Excess anhydrite
WQSP-6	C	0.33	Sulfatic weathering solution	Neither
SNL-16	C	0.38	Diagenetic	Excess anhydrite
SNL-13	C	0.38	Sulfatic weathering w/marine component	Excess anhydrite
H-14	C	0.39	Diagenetic	Excess anhydrite
SNL-18	C	0.40	Marine	Excess anhydrite
H-4b	C	0.44	Sulfatic weathering solution	Excess anhydrite
H-18	C	0.53	Marine	Excess anhydrite
SNL-9	C	0.56	Diagenetic	Excess anhydrite
P-14	C	0.58	Diagenetic	Excess anhydrite
WIPP-30	C	0.58	Sulfatic weathering w/marine component	Excess anhydrite
WIPP-25	C	0.58	Diagenetic	Excess anhydrite
WQSP-5	C	0.60	Sulfatic weathering w/marine component	Excess anhydrite
SNL-1	C	0.70	Marine	Excess anhydrite
AIS	C	0.79	Sulfatic weathering solution	Excess anhydrite & halite
WIPP-28	C	0.90	Sulfatic weathering w/marine component	Excess anhydrite & halite
SNL-3	C	0.92	Marine	Excess anhydrite & halite
WIPP-11	C	0.99	Marine	Excess anhydrite & halite
WIPP-27	D	2.59	Potash	Neither
WIPP-29	D	5.93	Potash	Excess halite
SNL-15	E	6.43	Diagenetic	Neither
SNL-6	E	8.61	Diagenetic	Neither

3.1 Hydrochemical Facies

Figures 10 and 11 display the Culebra hydrochemical facies plotted on a Piper (1944) diagram and geographically on a map of the WIPP site and surrounding area, respectively. The SNORM results also shown on Figure 10 will be discussed in Section 3.2. Piper diagrams plot the percentages of the major solutes (Ca, Mg, Na, K, Cl, SO_4, and HCO_3) with the cations plotting in the bottom left trilinear diagram, the anions in the bottom right trilinear diagram, and the cation-anion combined projection in the central diamond. Because the major element concentrations are expressed as percentages relative to each other and not as absolute concentrations, the degree of concentration of the waters cannot be discerned from this type of plot.

Figure 10 shows that the Culebra groundwaters are predominantly calcium-magnesium-sulfate to sodium-chloride type waters with very little bicarbonate. Predictably, the facies B waters plot in the calcium-sulfate corner of the Piper central diamond and facies A waters plot in the sodium-chloride corner, with the intermediate facies, B/C, C, and A/C plotting between facies A and B. Absent in Figure 10 is the presence of bicarbonate rich waters. Waters rich in bicarbonate are typically young, dilute, and may originate in shallow aquifers or limestone aquifers. The most dilute waters of the Culebra are the sulfate-rich facies B waters which are low in bicarbonate. The absence of bicarbonate waters in the Culebra is most likely due to the Culebra being sufficiently deep that the waters have had time to react along the flowpath with the abundant sulfate phases which would overwhelm any bicarbonate signature.

Information Only

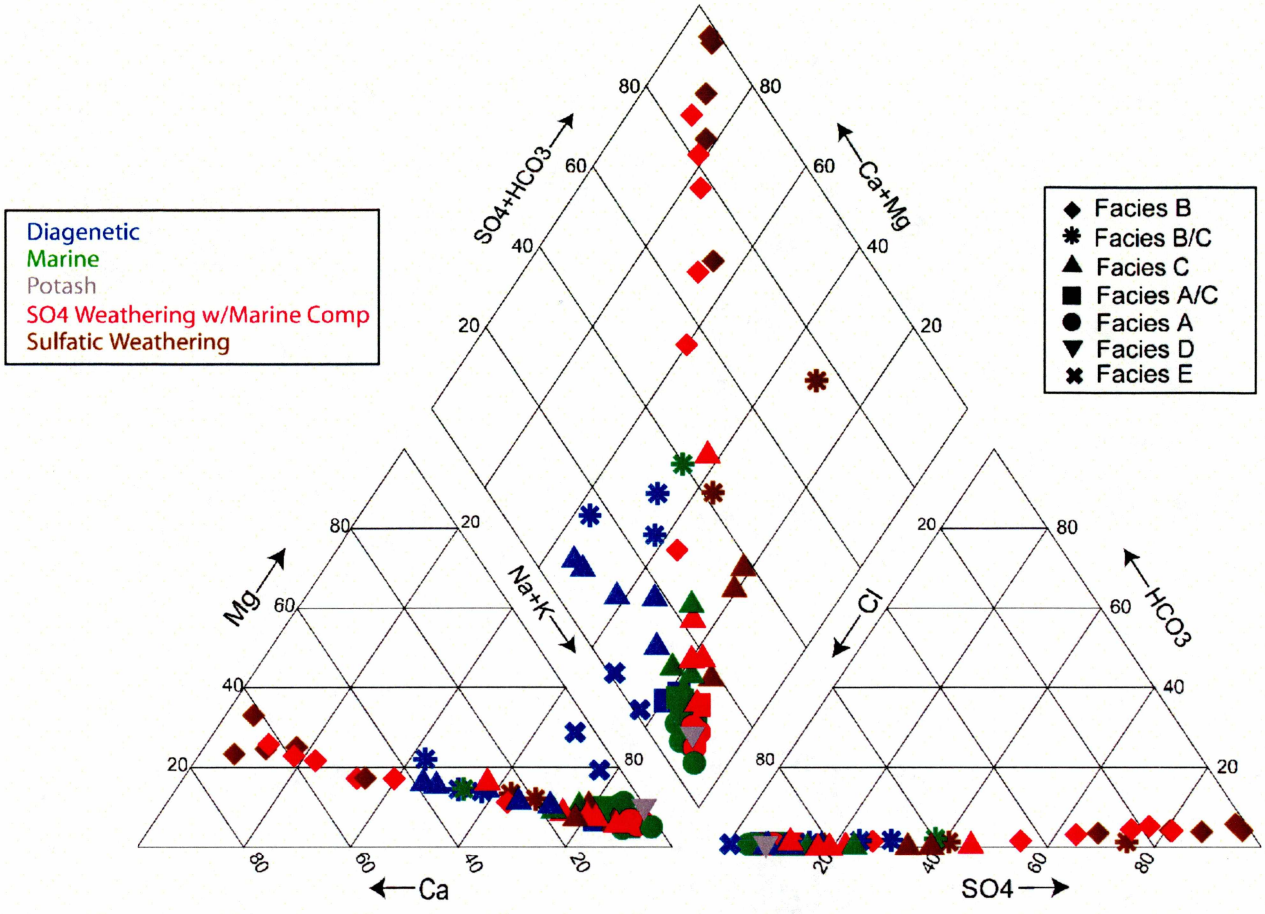

Figure 10. Piper plot of the Culebra wells symbol-coded to reflect their hydrochemical facies and color-coded to reflect their SNORM type.

A notable feature of Figure 10 is the data gap in the anion triangle along the sulfate axis between 40 to 60 percent. On the high-sulfate side of this gap, all of the wells are facies B wells, with the exception of SNL-10. On the low-sulfate side of the gap, no facies B wells are represented; the wells are all from facies B/C, C, A/C, A, D, and E.

Figure 11 shows the areal distribution of the different hydrochemical facies. The facies B waters all lie to the south and southwest of the WIPP site. The data gap along the sulfate axis on Figure 10 could be due to the area of facies B waters representing a recharge area, and/or to the possibility that this region is devoid of both significant evaporite phases such as halite and of high-concentration waters. In other words, this area may have been "flushed" to a greater degree than the surrounding areas.

Powers (2006) identified surface features where surface water could accumulate and potentially recharge the underlying strata. One of the features that Powers (2006) identified as extensive over the area encompassed by the facies B wells was drainage basin #6 (Figure 11), which included a karst valley with numerous caves and swallowholes, as well as a subbasin (drainage basin #7) that contains a major sinkhole. All of the features have the potential to funnel water from precipitation events into the subsurface for possible recharge to the Rustler Formation.

Information Only

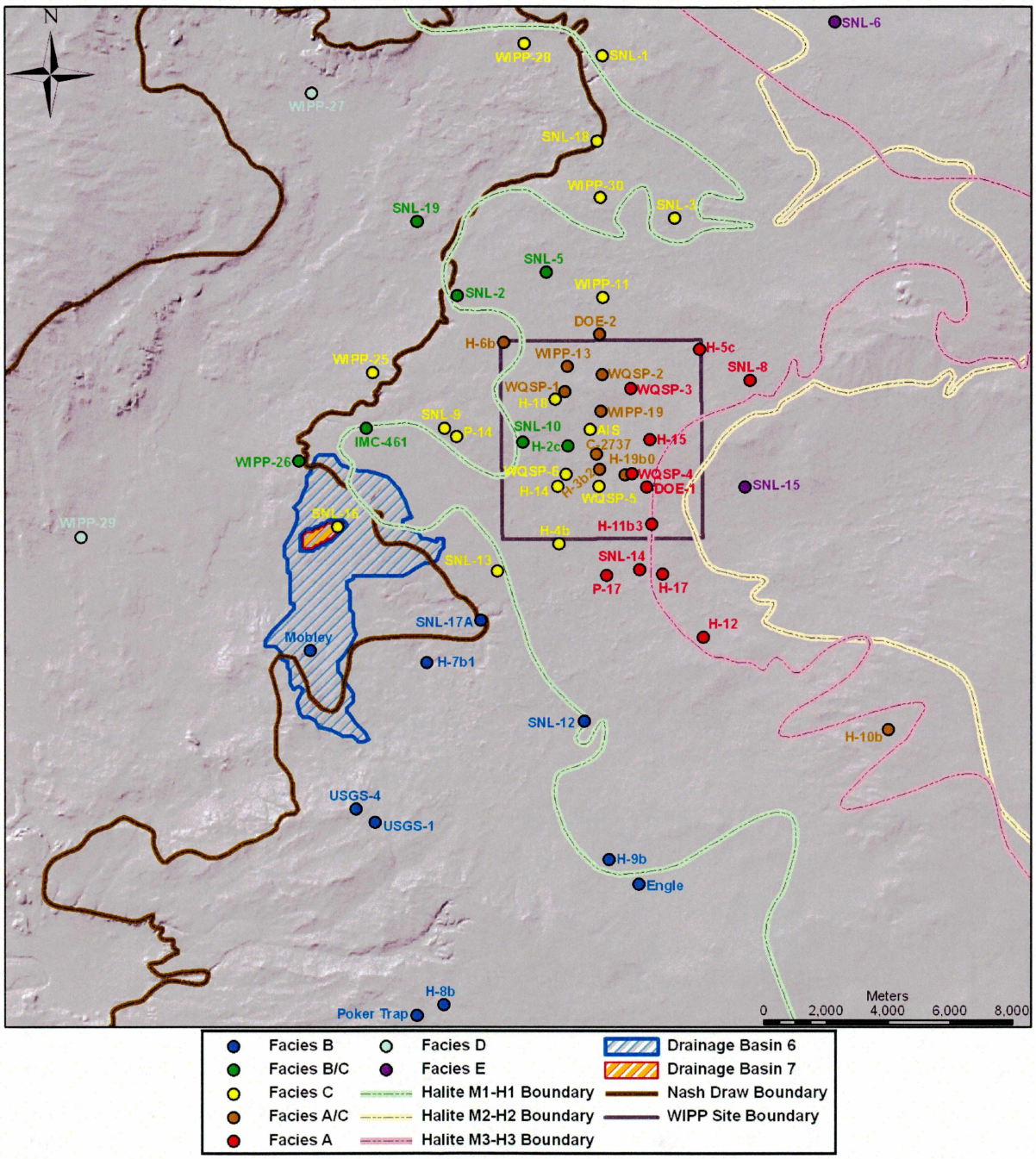

Figure 11. Culebra wells color-coded on the basis of hydrochemical facies.

Hillesheim et al. (2007) report that well SNL-16, located in drainage basin #7, responds rapidly to precipitation events with an increase in water level. This observation lends support to the contention of Powers et al. (2006) that a hydraulic pathway may exist between the surface geomorphic features and the Culebra. However, the water of SNL-16 is facies C and of a more evolved chemistry, with an ionic strength of 0.4 molal, than that of precipitation, suggesting that freshwater falling as precipitation is not directly entering the Culebra and being withdrawn at SNL-16. Rather, the observed water-level response at SNL-16 to precipitation events simply

Information Only

indicates that a hydraulic connection exists between the Culebra and an overlying water table that is recharged by precipitation.

If the geomorphic features identified by Powers (2006) are acting as recharge points for the facies B waters, the recharge may be creating a groundwater divide in that region that isolates the facies B wells hydraulically from the upgradient wells. The facies B waters may mix with other water types that have moved south across the WIPP site along a NE-SW trending line lying between SNL-16, SNL-17A, and SNL-13, and in the direction of H-10b.

Another possible explanation for the data gap along the sulfate axis in Figure 10 could be the lack of wells which tap waters of intermediate composition, i.e., the sample size of wells may be too small to represent all of the possible water compositions adequately.

As previously mentioned, the SNL-10 water is the only non-facies B water to plot along the sulfate axis with the facies B waters. While SNL-10 does not contain as much calcium and magnesium as the facies B waters, it does have high sulfate and is also relatively dilute (0.19 molal). The composition of SNL-10 is unique (anomalous) compared to the other Culebra wells and it will be discussed further in Section 3.2.

Facies E wells, SNL-6 and SNL-15, also lie outside the general trends observed in the Figure 10 Piper plot. The water from these wells is highly concentrated, 6.4 molal for SNL-15 and 8.6 molal for SNL-6, and dominated by sodium, magnesium, and chloride. During collection of the SNL-6 sample, what appeared to be halite crystals were observed precipitating from solution in the sample bottle illustrating the extreme concentration level of this brine. Both SNL-6 and SNL-15 lie on the eastern, halite side of the Rustler mudstone/halite margins (Powers et al., 2006), and the Culebra contained halite cements in both of these boreholes; therefore, these brines probably represent synsedimentary brines.

Figure 11 shows that the facies E wells, SNL-6 and SNL-15, are the only two Culebra wells located east of the M2-H2 boundary, and their unique water chemistry is a reflection of the geology in this area. Powers et al. (2006) provide a description and interpretation of the geology/depositional history of the Culebra in this area based on the cores from these holes. Halite was observed as filling fractures, occupying vuggy porosity, and as cements in zones of silty dolomite in the SNL-6 and SNL-15 Culebra cores. As a fracture filling, Powers et al. (2006) state that the Culebra halite accumulation must post-date the deposition of the primary Culebra dolomite, and that halite occupying vuggy porosity may be early diagenetic replacement of displacive gypsum nodules. Furthermore, Powers et al. (2006) hypothesize that halite accumulation in the Culebra may coincide with the deposition of the stratigraphically higher M3-H3 interval, i.e., that the M3-H3 transgression was the source of the fluids that initially dissolved the gypsum nodules of the Culebra and later laid down the halite observed in the cores.

If the Powers et al. (2006) hypothesis is true, then the brine samples from these wells do not represent the residual brine remaining after the deposition of the Culebra dolomite itself, but rather a residual fluid, still Permian in age, that remained after the deposition of the Culebra halite that has equilibrated with the surrounding rock. This will be further examined in Section 3.2.4.

Information Only

Waters of facies A plot in the sodium-chloride corner of the central diamond of the Piper plot (Figure 10). The facies A wells lie in a relatively well defined north-south cluster (Figure 11) along the Rustler halite margins with the M2-H2 being the most important of these margins. Facies A water is the high-concentration end member of a continuum of compositions from B/C→C→A/C→A where dissolution of evaporite phases (halite and accessory phases) by facies A/C or C waters and mixing with the facies E brines liberated at the dissolution front combine to produce the facies A composition.

Less saline waters of the A/C facies are likely the result of mixing between the relatively dilute facies C waters to the west with the facies A waters in the east (Figure 11). The facies A/C waters form a distinct wedge-shaped region that is widest on the north in the area of wells H-6b and DOE-2 and narrows down toward well H-3b2 (Figure 11) in the south.

The facies B/C and C wells form a broad band that roughly parallels Nash Draw and the M1-H1 margin (Figure 11). The purpose of creating the B/C facies was to examine the subtle differences in ionic strength of the facies C waters as defined by Siegel et al. (1991b), and to look for patterns in their occurrence.

Figure 11 shows that there are three clusters of B/C wells: SNL-2, SNL-5, and SNL-19 form a northern cluster; WIPP-26 and IMC-461 form a second cluster; and H-2c and SNL-10 form a third cluster. The first two clusters of B/C wells lie along the eastern margin of Nash Draw and they could represent upgradient precursors to facies C water, but the lack of wells in Nash Draw farther to the north and west makes it impossible to reach any conclusions.

The third cluster of B/C wells, H-2c and SNL-10 (ionic strength 0.22 and 0.19 molal, respectively), is separated from the other B/C waters and surrounded by waters of higher ionic strength, such as C-2737 which has an ionic strength of 1.5 molal. The presence of the B/C facies in this location is difficult to explain. In fact, the entire area around H-3b2, where the B/C, C, A/C, and A facies are all clustered together, seems to be a region of complex hydrogeology.

The final facies, facies D, is represented by the waters of WIPP-27 and WIPP-29. The most distinguishing feature of the chemistry of these wells is their K/Na weight ratio, which is 0.21 compared to the average value of 0.03 for all the other wells. Siegel et al. (1991b) attributed the unusually high potassium levels to contamination from potash refining activities at the nearby potash mining facilities.

3.2 Salt Norm Types

3.2.1 Sulfatic Weathering Solutions

The sulfatic weathering solutions are characterized by low to moderate ionic strength (0.06 to 0.78 molal) and normative assemblages heavy in sulfate phases (anhydrite - polyhalite – bloedite - epsomite). The mixed alkali/alkaline sulfate phase bloedite ($Na_2Mg(SO_4)_2 \cdot H_2O$) is indicative of continental recycling of sulfate phases, i.e., weathering and dissolution of sulfate-bearing minerals (Bodine and Jones, 1986). None of the other salt norm groups have either bloedite or epsomite in their normative assemblages, thus making these phases diagnostic minerals of this group.

Information Only

On a Piper plot (Figure 10), these waters span a wide range of sulfate/chloride ratios, with the facies B waters being high in sulfate and the B/C and C waters high in chloride. Geographically, we see two independent clusters (Figure 12) of this normative group, a northern and a southern cluster, both of which share similar normative assemblages, but are also chemically distinct and geographically separated by waters of different composition.

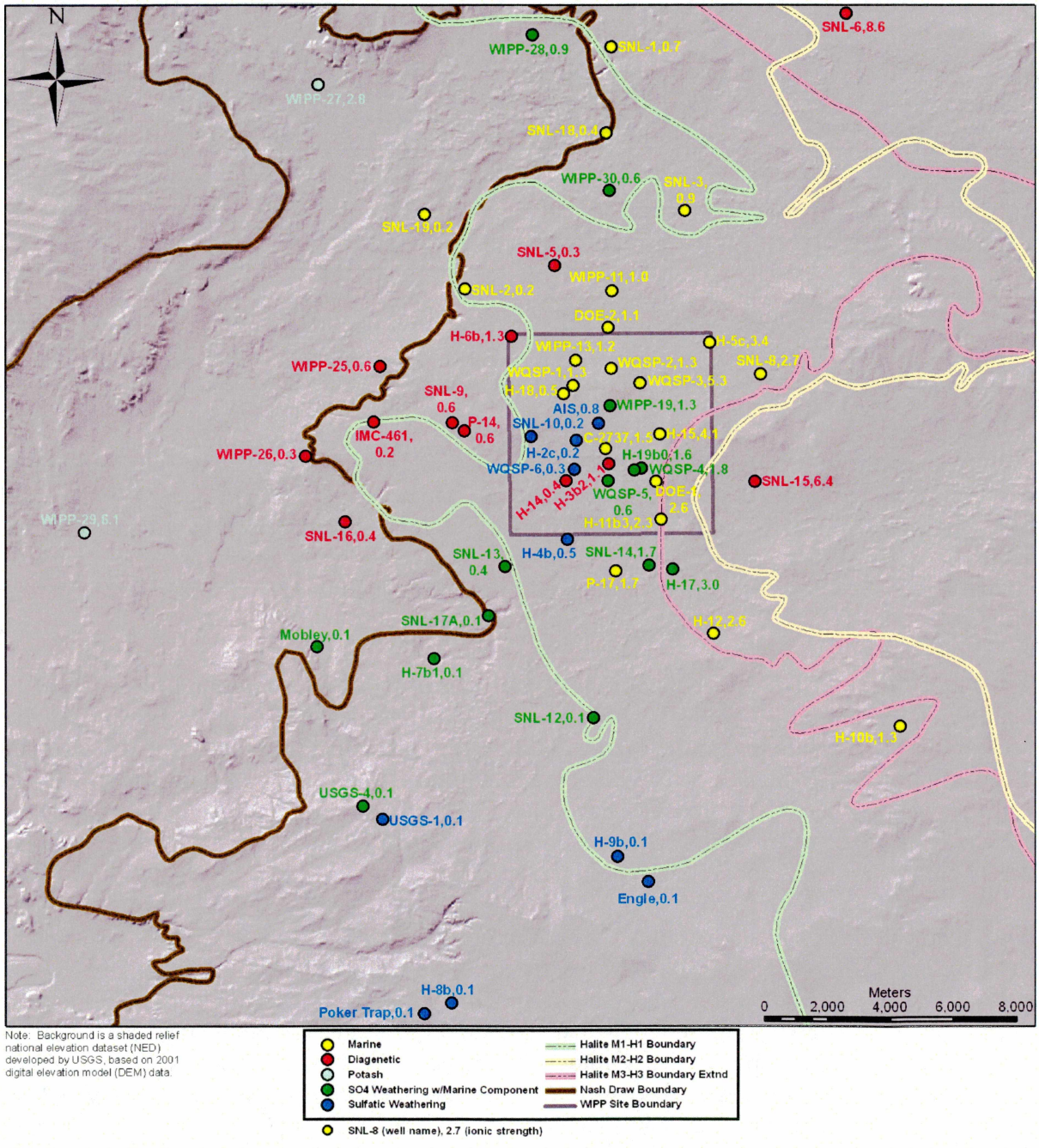

Figure 12. Culebra wells color-coded to water type based on SNORM output with corresponding ionic strength values.

Information Only

The northern cluster includes the following wells: AIS, H-2c, H-4b, SNL-10, and WQSP-6. The ionic strength of these waters varies from 0.19 molal at SNL-10 to 0.77 molal at the AIS. These wells are classified as hydrochemical facies B/C for SNL-10 and H-2c, and facies C for WQSP-6, H-4b, and AIS. The SNORM output for the northern cluster is listed in Table 6.

Table 6. Ionic strength (μ) and SNORM results for the northern cluster of sulfatic weathering solution wells.

Well	zone	μ	Halite (NaCl)	Anhydrite ($CaSO_4$)	Bloedite ($Na_2Mg(SO_4)_2 \cdot H_2O$)	Epsomite ($MgSO_4 \cdot 7H_2O$)	Glauberite ($Na_2Ca(SO_4)_2$)	Polyhalite ($K_2Ca_2Mg(SO_4)_4 \cdot 2(H_2O)$)	Magnesite ($MgCO_3$)	Thenardite (Na_2SO_4)	Aphthitalite ($K_3Na(SO_4)_2$)
SNL-10	B/C	0.19	22.2	0.0	0.4	0.0	21.3	0.0	42.5	11.1	2.5
H-2c	B/C	0.22	55.3	22.6	0.3	8.4	6.1	7.3	0.0	0.0	0.0
WQSP-6	C	0.33	57.8	1.4	0.2	8.8	11.1	0.0	20.9	0.0	0.0
H-4b	C	0.44	62.7	5.3	0.2	7.0	19.3	0.0	5.6	0.0	0.0
AIS	C	0.79	79.2	5.1	0.2	7.4	6.3	1.7	0.0	0.0	0.0
Max		0.79	79.2	22.6	0.4	8.8	21.3	7.3	42.5	11.1	2.5
Min		0.19	22.2	0.0	0.2	0.0	6.1	0.0	0.0	0.00	0.0
Average		0.39	55.4	6.9	0.3	6.3	12.8	1.8	13.8	2.2	0.5

Ionic strength in molal units, normative minerals are in anhydrous weight percent

Examination of the halite and anhydrite abundance for each well in Table 6 reveals that SNL-10 and WQSP-6 have neither excess halite nor excess anhydrite, while H-2c and H-4b both have excess normative anhydrite, and AIS is just above the thresholds for both halite and anhydrite. Thus, each water in this group shows a relatively low level of water-rock interaction and could have had a relatively short flow path, compared to other wells in the area, from infiltration to the well.

The composition of SNL-10 is unique among this group with the appearance of normative thenardite and aphthitalite, both of which are alkali sulfate phases. The occurrence of these phases in the salt norm is indicative of weathering solutions which may have dissolved sodium- and potassium-bearing silicate phases (Bodine and Jones, 1986). While this may be possible along a flowpath where the water may have interacted with the clastic sediments of the Dewey Lake, the appearance of this water composition in this location, surrounded as it is by waters of different compositions, is anomalous.

The southern cluster of wells includes the southernmost wells of facies B: Engle, H-8b, H-9b, Poker Trap, and USGS-1. The SNORM results for these wells are listed in Table 7. All of the waters in Table 7 contain excess normative anhydrite and none contain excess halite. The similarity in the chemistry combined with the relatively broad geographic occurrence of this water type makes this group somewhat unique for the Culebra. The low ionic strengths and low abundances of chloride phases in their salt norms suggests either that the waters are young and have not had the chance to react significantly with the host rock and/or mix with more saline waters, or that the waters are relatively old and there are very little chloride phases or high-salinity water, for mixing, remaining in the Culebra in this region. This second hypothesis implies that the hydrology of the Culebra in this area has been stable for a long period of time.

Information Only

Comparing the results presented in Tables 6 and 7 demonstrates the difference in the chemistry between the northern and southern wells. While both the northern and southern cluster wells shared the same normative assemblages, the percentages of the phases present vary between the two clusters, as do the ionic strength values. The northern wells have higher ionic strength and higher halite percentages, while the southern wells have lower ionic strength, higher percentages of normative sulfate phases, and low halite values. Based solely on the chemical differences, we surmise that these two clusters are hydraulically independent of one another. Furthermore, examination of Figure 12 reveals that waters of dissimilar chemistry lie between these two clusters, which supports the notion of the clusters being hydraulically isolated, or that a mixing zone lies between the two water types.

Table 7. Ionic strength (μ) and SNORM results for the southern cluster of sulfatic weathering solution wells.

Well	zone	μ	Halite (NaCl)	Anhydrite ($CaSO_4$)	Bloedite ($Na_2Mg(SO_4)_2 \cdot H_2O$)	Epsomite ($MgSO_4 \cdot 7H_2O$)	Glauberite ($Na_2Ca(SO_4)_2$)	Polyhalite ($K_2Ca_2Mg(SO_4)_4 \cdot 2(H_2O)$)	Magnesite ($MgCO_3$)
Poker Trap	B	0.06	2.2	73.2	7.7	12.4	0.0	1.1	3.4
H-8b	B	0.08	2.2	65.1	5.4	23.5	0.0	1.0	2.7
Engle	B	0.09	12.0	60.8	7.8	15.7	0.0	1.3	2.4
H-9b	B	0.09	8.9	66.6	3.2	17.7	0.0	1.6	2.0
USGS-1	B	0.10	27.1	51.3	8.2	8.6	0.0	2.9	1.9
Max		0.10	27.1	73.2	8.2	23.5	0.0	2.9	3.4
Min		0.06	2.2	51.3	3.2	8.6	0.0	1.0	1.9
Average		0.08	10.5	63.4	6.4	15.6	0.0	1.6	2.5

Ionic strength in molal units, normative minerals are in anhydrous weight percent

The average chemistry and salt norm of the northern cluster wells is anomalous with regard to the other wells in that area, most of which tend towards higher ionic strength and different normative assemblages (see Figure 12). Of the wells with sulfatic weathering signatures in the northern area, excluding the anomalous SNL-10, the lowest ionic strength occurs in well H-2c (0.22 molal), which also has the lowest percentage of normative halite, compared to the AIS which has the highest ionic strength (0.77 molal) and the greatest percentage of normative halite at 79%. The waters from these wells may have undergone geochemical processes similar to those responsible for the waters observed in the southern cluster – dissolution of sulfate phases possibly in the Tamarisk Member – and then mixed with waters of higher salinity in the Culebra. Given the closer proximity of the northern cluster wells to the M2-H2 salt margin and waters of higher ionic strength relative to the southern cluster wells, it is not surprising that the waters of the northern cluster have higher normative halite compared to the southern cluster of wells, as some mixing or dissolution of residual halite in the Culebra is highly probable. There was no previous interpretation of these waters, as they were grouped in hydrochemical facies C by Siegel et al. (1991b) and not recognized as compositionally different from other facies C waters.

3.2.2 Sulfatic Weathering Solutions with a Marine Component

The sulfatic weathering solutions with a marine component group of waters is characterized by ionic strengths that vary between 0.1 to 3.0 molal, and includes facies B, C, A/C, and A. The normative mineral assemblages are composed of halite, anhydrite, and the mixed alkali/alkaline

Information Only

chloride, carnallite ($KMgCl_3 \cdot 6H_2O$), and also includes alkaline sulfates as kieserite ($MgSO_4 \cdot H_2O$) and polyhalite ($K_2Ca_2Mg(SO_4)_4 \cdot 2H_2O$). In the norm of these waters, the diagnostic marine assemblage of halite-bischofite-kieserite-carnallite-anhydrite has been altered by the input of additional sulfate, which sacrifices bischofite ($MgCl_2 \cdot 6H_2O$) in favor of additional kieserite and polyhalite. Bodine and Jones (1986) further state that the presence of polyhalite in an otherwise marine-like norm is strong evidence for meteoric-marine water mixing. Compared to the sulfatic weathering type waters, this group lacks normative bloedite, while the diagnostic marine phase carnallite persists in these norms.

Table 8 shows the SNORM output for this group together with the ionic strengths calculated by PHREEQCI. Inspection of Table 8 reveals that two distinct groups are represented. The first group comprises the northernmost wells of hydrochemical facies B: SNL-17A, H-7b1, Mobley, and SNL-12. The low ionic strength and high calcium-sulfate content of these wells is very similar to the southern cluster of sulfatic waters, also of facies B, discussed in the previous section. However, the presence of carnallite and kierserite in the salt norms of the northern facies B wells, combined with the lack of bloedite, suggests the addition of marine-derived solutes to the sulfatic weathering solution of the other wells of facies B. This may be a reflection of mixing with the more concentrated waters to the north, and the salt norm may be able to detect more subtle variations in the solute makeup of the waters than the hydrochemical facies approach allows. This mixing hypothesis is evaluated in Section 4.3.1.

Table 8. Ionic strength (μ) and SNORM results for the sulfatic weathering solution with marine component waters.

Well	Zone	μ	Halite (NaCl)	Anhydrite ($CaSO_4$)	Carnallite ($KMgCl_3 \cdot 6H_2O$)	Bischofite ($MgCl_2 \cdot 6H_2O$)	Kieserite ($MgSO_4 \cdot H_2O$)	Magnesite ($MgCO_3$)	Polyhalite ($K_2Ca_2Mg(SO_4)_4 \cdot 2H_2O$)
H-7b1	B	0.09	13.5	65.2	1.1	2.2	14.9	3.1	0.0
SNL-17A	B	0.09	10.5	67.1	0.7	2.2	17.2	2.2	0.0
Mobley	B	0.10	20.4	59.7	0.5	0.0	15.7	2.5	1.3
SNL-12	B	0.10	29.6	54.7	1.5	0.0	12.2	1.6	0.3
USGS-4	B	0.10	36.6	48.0	1.7	3.0	10.0	0.6	0.0
SNL-13	C	0.38	71.6	17.6	3.8	0.0	5.7	0.2	1.2
WIPP-30	C	0.58	77.1	13.8	3.9	0.4	4.8	0.1	0.0
WQSP-5	C	0.60	77.6	7.6	0.7	0.0	5.0	0.1	8.9
WIPP-28	C	0.90	84.0	6.6	2.3	0.0	2.7	0.5	3.8
WIPP-19	A/C	1.37	85.1	5.7	1.3	0.0	4.9	0.0	3.0
H-19b0	A/C	1.55	85.9	6.8	3.7	2.3	1.2	0.0	0.0
SNL-14	A	1.68	86.9	5.2	2.3	0.0	4.3	0.0	1.3
WQSP-4	A	1.71	85.8	4.4	4.7	0.0	2.3	0.0	2.9
H-17	A	2.95	90.1	3.2	3.8	0.0	2.7	0.0	0.3
Max		2.95	90.1	67.1	4.7	3.0	17.2	3.1	8.9
Min		0.09	10.5	3.2	0.5	0.0	1.2	0.0	0.0
Average		0.87	61.1	26.1	2.3	0.7	7.4	0.8	1.7

Ionic strength in molal units, normative minerals are in anhydrous weight percent

The second group represented in Table 8 comprises wells from hydrochemical facies C, A/C, and A (SNL-13, WIPP-30, WQSP-5, WIPP-28, WIPP-19, H-19b0, SNL-14, WQSP-4, and H-17). This second group has much higher normative halite, lower anhydrite, and higher ionic strength.

Information Only

These differences could be due to dissolution of marine-derived non-sulfate phases, or mixing with water of high salinity. These waters appear to originate from mixing of dilute sulfatic weathering type waters with more concentrated waters with a marine normative signature.

3.2.3 Marine-type Waters

Waters with marine-type salt norms are characterized by halite-bischofite-kieserite-carnallite-anhydrite assemblages with the carnallite-bischofite pair in the norm as a single unique diagnostic feature (Bodine and Jones, 1986). The waters listed in Table 9 all share this normative assemblage, which suggests a marine solute origin. However, the halite and anhydrite values for the majority of the samples suggest that the solutes of these waters do not have a purely marine origin, but rather are mixtures of sulfate-rich meteoric-derived waters with waters that have dissolved significant marine-derived phases. Bodine and Jones (1990) state that mixing, continental cycling, and water-rock interactions, including re-solution of marine evaporite salts, can be expected to produce quantitative variations in a marine-like norm, as well as variation in the normative mineralogy.

Table 9. Ionic strength (μ) and SNORM results for the Culebra waters with marine-type normative assemblages.

Well	Zone	μ	Halite ($NaCl$)	Anhydrite ($CaSO_4$)	Carnallite ($KMgCl_3 \cdot 6H_2O$)	Bischofite ($MgCl_2 \cdot 6H_2O$)	Kieserite ($MgSO_4 \cdot H_2O$)	Magnesite ($MgCO_3$)
SNL-19	B/C	0.18	50.9	36.2	2.3	4.0	5.8	0.8
SNL-2	B/C	0.24	61.4	29.3	1.9	6.0	0.9	0.6
SNL-18	C	0.40	70.2	19.8	2.8	0.6	6.3	0.3
H-18	C	0.53	76.1	14.0	3.6	0.1	6.1	0.1
SNL-1	C	0.70	75.4	14.1	4.4	5.6	0.4	0.1
SNL-3	C	0.92	80.6	10.8	3.5	2.5	2.5	0.1
WIPP-11	C	0.99	79.5	11.3	3.3	0.4	5.3	0.1
DOE-2	A/C	1.07	81.0	10.5	3.6	3.6	1.2	0.2
WIPP-13	A/C	1.19	83.3	8.5	2.5	4.3	1.2	0.1
WQSP-2	A/C	1.24	80.8	9.0	4.9	3.0	2.2	0.0
WQSP-1	A/C	1.24	81.1	9.6	3.8	4.3	1.2	0.1
H-10b	A/C	1.28	83.2	8.5	3.5	1.7	3.0	0.0
C-2737	A/C	1.53	88.1	6.7	1.7	0.0	3.4	0.1
P-17	A	1.69	83.3	6.1	4.6	3.2	2.7	0.0
H-11b3	A	2.21	88.6	5.0	3.1	0.1	3.2	0.0
H-12	A	2.59	87.9	4.5	4.4	0.6	2.7	0.0
DOE-1	A	2.62	89.5	3.6	3.3	0.8	2.7	0.0
SNL-8	A	2.73	84.3	4.8	4.6	4.6	1.7	0.0
H-5c	A	3.00	88.3	3.9	3.8	1.4	2.6	0.0
H-15	A	4.13	90.2	2.7	3.9	2.6	0.6	0.0
WQSP-3	A	4.50	92.4	2.2	3.0	0.1	2.3	0.0
Max		4.50	92.4	36.2	4.9	6.0	6.3	0.8
Min		0.18	50.9	2.2	1.7	0.0	0.4	0.0
Average		1.67	80.8	10.5	3.5	2.4	2.8	0.1

Ionic strength in molal units, normative minerals are in anhydrous weight percent

The results in Table 9 show that these waters encompass a wide range of ionic strength from 0.2 molal to 5 molal, and that normative anhydrite is very high in the low ionic strength waters and normative halite prevails in the high ionic strength waters. The Figure 10 Piper plot shows the

Information Only

marine waters plotting in the sodium-chloride corner of the central diamond with significant overlap with the waters of the sulfatic weathering with a marine component group.

Figure 12 shows that these waters have a wide geographic distribution with little tendency to cluster near the M2-H2 halite margin. As the distance from the well to the M2-H2 margin decreases, so does the percent of normative anhydrite while the ionic strength and normative halite increase. This suggests that this water type encompasses a broad mixing zone between more sulfate-rich marine-like solutions to the west and high-salinity waters along the M2-H2 margin where dissolution of Culebra halite cements and liberation of marine connate pore fluids may be occurring.

3.2.4 Diagenetic-type Waters

The final set of wells contains waters with a diagenetic salt norm signature as defined by Bodine and Jones (1986). The alkaline (calcium and magnesium) association with chloride in tachyhydrite ($Mg_2CaCl_6 \cdot 12H_2O$) and antarcticite ($CaCl_2 \cdot 6H_2O$) of this norm (Table 10) suggests dolomitization as the reaction (Bodine and Jones, 1986). Tachyhydrite, carnallite, and, in some cases, antarcticite are the diagnostic phases for this group of Culebra waters. Dolomite is also unique to these norms.

Table 10. Ionic strength (μ) and SNORM results for the Culebra waters with diagenetic-type normative assemblages.

Well	Zone	μ	Halite (NaCl)	Anhydrite ($CaSO_4$)	Tachyhydrite ($Mg_2CaCl_6 \cdot 12H_2O$)	Antarcticite ($CaCl_2 \cdot 6H_2O$)	Carnallite ($KMgCl_3 \cdot 6H_2O$)	Dolomite ($CaMg(CO_3)_2$)	Bischofite ($MgCl_2 \cdot 6H_2O$)
IMC-461	B/C	0.21	51.2	34.2	7.2	0.0	1.5	0.8	5.2
WIPP-26	B/C	0.28	54.2	27.8	10.3	0.4	6.7	0.7	0.0
SNL-5	B/C	0.29	43.1	18.0	25.6	10.2	2.6	0.4	0.0
SNL-16	C	0.38	62.3	20.2	8.3	1.8	7.0	0.4	0.0
H-14	C	0.39	56.6	12.9	13.8	10.6	6.1	0.1	0.0
SNL-9	C	0.56	49.4	9.3	19.7	20.4	0.8	0.4	0.0
P-14	C	0.58	46.7	8.9	20.8	22.5	0.8	0.3	0.0
WIPP-25	C	0.58	67.7	13.9	4.2	3.6	10.4	0.3	0.0
H-3b2	A/C	1.09	80.3	11.7	3.2	0.0	3.9	0.1	0.8
H-6b	A/C	1.25	79.8	7.8	7.7	1.4	3.2	0.1	0.0
SNL-15	E	6.43	75.6	0.8	10.1	0.0	9.8	0.1	3.6
SNL-6	E	8.61	68.9	0.7	9.9	0.0	5.8	0.0	14.6
Max		8.61	80.3	34.2	25.6	22.5	10.4	0.8	14.6
Min		0.21	43.1	0.7	3.2	0.0	0.8	0.0	0.0
Average		1.72	61.3	13.9	11.7	5.9	4.9	0.3	2.0

Ionic strength in molal units, normative minerals are in anhydrous weight percent

Examination of the data in Table 10 reveals that all but four of the wells (H-3b2, IMC-461, SNL-6, and SNL-15) contain both tachyhydrite and antarcticite, with the four exceptions containing only tachyhydrite. Wells SNL-6 and SNL-15 are unique among all of the Culebra wells in that they contain water characteristic of a truly primitive syndepositional nature that will be discussed separately from the other diagenetic waters.

Information Only

Only two Culebra wells, SNL-6 and SNL-15, are located east of the M2-H2 margin where halite is present below the Culebra. The core from these wells was unique for the Culebra, as discussed in the previous section, due to the presence of halite cement and fracture fillings. As result of the halite cement, the Culebra has very low transmissivity (T) at these wells: log T (m^2/s) = -13 at SNL-15 (Roberts, 2007), and SNL-6 has a log T = -11 (Bowman and Roberts, 2008). Both of these wells were drilled using compressed air as the circulation medium, thereby eliminating any potential drilling fluid contamination of the formation water. Therefore, based on the hydrology and chemistry of these samples, they are believed to represent primitive brine that has been present in the Culebra since its deposition, or as hypothesized by Powers et al. (2006), since the deposition of the halite cements which may have accompanied deposition of the overlying M3-H3 strata.

Examination of the data for SNL-6 and SNL-15 (Table 10) shows that they are both highly concentrated primitive brines with virtually no normative anhydrite, and with normative halite values (<78%) that do not indicate re-solution of halite. The normative assemblages for both of these wells are very similar to those listed in Bodine and Jones (1986) from the sabkhas of the Bardawil Lagoon, Egypt, in the northern Sinai desert along the Mediterranean coast. The salt norms of the fluids from the innermost isolated lagoons, or salt pans, are very similar to those of SNL-6 and SNL-15 (Bodine and Jones, 1986). The fluids from these salt pans are reported by Levy (1977) to have undergone extensive evaporative concentration, depositing gypsum and halite during the summer months. Levy (1977) reports the presence of soft, chalky, unlithified dolomite in these areas as well. During the rainy winter months, Levy (1977) reports that the water table rises in the inland sabkhas, and gypsum and halite redissolve. The depositional environment for the current-day dolomite in the Bardawil lagoon is similar to the salt pan environment described by Powers et al. (2006) for the deposition of the Culebra with periodic freshening of the basin's waters by flood events.

Based solely on the available chemistry data, the model of Powers et al. (2006) for Culebra halite deposition as a contemporaneous event with M3-H3 deposition can be neither proved nor disproved. For the Powers et al. (2006) model to function, the water flooding the basin would have had to dissolve previously deposited vug-filling gypsum in the Culebra, and then gone through an evaporative sequence of gypsum to halite deposition. However, the re-deposited gypsum could not be allowed to form in the same vugs from where it was originally deposited, that space being reserved for halite.

The normative assemblages for SNL-6 and SNL-15 have halite and anhydrite at levels that are consistent with the deposition of these phases as observed in their cores. Powers et al. (2006) based their model on the premise that halite occurring in fractures would have to post-date Culebra deposition – a premise the chemistry cannot address.

Notice in Figure 10 that the diagenetic waters form a separate cluster in the central diamond on the left side of a vertical line that would divide the diamond in half. Waters that lie along the vertical line connecting the apices of the central diamond are primarily derived from the dissolution of halite, while those to the left contain alkalines coordinated with chloride, and those to the right contain alkaline metals coordinated with sulfate.

Information Only

Excluding SNL-6 and SNL-15, the remainder of the wells in the diagenetic group – the "dilute diagenetic" waters - tend toward lower normative halite and higher normative anhydrite. Combined with the presence of normative dolomite, this suggests dolomite and sulfate-phase dissolution, or possibly dissolution of an accessory phase such as the clay mineral corrensite, as a possible geochemical process in their evolution. In addition, the ionic strengths of these waters are much lower, 0.2 to 1.3 molal, compared to the concentrated brines, 6.4 to 8.6 molal, of SNL-15 and SNL-6.

Bodine et al. (1991) identified waters from two wells in this group, P-14 and P-18, as being of diagenetic origin. Drilling and sampling of new well SNL-15 on the old P-18 drillpad has shown that the original P-18 sample was contaminated by drilling fluid and not representative of the Culebra, leaving only the P-14 sample as having a diagenetic origin. Based on its normative assemblage, Bodine et al. (1991) classified the P-14 sample as a "primitive-diagenetic Culebra fluid", and yet were not able to reconcile this with its meteoric stable isotope composition, dilute concentration, and presence in a high-T region (log T (m^2/s) at P-14 = -3.5), and as such labeled it as "anomalous". Since publication of Bodine et al. (1991), nine new Culebra wells in the same general vicinity of P-14 show similar normative assemblages. Well SNL-9, which is closest to P-14, has a nearly identical assemblage which adds confidence to the P-14 analysis. Figure 12 shows that these waters are distributed in close proximity to the margin of Nash Draw.

Figure 13 is a plot of the molal values of sodium versus chloride as coded by the SNORM type. It shows that for the most part, the Culebra waters fall on the 1:1 slope line characteristic of halite dissolution. Waters in the 0.1 to 1.0 molal chloride range with a diagenetic salt norm tend to have excess chloride, or depleted sodium, and fall to the right of the 1:1 molar line. The apparent excess chloride is reflected in the salt norm by the presence of the diagnostic diagenetic phases tachyhydrite and antarcticite. A possible source of the characteristic excess chloride and magnesium in these waters could be dissolution of an accessory phase such as carnallite ($KMgCl_3$ $6H_2O$), though this phase has not been documented as present in the Rustler Formation, or from the dissolution of corrensite.

Based on observational evidence, these dilute diagenetic-type waters are not the product of primitive diagenetic fluids, like those found in SNL-6 and SNL-15, released from isolated "islands" of low-T halite-cemented Culebra in the vicinity of the wells. We do not observe fluids with a diagenetic signature in the vicinity, i.e. west of the M2-H2 boundary, where water of a composition similar to that found in SNL-6 and SNL-15 is likely mixing with the more dilute waters west of the boundary. The probable reason that we do not observe diagenetic compositions in this region is that the diagenetic signature is obliterated because the relative volume of these primitive waters is small compared to the waters west of the M2-H2 boundary with which they are mixing. Thus, the waters west of the M2-H2 boundary reflect a marine or marine sulfate signature from halite and sulfate phase dissolution, and not a diagenetic signature. The dilute diagenetic waters most likely result from dissolution of a unique combination of dolomite and phases present in trace amounts, such as corrensite, or possibly through ion exchange (Siegel and Anderholm, 1994).

Information Only

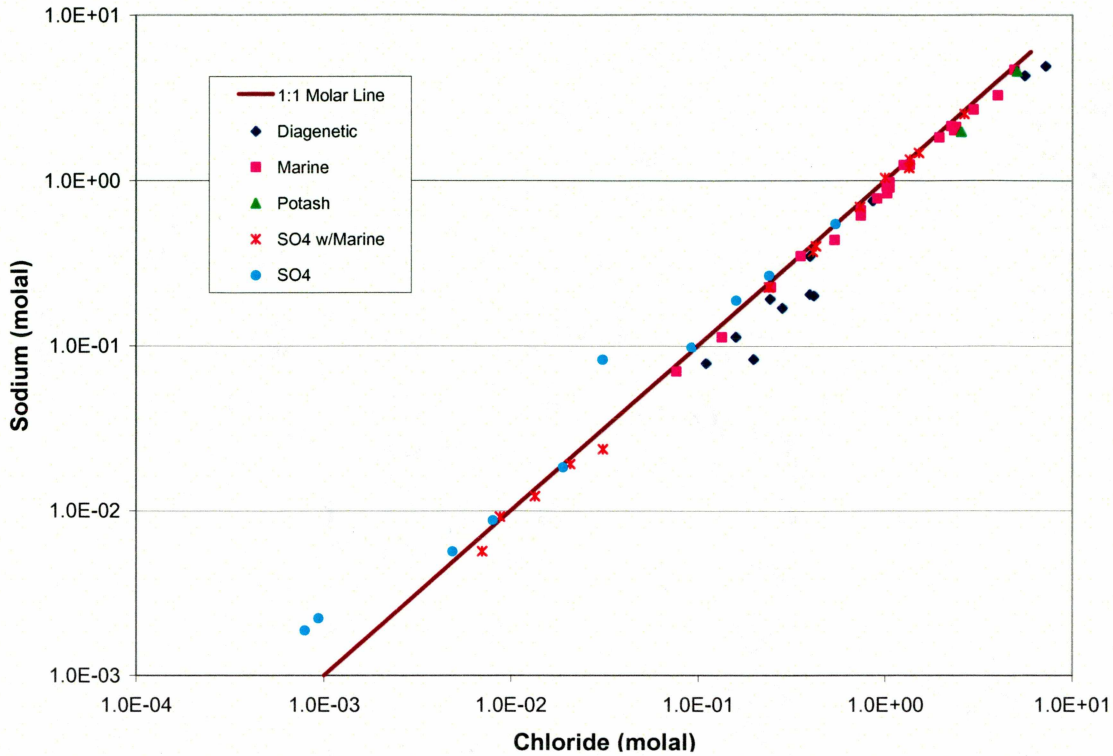

Figure 13. Sodium versus chloride for the Culebra waters coded by SNORM type.

3.3 Excess Normative Halite and Anhydrite

Figure 14 shows the locations of the Culebra wells color-coded by normative excess. This method of sorting the wells provides a broad view of the solute distribution within the Culebra, and provides some clues about the hydrogeology.

A group of wells located along the M2-H2 and M3-H3 margins, some having exclusively excess halite (H-5c, WQSP-3, H-15, DOE-1, and H-17), and some with both excess halite and anhydrite (SNL-8, WQSP-4, H-19b0, H-11b3, SNL-14, P-17, H-12, and H-10b), will be discussed together.

The wells with excess halite are located in close proximity to the M2-H2 and M3-H3 margins and may reflect the addition of dissolved halite from dissolution along the halite margins and addition of primitive brines similar in composition to those of SNL-6 and SNL-15. After SNL-6 and SNL-15, these wells have the highest ionic strength values of all the Culebra wells, 2.6 to 5.3 molal.

The wells containing both excess halite and anhydrite are also in close proximity to the M2-H2 and M3-H3 margins. Assuming the possibility of vertical flow to the Culebra, the excess anhydrite could originate from dissolution of the A2 anhydrite in the overlying Tamarisk Member of the Rustler Formation. This group of wells contains waters with the next highest ionic strength compared to the excess halite wells and, considered together, these two groups form a group of continuously increasing ionic strength. Table 11 provides the ionic strength and normative halite and anhydrite values for these wells.

Information Only

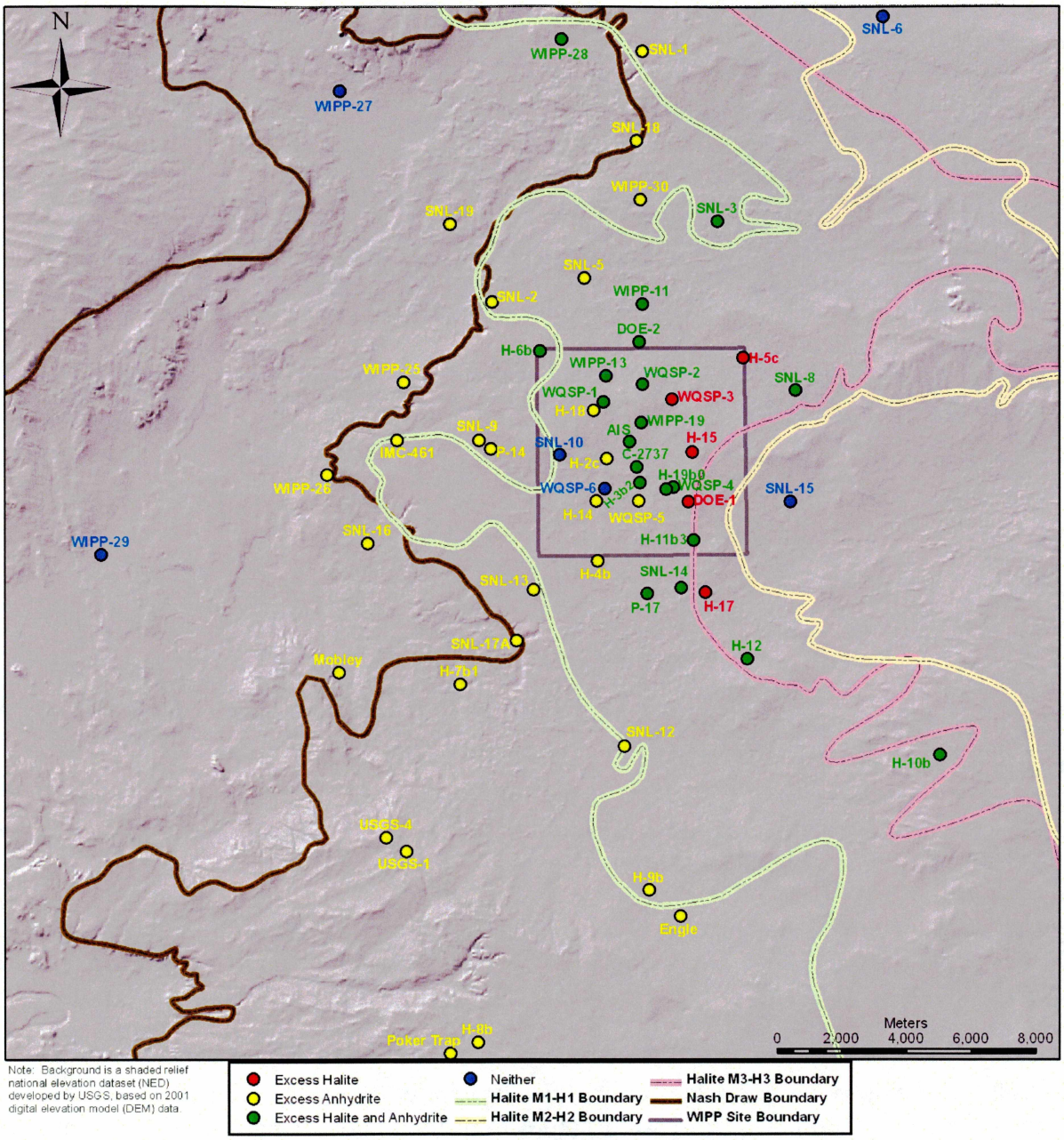

Figure 14. Culebra wells color-coded based on the abundance of normative halite and anhydrite.

The differences in the compositions between these two groups are subtle for the wells in the middle of Table 11, and well defined for the wells near the top and bottom of Table 11. The data in Table 11 show that as anhydrite values decrease, the ionic strength and halite values increase. A simple explanation for this trend would be halite dissolution; in other words, the addition of halite to a water composition such as that from H-10b would result in a composition that would have a higher ionic strength and be higher in normative halite and lower in normative anhydrite. To test this hypothesis, the H-10b composition was input into PHREEQCI (file name: *H-10b_halite.pqi*) and three moles of halite were equilibrated with the solution to bring its ionic strength into the range of H-15 and WQSP-3. The PHREEQCI results were then run through

Information Only

SNORM (file name: *H-10b*) to obtain the normative assemblage. The results are tabulated in Table 12.

Table 11. Excess normative halite and anhydrite for the wells along the M2-H2 margin.

Well	Excess	μ (molal)	Normative Percent	
			Halite	Anhydrite
H-10b	both	1.3	83.2	8.5
H-19b0	both	1.6	85.9	6.8
P-17	both	1.7	83.2	6.1
SNL-14	both	1.7	86.9	5.2
WQSP-4	both	1.8	85.8	4.4
H-11b3	both	2.3	88.6	5.0
H-12	both	2.6	87.9	4.5
SNL-8	both	2.7	84.3	4.8
DOE-1	halite	2.6	89.5	3.6
H-17	halite	3.0	90.0	2.7
H-5c	halite	3.4	88.3	3.9
H-15	halite	4.1	90.2	2.7
WQSP-3	halite	5.3	92.4	2.2

Table 12. Comparison of H-10b water to H-10b water with three moles of halite added.

Well	Excess	μ (molal)	Normative Percent	
			Halite	Anhydrite
H-10b	both	1.3	83.2	8.5
H-10b w/3 moles halite	halite	4.3	95.5	2.3

The exercise showed that the addition of halite did change the normative excess from both excess halite and anhydrite to purely excess halite. However, in comparing the theoretical H-10b composition to those of H-15 and WQSP-3, it appears that the magnitude of the normative halite in the theoretical water is greater for its ionic strength compared to H-15 and WQSP-3. This may suggest that in addition to dissolution of halite, mixing is also occurring between concentrated halite-rich waters and more dilute calcium-sulfate waters.

The occurrence of more dilute waters with both excess halite and anhydrite in such close proximity to the halite margins, and to wells with higher concentration and only excess normative halite, suggests localized regions where water may be entering the Culebra from the overlying strata. If this is the situation, then the water entering the Culebra from above may have traveled laterally through the Tamarisk M3 mudstone and then vertically through the Tamarisk A2 anhydrite to reach the Culebra. This scenario is consistent with the location of the Tamarisk H3 halite margin where the decrease in transmissivity in transitioning from the M3 mudstone to the H3 halite could focus flow through a fractured area in the A2 anhydrite and into the Culebra. This is a highly speculative hypothesis and one that would be very difficult to test in the field.

Holt and Powers (1988) and Beauheim and Holt (1990) suggested that Rustler halite was most likely to dissolve along the depositional margins, where it could be attacked by water flowing

Information Only

(slowly) through the halite-poor mudstone. Collapse and brecciation of the A3 anhydrite at WIPP-19 and H-11 is attributed to dissolution of H3 along its margin (Holt and Powers, 1988). Powers and Holt (2000) describe erosional channels through M3 and A3 filled with intraclast conglomerates and siltstones that could provide localized sources of Tamarisk waters to the Culebra.

The remainder of the wells with waters containing both excess anhydrite and halite are numerous and widespread, and generally are located between the wells with excess halite and those with excess anhydrite, with a greater number lying to the north of the site compared to the south. The presence of the combined excess halite-anhydrite is evidence of widespread mixing between the concentrated brines to the east with the more dilute $CaSO_4$ waters to the west.

The prevalence of waters with excess normative anhydrite along the western margin of the study area is suggestive of a greater vertical flow component in that area, and the absence of significant halite in the Culebra and overlying units. There are 26 wells in this group with ionic strengths that range from 0.08 molal at Poker Trap in the far southwest to 0.7 molal at SNL-1 located at the northern extreme of the study area. Based solely on their percentage of normative anhydrite, the waters in this group may be considered as the starting composition for the more evolved Culebra waters.

The *neither* designation can represent two types of waters that lie on opposite ends of a continuum of possible water compositions. The first type includes waters (SNL-10 and WQSP-6) which appear to have had a minimal amount of water-rock interaction such that neither halite nor anhydrite exceeds the threshold values. On the opposite end of the spectrum are waters (SNL-6 and SNL-15) which have undergone an extreme level of water-rock interaction to the point where halite and anhydrite have been removed from solution via precipitation.

Five Culebra wells were identified with norms containing neither excess halite nor anhydrite: SNL-6, SNL-15, SNL-10, WQSP-6, and WIPP-27. SNL-10 and WQSP-6 represent the first water type discussed above, in which the water-rock interaction has been minimal. They are anomalous in their occurrence; neither contain excess halite or anhydrite, and both have low ionic strengths, yet they are surrounded by waters of higher concentration whose norms contain excess halite and anhydrite How these waters came to be in this location is unknown and, without installation of additional wells and collection of additional data, the mystery of their occurrence is not likely to be resolved.

SNL-6 and SNL-15 represent the second type of water discussed above with neither excess halite nor anhydrite. They are representative of primary synsedimentary brines whose chemistries reflect gypsum and halite deposition and, as such, their norms should be depleted in both of these phases. The locations of SNL-6 and SNL-15, to the east of the M2-H2 margin, are in accordance with the current understanding of the geology and hydrology of that area.

The water of WIPP-27 is the product of potash-refining activities, rendering its composition meaningless for the purpose of this report.

Information Only

4. Chemical Evolution of the Culebra Groundwater

In this section, trends in the chemistry of the Culebra waters will be examined by plotting the data in various formats and discussing the possible chemical processes that may be responsible for the observed chemistry. The data were plotted depending on which classification scheme, hydrochemical facies or SNORM type, provided the most information for the parameters plotted.

4.1 Ionic Strength Effect and Partial Equilibrium

In this section, the role of increasing ionic strength will be investigated as a driving force in the evolution of the Culebra water chemistry. Figure 15 clearly illustrates that sodium and chloride concentrations are controlling the ionic strength of the Culebra waters. Based on this observation, we conclude that halite dissolution is a driving force in the evolution of the chemistry of the Culebra waters. Note that above an ionic strength of about 6 molal, magnesium and, to a lesser degree, calcium become bigger contributors to ionic strength.

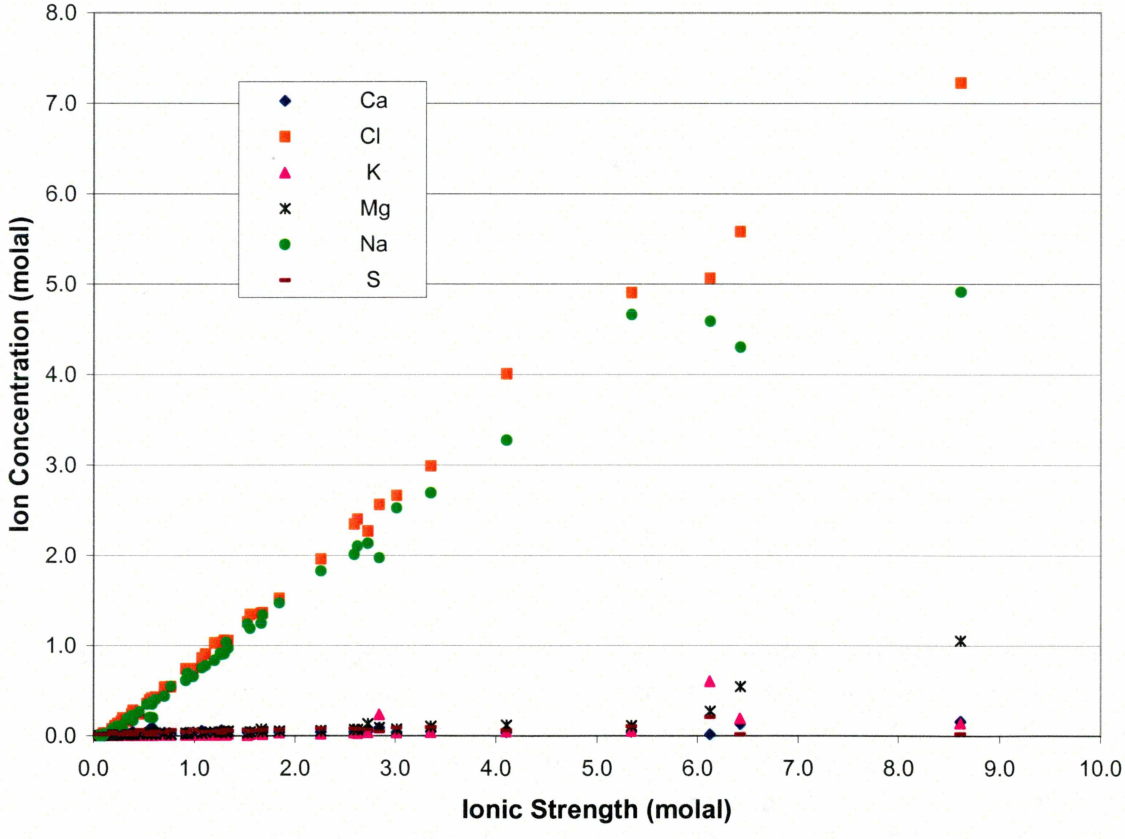

Figure 15. Culebra waters' ion concentrations versus ionic strength.

Figure 16 displays the saturation index of halite versus the ionic strength as calculated in PHREEQCI. The linear portion of the graph illustrates that for all of the waters, with the exception of the Facies B waters, halite dissolution controls the ionic strength, and is a dominant process in the evolution of the Culebra waters. With the exception of the wells in the neighborhood of the M2-H2 margin, there is no current or nearby source of halite; the H1 halite

Information Only

of the Los Medaños underlies the Culebra wells (see Figure 14 for the margin locations) with the exception of the facies B wells, but is an improbable source because of the intervening A1 anhydrite unit. Therefore, at some time in the past, halite may have existed in the Culebra that has since been dissolved away, and which is reflected in the current chemistry of the Culebra wells. Alternatively, or in conjunction with widespread halite dissolution, more localized dissolution along the M2-H2 margin combined with mixing due to groundwater flow and chemical diffusion could result in the trend observed in Figure 16.

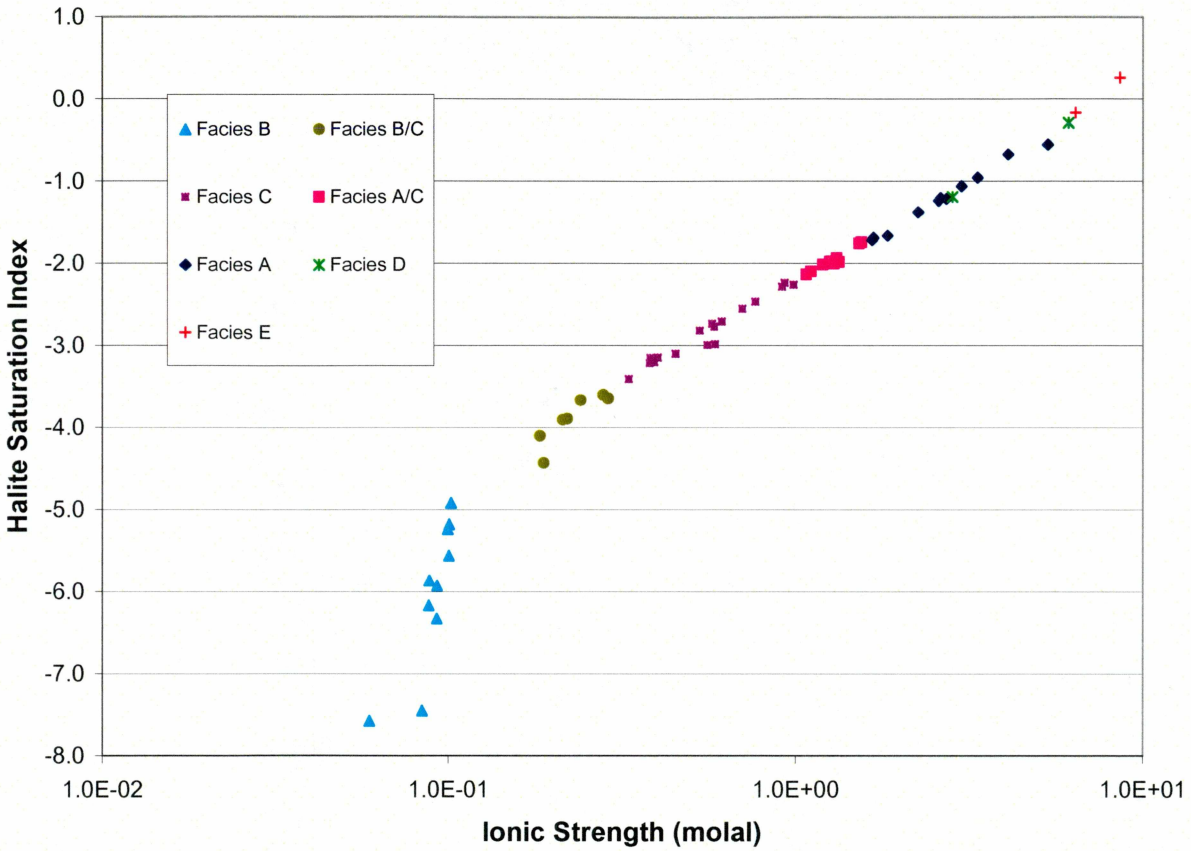

Figure 16. Halite saturation index versus ionic strength color coded by hydrochemical facies.

The importance of halite dissolution on the evolution of the chemistry of the Culebra waters is that its solubility relative to other common minerals present in the Culebra is very high. Thus, halite can dissolve to very high concentrations without approaching its solubility limit, and in doing so raises the ionic strength of the water which increases the solubility of the other non-halite phases. This creates a partial equilibrium condition where a phase may be at saturation (saturation index = 0) but the molar concentration of its constituent ions continues to increase as the ionic strength of the solution increases, which is known as the *ionic strength effect*.

This *ionic strength effect* can best be illustrated by consideration of the definition of the solubility product:

$$CA \Leftrightarrow C^{+} + A^{-}$$
$$K_{sp} = a_{C+}\, a_{A-}$$

Information Only

Where:

CA = ionic solid

C^+ and A^- are the cation and anion

a_{C+} and a_{A-} are the activities of the cation and anion

K_{sp} is the solubility product, or equilibrium constant at a specific temperature and pressure

where:

$$a_{C+} = \gamma_{C+} m_{C+}$$
$$a_{A-} = \gamma_{A-} m_{A-}$$

where:

γ_{C+} and γ_{A-} are the cation and anion activity coefficients

m_{C+} and m_{A-} are the cation and anion molalities

The activity coefficients (γ values) decrease as the ionic strength increases, thus allowing more of the ionic solid (mineral phase) to dissolve.

The activity coefficients for the Culebra waters were calculated in PHREEQCI and are plotted in Figure 17 as a function of ionic strength. Figure 17 shows that trends of the activity coefficients versus ionic strength are complex and different for cations and anions as well as different for monovalent versus divalent ions. Based on these trends, it is difficult to determine by visual inspection alone how the solubility of complex ionic solids would change as ionic strength increases. To aid in this determination, the data were manipulated such that the activity coefficient product, or gamma product, was calculated for several phases of interest. The gamma product is simply the product of the phases' activity coefficients:

$$K_{sp} = \gamma_{C+} m_{C+} \gamma_{A-} m_{A-}$$
$$\textit{Gamma product} = K_{sp} / m_{C+} m_{A-} = \gamma_{C+} \gamma_{A-}$$

If the gamma product decreases as a function of ionic strength, then the partial equilibrium saturation concentration of the phase specific ions will also increase. If the gamma product is constant, then the ionic strength effect is no longer influencing the molar concentrations of the phase specific ions. The gamma products were calculated in Excel for the phases of interest using the activity coefficients calculated in PHREEQCI.

The gamma product for the key minerals of interest (Figure 18) decreases up to an ionic strength of approximately 2.5 to 3 molal. In other words, for 48 to 52 of the 59 Culebra waters, the ionic strength effect and partial equilibrium conditions dominate the evolution of the water chemistry. At ionic strength values greater than 3 molal, the gamma product for the phases plotted on Figure 18 increases, indicating that the ionic strength effect is acting to decrease solubility.

Information Only

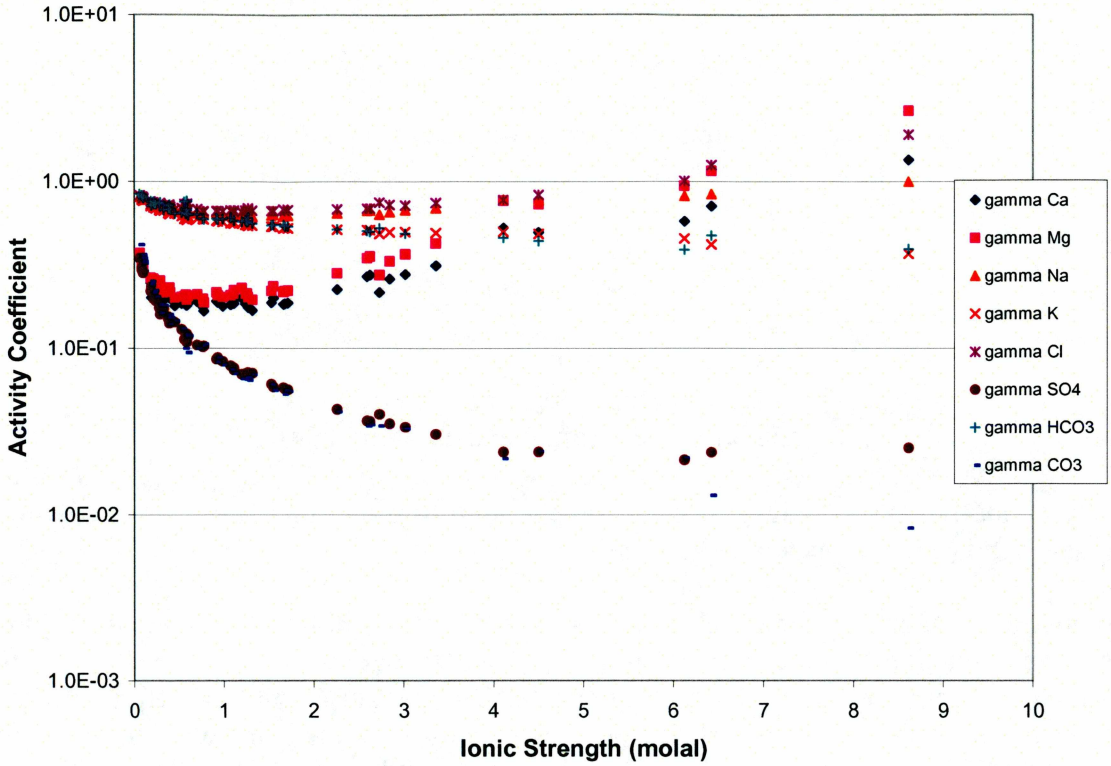

Figure 17. Ion activity coefficients for the Culebra waters versus ionic strength.

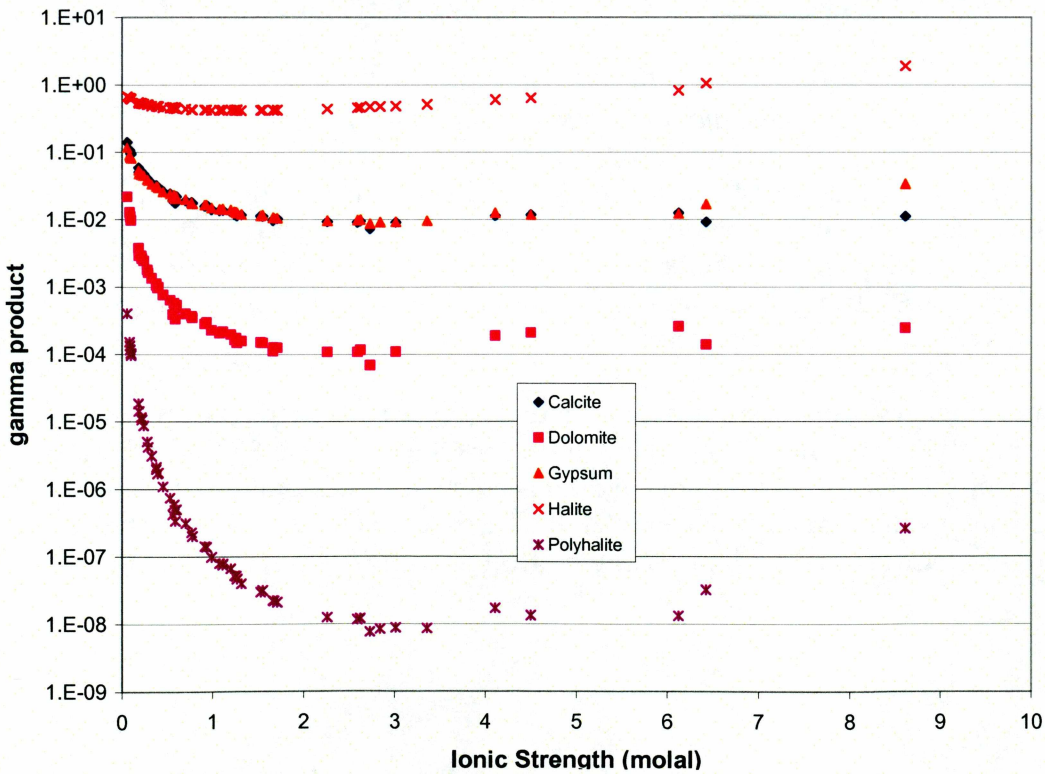

Figure 18. Gamma product values for phases of interest for the Culebra waters.

Information Only

4.2 Mineral Phases Contributing to the Evolution of Culebra Waters

As water flows through the subsurface, it encounters various mineral phases, some more soluble than others, and by examining the saturation state of phases known or suspected to be present in an aquifer, we may gain an understanding of the role of these phases in the chemical evolution of the waters.

The mineral saturation index values for the Culebra waters as calculated using PHREEQCI for calcite, dolomite, CO_2 gas, gypsum, polyhalite, carnallite, and halite are listed in Table 13.

Table 13. Ionic strength (μ) and mineral saturation index values for the Culebra waters.

Well	μ (molal)	Saturation Index							
		Calcite[1]	Dolomite[2]	CO_2 (g)	Gypsum[3]	Polyhalite[4]	Carnallite[5]	Halite[6]	Sylvite[7]
AIS	0.79	0.61	1.46	-3.19	0.00	-6.63	-10.22	-2.44	-3.53
C-2737	1.53	-0.33	-0.41	-2.29	0.01	-7.04	-9.17	-1.76	-3.33
DOE-1	2.62	-0.89	-1.11	-2.05	-0.07	-5.96	-7.37	-1.20	-2.54
DOE-2	1.07	-0.48	-0.68	-1.55	0.01	-6.67	-9.44	-2.14	-3.33
Engle	0.09	0.25	0.44	-2.44	-0.02	-10.52	-17.87	-6.04	-7.15
H-10b	1.28	0.66	1.66	-4.07	0.04	-6.39	-9.08	-1.97	-3.19
H-11b3	2.21	-0.11	0.25	-2.80	0.03	-5.99	-7.95	-1.40	-2.75
H-12	2.59	-0.31	-0.02	-2.54	0.06	-5.38	-7.30	-1.24	-2.45
H-14	0.39	0.13	0.29	-3.25	-0.09	-7.91	-11.13	-3.22	-4.00
H-15	4.13	-0.55	-0.23	-2.21	-0.04	-5.30	-5.89	-0.67	-2.02
H-17	2.95	-0.72	-0.78	-2.24	-0.06	-5.64	-7.09	-1.07	-2.35
H-18	0.53	-0.34	-0.52	-2.63	-0.01	-7.31	-11.05	-2.82	-3.97
H-19b0	1.55	0.00	0.39	-2.99	-0.08	-6.61	-8.58	-1.74	-2.97
H-2c	0.22	0.07	0.17	-3.08	0.03	-7.72	-13.17	-3.90	-4.77
H-3b2	1.09	-0.12	-0.18	-2.56	0.13	-6.48	-9.46	-2.12	-3.28
H-4b	0.44	-0.17	0.01	-3.02	0.01	-6.92	-11.66	-3.12	-4.18
H-5c	3.00	0.83	2.37	-3.29	0.05	-5.32	-6.95	-1.08	-2.37
H-6b	1.25	-0.03	0.14	-2.28	0.01	-6.91	-9.08	-1.98	-3.22
H-7b1	0.09	0.33	0.57	-2.34	-0.05	-10.41	-17.31	-5.98	-6.86
H-8b	0.08	0.67	1.36	-3.01	-0.06	-10.95	-20.44	-7.44	-8.15
H-9b	0.09	-0.02	-0.16	-2.26	0.04	-10.25	-18.17	-6.33	-7.20
IMC-461	0.21	-0.26	-0.61	-1.90	0.04	-9.10	-13.44	-3.91	-5.26
Mobley	0.10	0.08	0.04	-2.03	0.02	-9.94	-16.82	-5.61	-6.62
P-14	0.58	0.04	0.02	-1.77	0.04	-9.23	-11.21	-3.00	-4.56
P-17	1.69	-1.15	-1.69	-1.69	-0.07	-6.03	-8.23	-1.70	-2.83
Poker Trap	0.06	-0.16	-0.50	-2.15	-0.16	-11.60	-21.17	-7.64	-8.33
SNL-1	0.70	0.00	0.25	-2.52	0.00	-6.96	-10.16	-2.55	-3.62
SNL-2	0.24	0.34	0.59	-2.69	-0.01	-8.88	-13.06	-3.67	-4.99
SNL-3	0.92	0.09	0.43	-2.81	0.02	-6.82	-9.77	-2.28	-3.48
SNL-5	0.29	0.33	0.73	-2.77	-0.05	-8.77	-12.06	-3.65	-4.68
SNL-6	8.61	0.61	2.61	-1.15	0.32	-3.08	-2.74	0.26	-1.04
SNL-8	2.73	-0.01	0.77	-2.80	0.00	-5.32	-7.02	-1.21	-2.38
SNL-9	0.56	0.36	0.66	-1.85	0.02	-9.34	-11.31	-3.00	-4.61
SNL-10	0.19	0.10	0.27	-3.40	0.01	-7.89	-14.95	-4.43	-5.42
SNL-12	0.10	0.67	1.16	-3.04	-0.03	-9.85	-16.02	-5.18	-6.21

Information Only

Well	μ (molal)	Saturation Index							
		Calcite[1]	Dolomite[2]	CO_2 (g)	Gypsum[3]	Polyhalite[4]	Carnallite[5]	Halite[6]	Sylvite[7]
SNL-13	0.38	0.88	1.81	-4.05	0.00	-7.49	-11.69	-3.15	-4.17
SNL-14	1.68	-0.05	0.33	-2.96	0.01	-6.22	-8.63	-1.69	-3.01
SNL-15	6.43	0.85	2.80	-1.55	-0.04	-4.39	-3.77	-0.17	-1.15
SNL-16	0.38	0.16	0.33	-2.34	0.03	-7.22	-11.35	-3.22	-3.98
SNL-17A	0.09	0.37	0.66	-2.65	-0.01	-10.61	-17.74	-6.17	-7.12
SNL-18	0.40	0.22	0.49	-2.79	0.07	-7.64	-11.83	-3.15	-4.36
SNL-19	0.18	0.55	1.03	-2.91	0.01	-8.78	-13.78	-4.10	-5.25
USGS-1	0.10	0.15	0.14	-2.39	-0.03	-9.84	-16.36	-5.29	-6.33
USGS-4	0.10	-0.88	-1.89	-2.33	-0.10	-10.04	-15.50	-4.92	-6.04
WIPP-11	0.99	-0.17	-0.09	-2.33	0.16	-6.31	-9.76	-2.26	-3.48
WIPP-13	1.19	-0.27	-0.15	-1.86	-0.06	-7.09	-9.24	-2.01	-3.37
WIPP-19	1.37	0.08	0.52	-3.18	0.06	-6.25	-9.14	-1.90	-3.20
WIPP-25	0.58	0.55	1.19	-2.71	0.00	-6.55	-10.24	-2.77	-3.40
WIPP-26	0.28	-0.11	-0.27	-1.94	0.07	-7.42	-12.14	-3.62	-4.33
WIPP-27	2.59	-0.30	-0.23	-1.34	0.02	-4.44	-6.45	-1.28	-1.65
WIPP-28	0.90	-0.14	-0.06	-1.12	-0.08	-6.89	-9.83	-2.26	-3.36
WIPP-29	5.93	-0.55	0.60	-1.27	0.00	-1.72	-4.02	-0.33	-0.79
WIPP-30	0.58	0.99	2.11	-4.61	0.01	-7.18	-10.79	-2.72	-3.84
WQSP-1	1.24	-0.52	-0.67	-2.28	0.03	-6.40	-9.01	-2.00	-3.18
WQSP-2	1.24	-0.43	-0.46	-2.96	0.02	-6.14	-8.91	-2.01	-3.07
WQSP-3	4.50	-0.81	-0.82	-2.10	0.06	-5.02	-6.01	-0.55	-2.04
WQSP-4	1.71	-0.32	-0.21	-2.83	-0.03	-5.75	-8.23	-1.66	-2.65
WQSP-5	0.60	0.09	0.34	-3.25	0.02	-6.61	-10.62	-2.71	-3.64
WQSP-6	0.33	-0.02	0.00	-3.21	0.04	-7.19	-12.42	-3.41	-4.36

1 – Calcite: ($CaCO_3$)
2 – Dolomite: ($CaMg(CO_3)_2$)
3 – Gypsum: ($CaSO_4 \cdot 2H_2O$)
4 – Polyhalite: ($K_2Ca_2Mg(SO_4)_4 \cdot 2H_2O$)
5 – Carnallite: ($KMgCl_3 \cdot 6H_2O$)
6 – Halite: (NaCl)
7 – Sylvite: (KCl)

Inspection of Table 13 shows that only calcite, dolomite, and gypsum saturation index values regularly exceed zero. Halite was at saturation in SNL-6 (SI = 0.26), where it was observed to form during sampling. Neither polyhalite, carnallite, nor sylvite are at saturation for any of the locations and their saturation index values span very wide ranges: ten orders of magnitude for polyhalite, eighteen orders of magnitude for carnallite, and nine orders of magnitude for sylvite.

The dolomite saturation index for USGS-4 was lower than for any of the other waters. The likely cause is the high %CBE (-7%, Table 2) which suggests that the reported magnesium, calcium, sulfate, and/or carbonate (alkalinity) concentrations may be subject to analytical error. As described in Section 1.4, the USGS-4 composition was charge-balanced on all of the ions so as not to change the salt norm. However, the calculated saturation indices of calcite and dolomite may be too low.

Information Only

The following sets of figures (Figures 19 through 28) plot the saturation index of a specific phase versus ionic strength, with the second plot in each set plotting the constituent ions of the phase versus the phase's saturation index.

Figure 19 shows gypsum saturation versus ionic strength. The saturation index varies between -0.16 to 0.32, with the majority of the values in the -0.1 to 0.1 range. All of the Culebra waters are very close to gypsum saturation and for all practical purposes, within the range of thermodynamic and analytical uncertainty, can be considered saturated with respect to gypsum. This is not surprising given the widespread distribution of gypsum in the Culebra and in the overlying strata. There is no systematic variation of gypsum saturation with ionic strength, which suggests that the Culebra waters came into contact with gypsum or anhydrite early along their evolutionary paths and maintained equilibrium as the waters evolved and became increasingly concentrated.

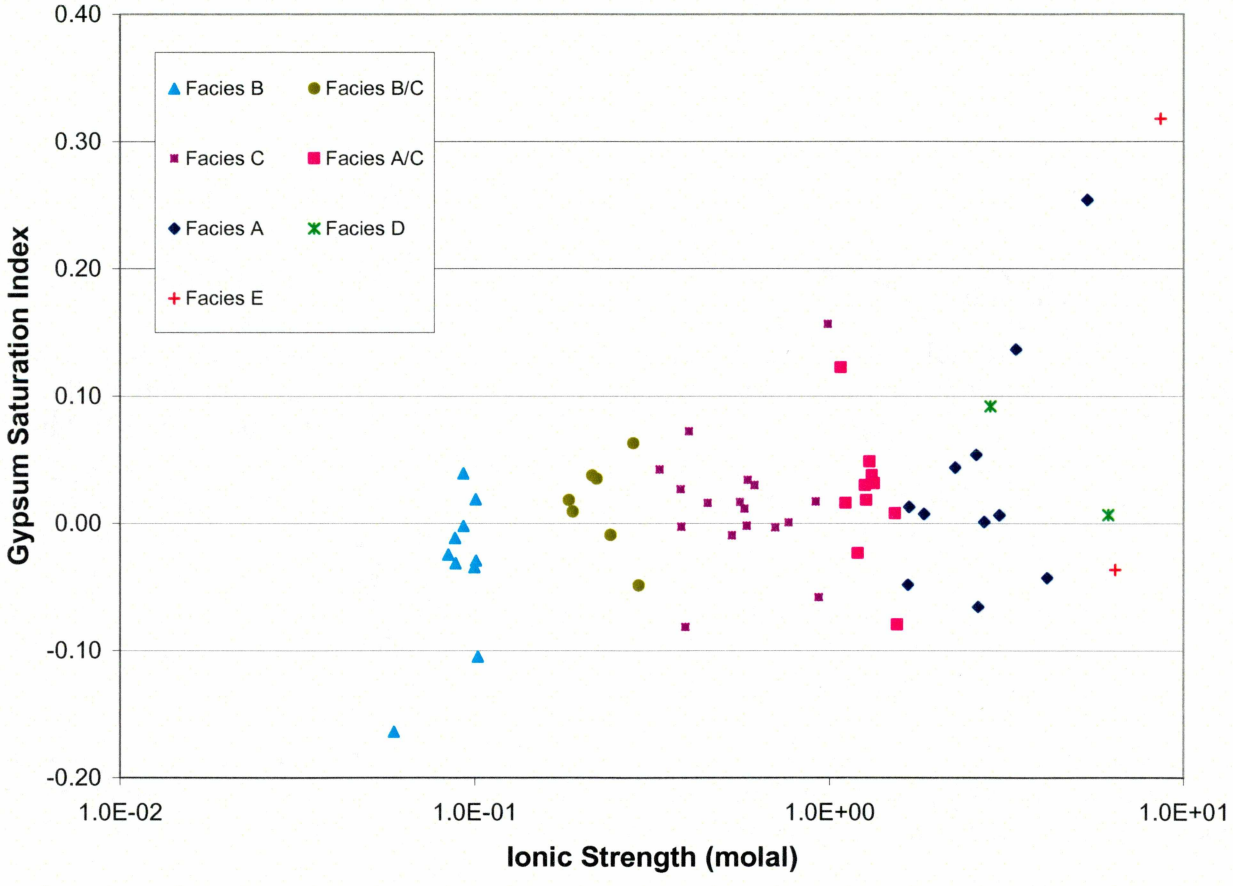

Figure 19. Gypsum saturation index versus ionic strength for the Culebra waters.

Figure 20 shows that calcium concentration shows no discernable correlation to the gypsum saturation index. Most of the gypsum SI values are clustered around zero where the calcium concentration varies by nearly a factor of ten, suggesting that the ionic strength effect may be controlling the concentration.

Information Only

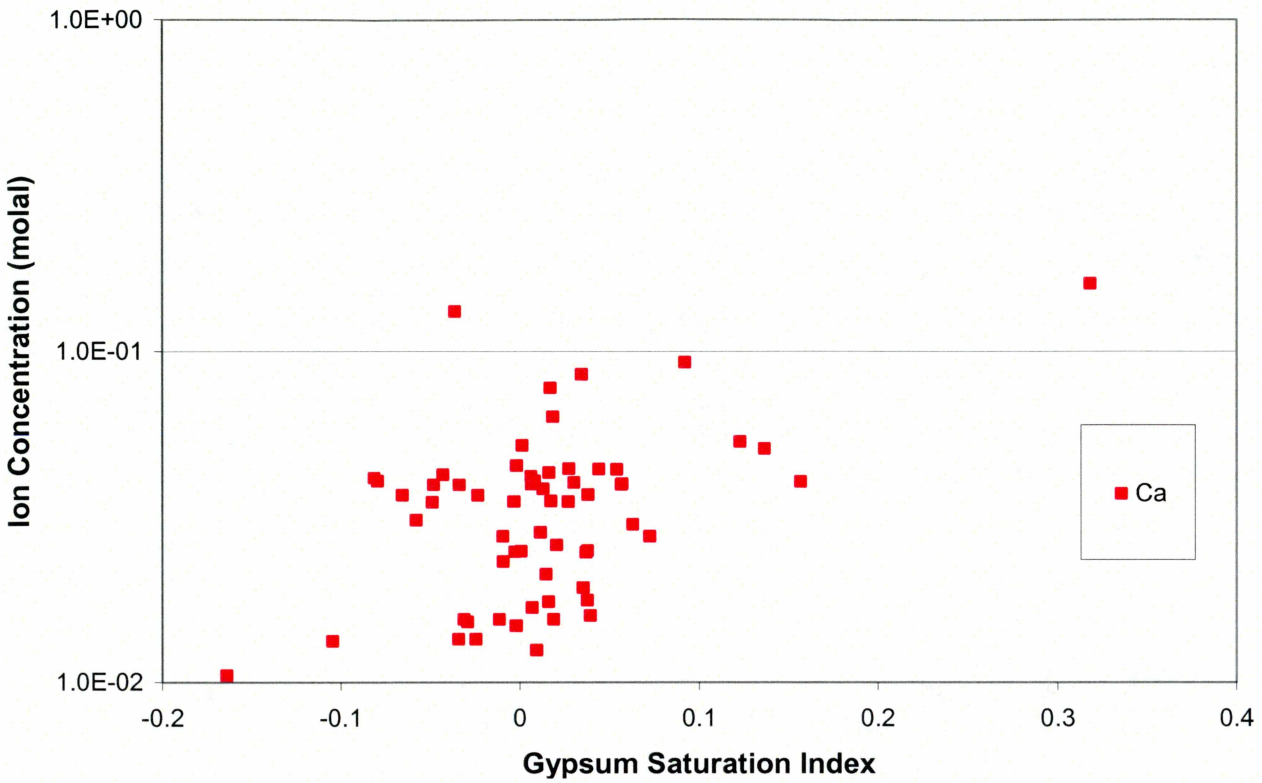

Figure 20. Calcium concentration versus gypsum saturation index for the Culebra waters.

Figure 21 shows that dolomite saturation ranges from -1.7 to 2.8, with the majority of the wells having a saturation index greater than zero indicating oversaturation. Loss of carbon dioxide from solution during sampling will cause the pH of a sample to increase slightly, which results in carbonate phases (calcite and dolomite) becoming oversaturated in solution. This is probably the situation with most of the Culebra samples with carbonate-phase saturation index values greater than zero. However, even with CO_2 degassing, it is safe to assume that the Culebra waters were all at, or very close to, dolomite saturation due to the waters having been in contact with dolomite for very long periods. Dolomite saturation does not show any correlation to ionic strength, and like the gypsum saturation data, suggests that the Culebra waters were in contact with dolomite for extended durations and maintained equilibrium.

Figure 22 illustrates that there is no correlation between either calcium or magnesium concentration and dolomite saturation index. The large range in concentrations at nearly constant values of saturation is to be expected in a system controlled by the ionic strength effect.

Information Only

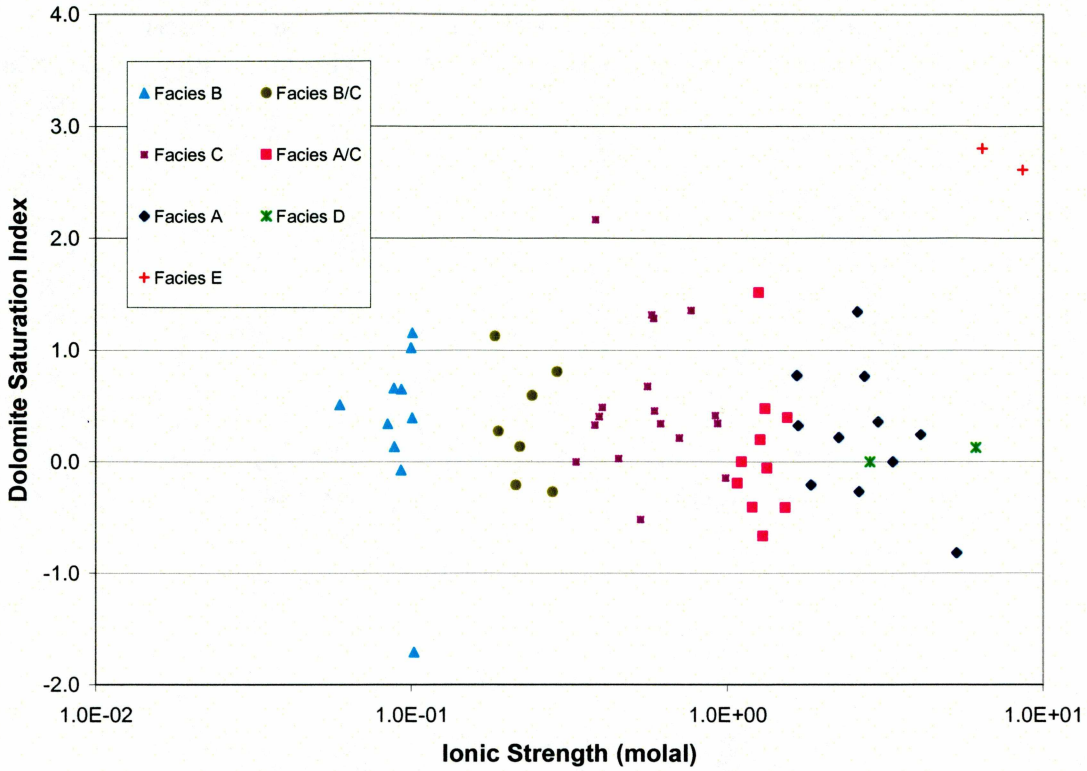

Figure 21. Dolomite saturation index versus ionic strength for the Culebra waters.

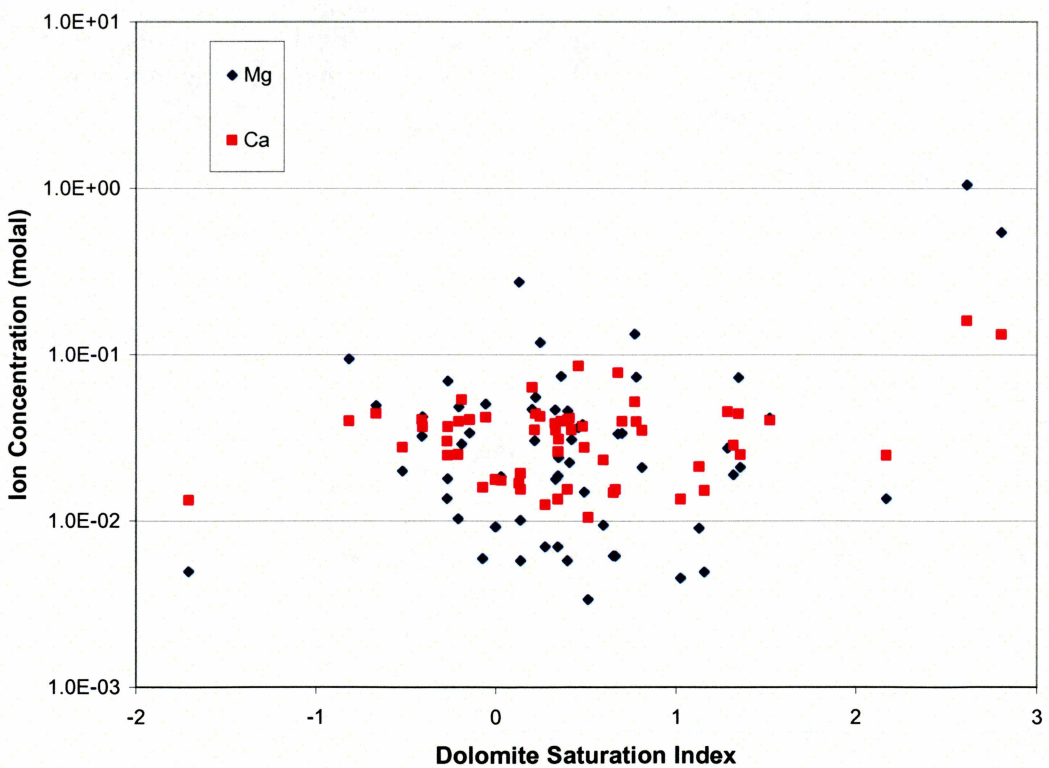

Figure 22. Calcium and magnesium concentrations versus dolomite saturation index for the Culebra waters.

Information Only

Like dolomite, calcite saturation tends to be biased toward positive values (Figure 23), again suggesting CO_2 degassing during sampling as a possible process for increasing calcite saturation.

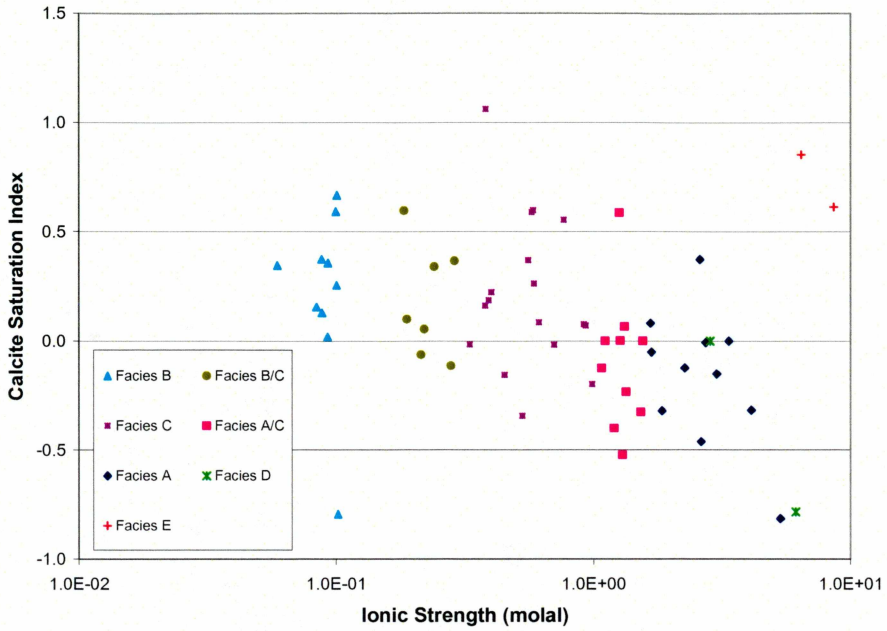

Figure 23. Calcite saturation index versus ionic strength for the Culebra waters.

Similar to dolomite, there is no correlation between calcite saturation and calcium concentration (Figure 24). As is the case with dolomite, the concentration of calcium is probably more greatly influenced by the ionic strength effect which should show increasing calcium as ionic strength increases and calcite remains at equilibrium.

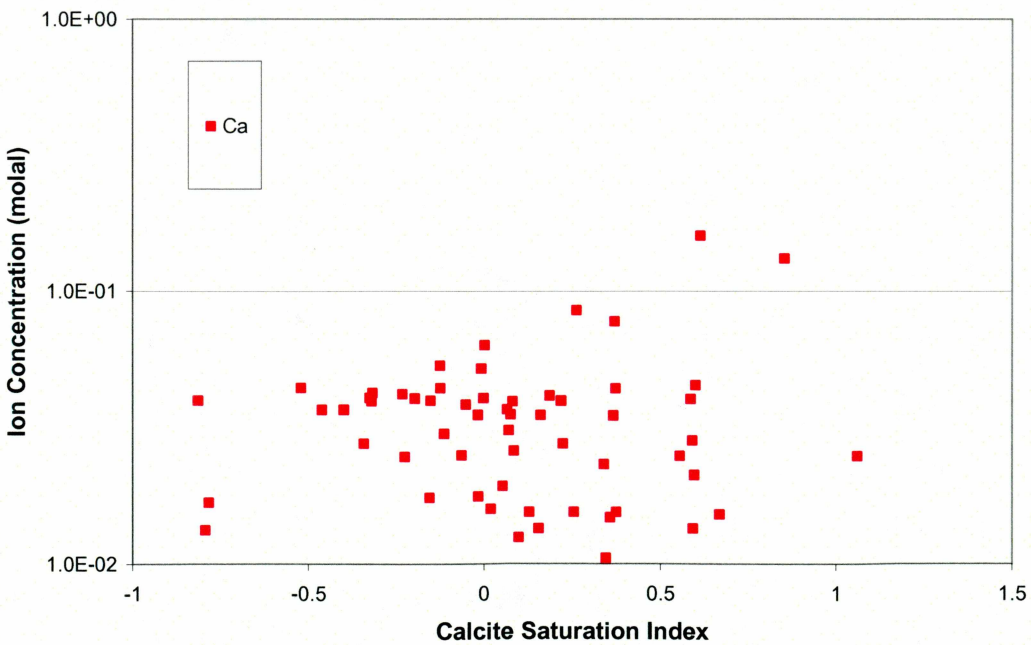

Figure 24. Calcium concentration versus calcite saturation index for the Culebra waters.

Information Only

Polyhalite saturation increases with increasing ionic strength (Figure 25). This correlation is a reflection of the fact that polyhalite is strongly undersaturated in the Culebra waters, and as the concentrations of its constituent ions (K, Ca, Mg, and SO_4) increase with ionic strength, so does its saturation index. This does not identify polyhalite dissolution as the source of these ions, although polyhalite has been identified as occurring in the overlying Tamarisk near and east of the M3-H3 margin (Snyder, 1985, Powers et al., 2006) and may contribute to the solutes of the Culebra waters.

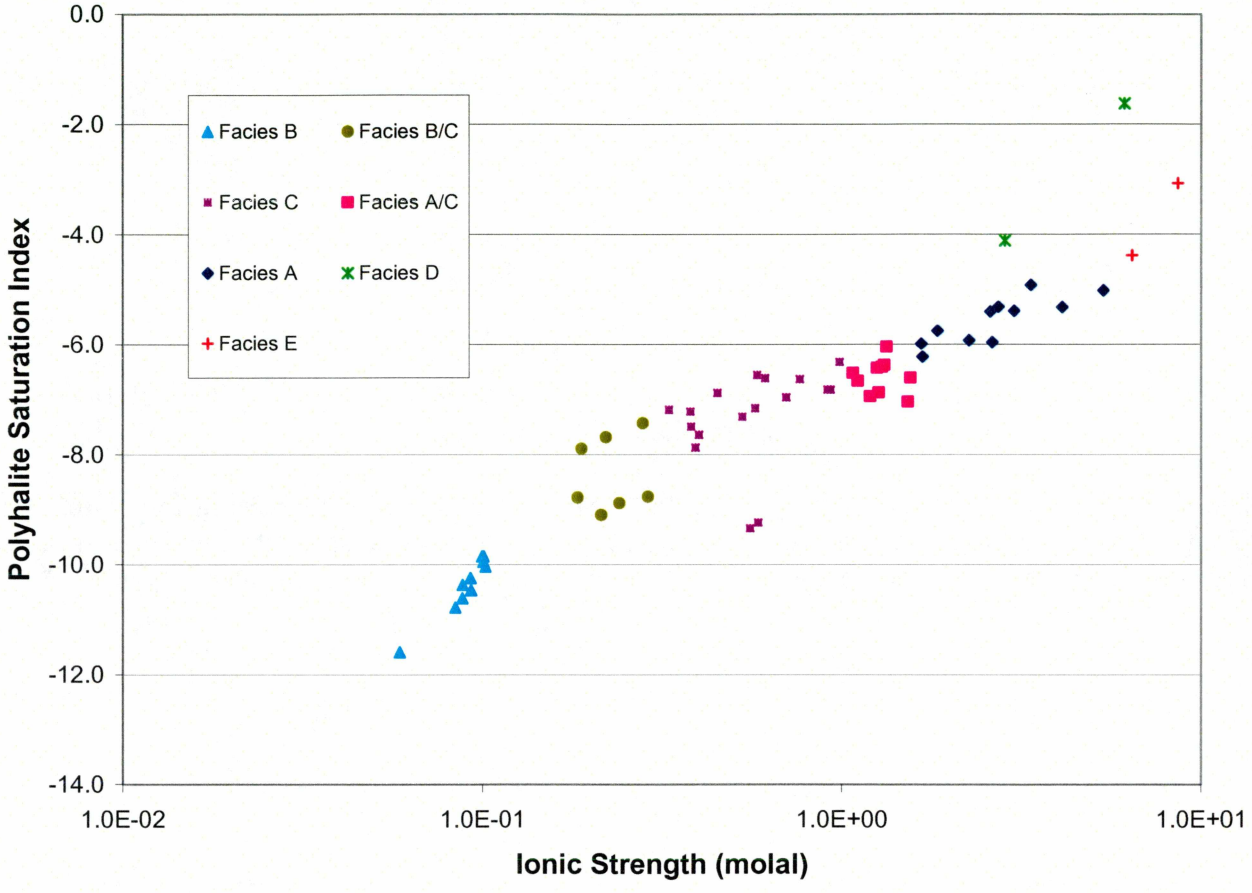

Figure 25. Polyhalite saturation index versus ionic strength for the Culebra waters.

Figure 26 shows that potassium concentration is strongly correlated with the saturation index of polyhalite, and that calcium and magnesium concentrations also appear to be correlated, but less so than potassium. Polyhalite dissolves incongruently, via:

$$K_2Ca_2Mg(SO_4)_4{\cdot}2H_2O \Leftrightarrow 2K^+ + Mg^{+2} + 2SO4^{-2} + 2CaSO_4{\cdot}2H_2O_{(s)}$$

Thus, in a system saturated with respect to gypsum, polyhalite dissolution does not contribute to the dissolved calcium budget because two moles of gypsum will precipitate per mole of polyhalite that dissolves. Since polyhalite is undersaturated for each of the Culebra waters, the ionic strength effect does not influence its solubility.

Information Only

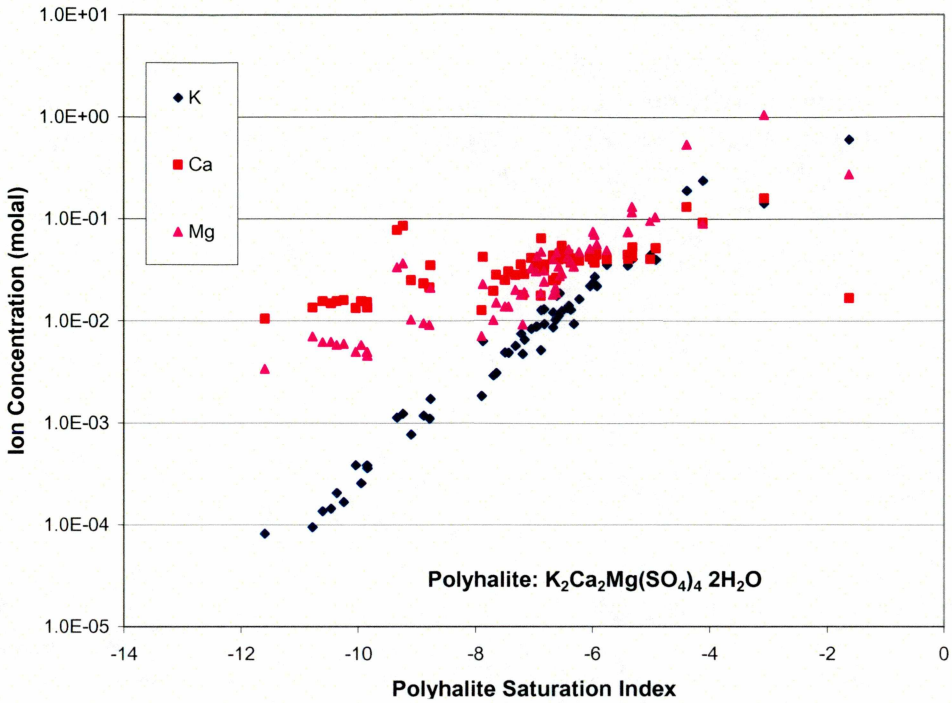

Figure 26. Calcium, magnesium, and potassium concentrations versus polyhalite saturation index for the Culebra waters.

The saturation index for carnallite displays a linear correlation with increasing ionic strength (Figure 27). Like the correlation of polyhalite saturation with ionic strength, this correlation is not an indication that carnallite is present in the system and contributing ions to solution.

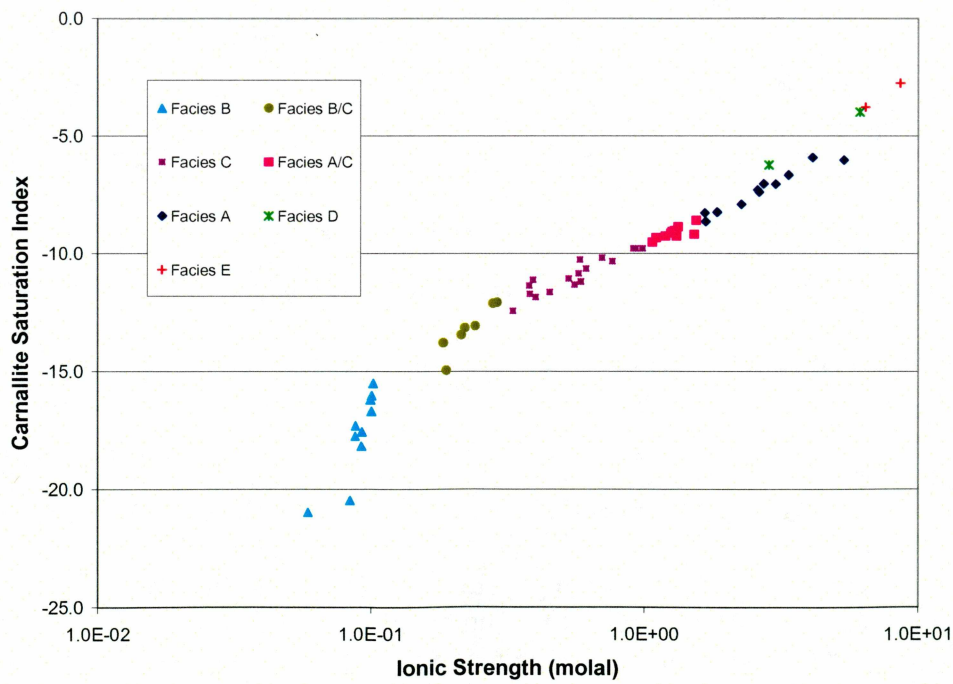

Figure 27. Carnallite saturation index versus ionic strength for the Culebra waters.

Information Only

Figure 28 shows that both magnesium and potassium concentrations are strongly correlated to the saturation index of carnallite. Carnallite is not reported as being present in either the Culebra or Tamarisk, and the observed correlation is a reflection of the increasing concentrations of these ions with ionic strength.

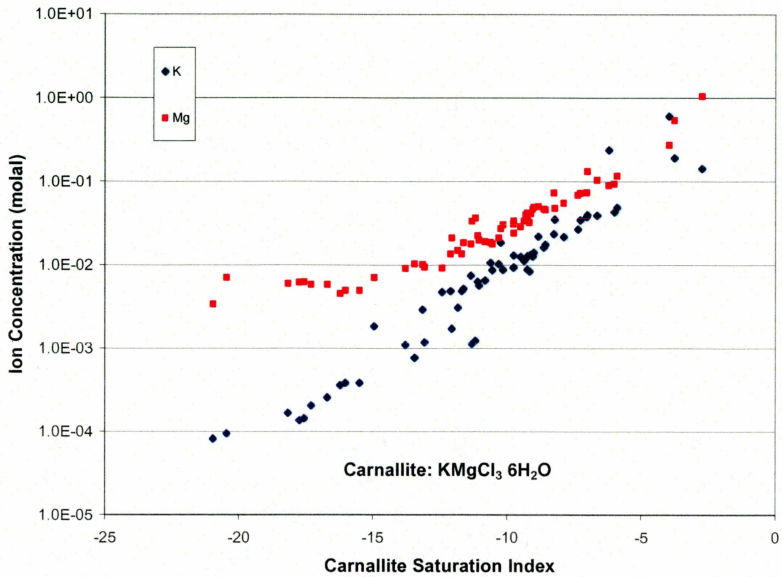

Figure 28. Magnesium and potassium concentrations versus carnallite saturation index for the Culebra waters.

Figure 29 shows the major ions, minus chloride and sodium, plotted as a function of ionic strength. All of the ions display increasing concentration as a function of ionic strength, which is a reflection of the ionic strength effect caused by the increase in sodium chloride in the system.

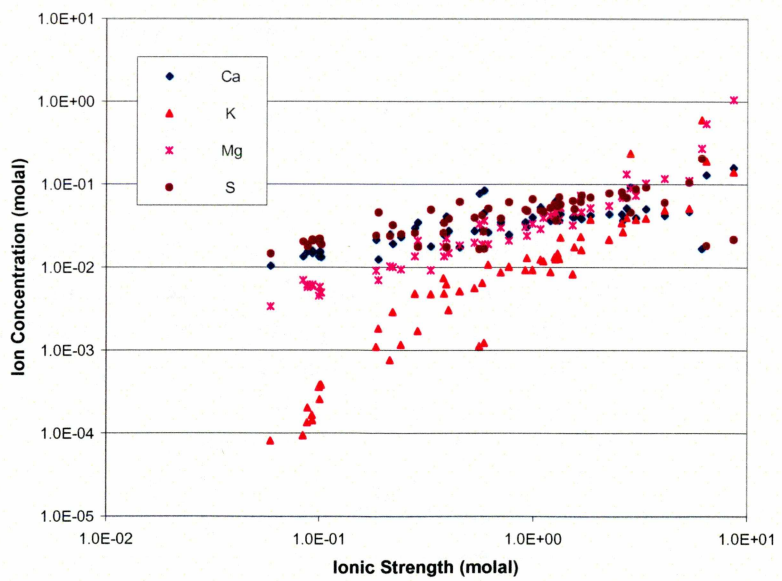

Figure 29. Calcium, magnesium, potassium, and sulfate concentrations versus ionic strength for the Culebra waters

Information Only

4.3 Forward Geochemical Modeling with PHREEQCI

The knowledge gained in Section 4.2 was used as the starting point for a set of theoretical calculations to evaluate potential fluid-rock interactions important in the evolution of the Culebra waters. Two types of simulations were performed -- reaction-path simulations and large-scale mixing calculations. The reaction-path simulations included defining an irreversible reaction and mineral equilibria where minerals were allowed to dissolve and precipitate as a chemical reaction progressed. The underlying assumption of the reaction-path models is that the entire range of observed Culebra water compositions can be derived from a single dilute starting solution into which solutes are added while equilibrium is maintained with various phases, i.e., a homogeneous evolution. These models do not account for mixing of different composition waters which may have undergone processes unique unto themselves, i.e., a heterogeneous chemical evolution. The large-scale mixing simulations (Section 4.4) investigated the mixing of different types of Culebra waters. Both PHREEQCI and SNORM were used in the simulations and evaluation of the results.

4.3.1 The Run 10 Model

Siegel et al. (1991b) extensively investigated the geochemical evolution of the Culebra groundwater using forward geochemical modeling. Siegel et al. (1991b) pursued various approaches to approximate the observed Culebra water compositions and the reader is referred to that reference for the details of the attempted models. The Siegel et al. (1991b) best-fit model, "Run 10" (Run 10 will be used from here forward to note the model), implemented irreversible halite dissolution in a partial-equilibrium system, closed to carbon dioxide exchange, in which gypsum and calcite equilibrium were maintained and polyhalite and carnallite dissolved as halite was added.

The initial water used in Run 10 was set to equilibrium with calcite, dolomite, gypsum, and carbon dioxide at a partial pressure of 10^{-2} atmospheres. This initial water was then reacted with halite in small increments until 8 moles of halite were added to 1 L of initial water. Also added were leonite in a ratio of 0.007 moles to 1 mole of halite, and magnesium chloride at 0.025 moles to each mole of halite. Calcite and gypsum saturations were maintained while halite, leonite, and magnesium chloride were added to solution. Dolomite equilibrium was not maintained during the reaction sequence of Run 10; in other words, dolomite was not allowed to dissolve or precipitate during the simulation.

Siegel et al. (1991b) determined the ratio of leonite to halite (0.007) and $MgCl_2$ to halite from the Culebra water chemistry by plotting the K:Cl and Mg:Cl ratios versus ionic strength (Figures 30 and 31). Figures 30 and 31 show that the potassium:chloride ratio and the magnesium:chloride ratio have a wide range of values, and that the magnesium:chloride ratio varies as a function of ionic strength. Siegel et al. (1991b) do not indicate what their reasoning was in choosing the average K:Cl ratio while choosing the minimum Mg:Cl ratio. Because one mole of leonite contains two moles of potassium, the observed K:Cl ratio of the Culebra waters (0.014) was divided in half to get the value used in the Run 10 model.

Information Only

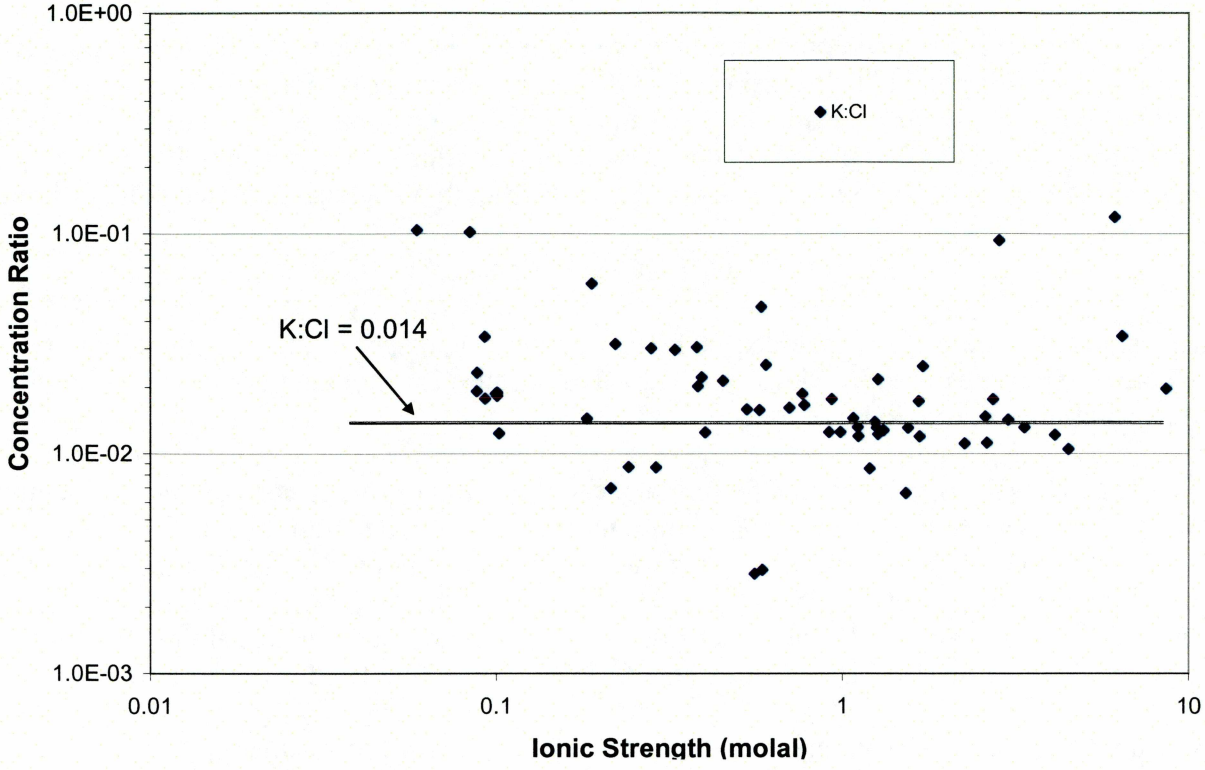

Figure 30. Potassium:chloride ratio versus ionic strength.

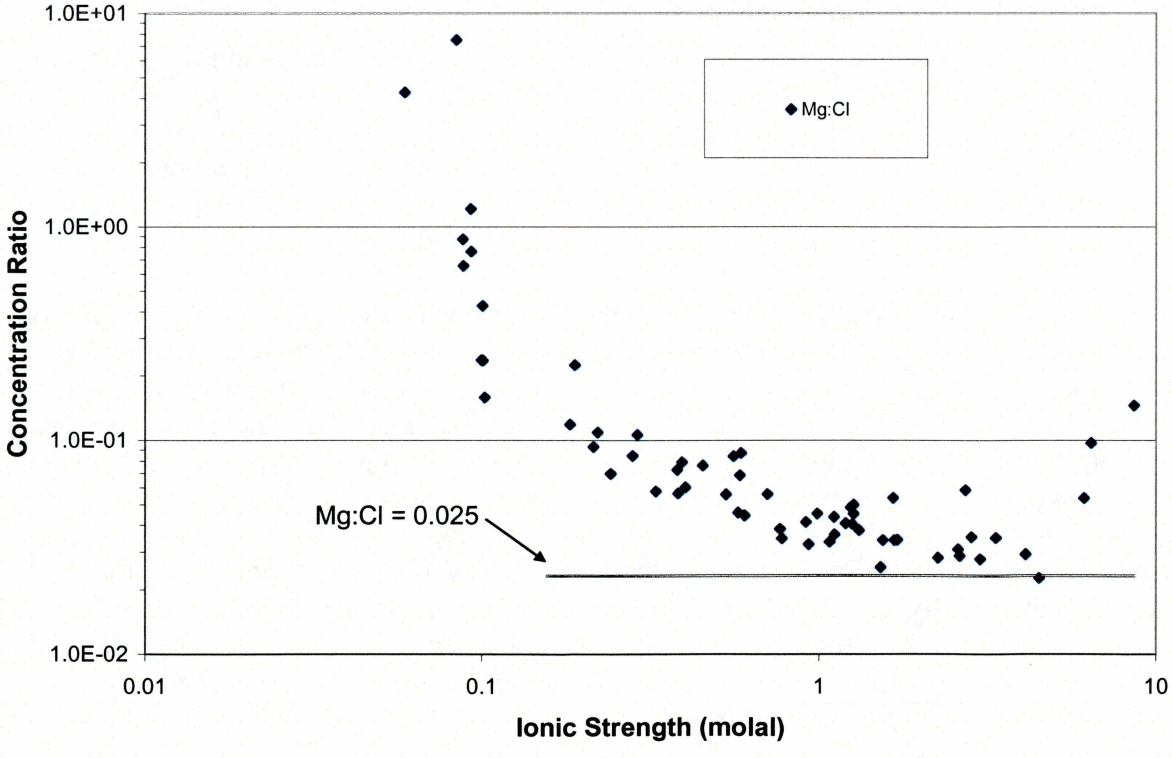

Figure 31. Magnesium:chloride ratio versus ionic strength.

Information Only

The Run 10 model included some surrogate reactions for incongruent dissolution of polyhalite and carnallite. For polyhalite, Siegel et al. (1991b) used leonite ($K_2Mg(SO_4)_2 \cdot 4H_2O$) because it dissolves congruently and results in the same fluid composition as incongruent polyhalite dissolution (see Section 4.2 for polyhalite dissolution reaction). Magnesium chloride ($MgCl_2$) was used rather than carnallite, which dissolves incongruently in sylvite-saturated solutions via:

$$KMgCl_3 \cdot 6H_20 \Leftrightarrow KCl_{(s)} + Mg^{+2} + 2Cl^- + 6H_20$$

Magnesium chloride was not included in the thermodynamic database and was input directly into the Run 10 input files used by Siegel et al. (1991b) because it is not a naturally occurring phase, and its solubility was set to be infinite.

Siegel et al. (1991b) concluded that dolomite plays only a minor role in controlling the chemistry of the Culebra waters, and that the concentrations of potassium, magnesium, calcium, and sulfate are consistent with a partial equilibrium system in which saturation is maintained with calcite and gypsum by the irreversible dissolution of halite with trace amounts of polyhalite and carnallite. Siegel et al. (1991b) note that results of the reaction-path models are non-unique, and that fluid compositions similar to those of the Culebra can be simulated using other reactants.

The Run 10 model was re-created in PHREEQCI for the purposes of this report to create new plots which included the additional Culebra water chemistry data that have become available, and to compare the Run 10 results to an alternate model.

4.3.2 Alternate Conceptual Model

A simplified alternative model was developed to examine some of the assumptions in the Run 10 model. Aspects of the Run 10 model that were scrutinized included: 1) The assumption that dolomite equilibrium is not maintained with the Culebra fluids, and that calcite equilibrium is maintained, 2) the assumption that carnallite contributes to the Culebra solute budget and that it dissolves incongruently in solutions undersaturated with respect to sylvite, and 3) the need to use leonite as a surrogate for polyhalite in gypsum-saturated fluids.

The starting water composition for the alternate model was equivalent to the water from the Poker Trap well. This well was chosen because it is the most dilute water of the 59 Culebra samples, and as such is the least evolved of all the Culebra waters and may represent an end member composition. The water was created in PHREEQCI by using the calculated saturation index values of the Poker Trap water (Table 13) for calcite, dolomite, gypsum, pCO_2, polyhalite, and halite and equilibrating distilled water to the phases at those saturations. The initial solution was then reacted with eight moles of halite in small increments while polyhalite simultaneously reacted in a ratio of 0.0125 moles per mole halite. This ratio of polyhalite to halite was determined by iteratively running the model until a reasonably good fit of the simulated potassium to the measured potassium of the Culebra waters was attained. Both dolomite and gypsum equilibrium were maintained such that they could either dissolve or precipitate during the reaction sequence. A comparison of the Run 10 and alternate model constraints is provided in Table 14.

Information Only

Table 14. Summary of the Run 10 and alternate model constraints.

Model	Initial Solution	Fixed Saturation Phases	Accessory phases (ratio to halite)
Run 10	Calcite, dolomite, gypsum, & pCO_2 (10^{-2}) equilibria	Calcite and gypsum at saturation	Leonite (0.007) $MgCl_2$ (0.025)
Alternate	Poker Trap	Dolomite and gypsum at saturation	Polyhalite (0.0125)

Inspection of Figures 32 through 39 of model results reveals that on the whole, both models provide a reasonably good fit to the measured data. The exception would be the fit of the alternate model to the magnesium data (Figure 32), where the alternate model underpredicts the measured data, and the Run 10 model clearly has a superior match to the measured data. The reason that the alternate model did not attain a better fit to the magnesium data was because the addition of magnesium chloride to the simulated solution, as was used in Run 10, was not included in the alternate model. The Siegel et al. (1991b) rationale for using magnesium chloride was to simulate the dissolution of carnallite ($KMgCl_3 \cdot 6H_2O$), where carnallite dissolves incongruently to form sylvite (KCl) and aqueous magnesium and chloride ions. However, sylvite is highly soluble and is stable only in solutions in which it is saturated. Therefore, in solutions not saturated with sylvite, such as all of the Culebra waters (Table 13), carnallite would completely dissolve without forming sylvite. Thus, the use of magnesium chloride in the Run 10 model may not have been wholly correct. Had Siegel et al. (1991b) used carnallite instead of magnesium chloride, then the modeled potassium budget would have been exceeded, i.e., the Run 10 simulated potassium concentration (Figure 33) would have overpredicted the measured potassium data because in Run 10, Siegel et al. (1991b) used leonite ($K_2Mg(SO_4)_2 \cdot 4H_2O$) dissolution to fit the potassium data, and the additional potassium from carnallite dissolution would have exceeded the measured data.

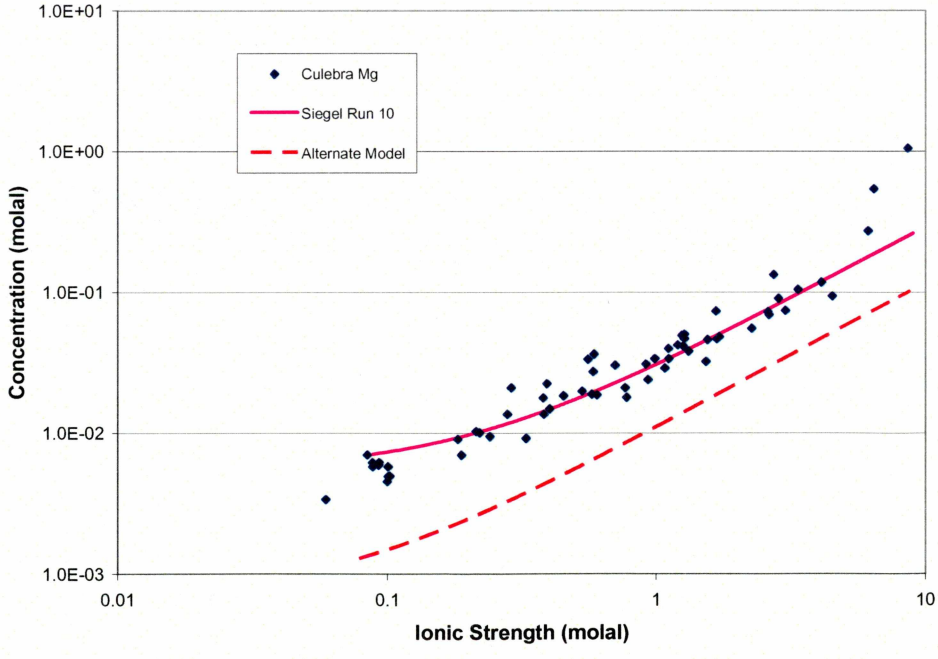

Figure 32. Measured and simulated magnesium concentration versus ionic strength.

Information Only

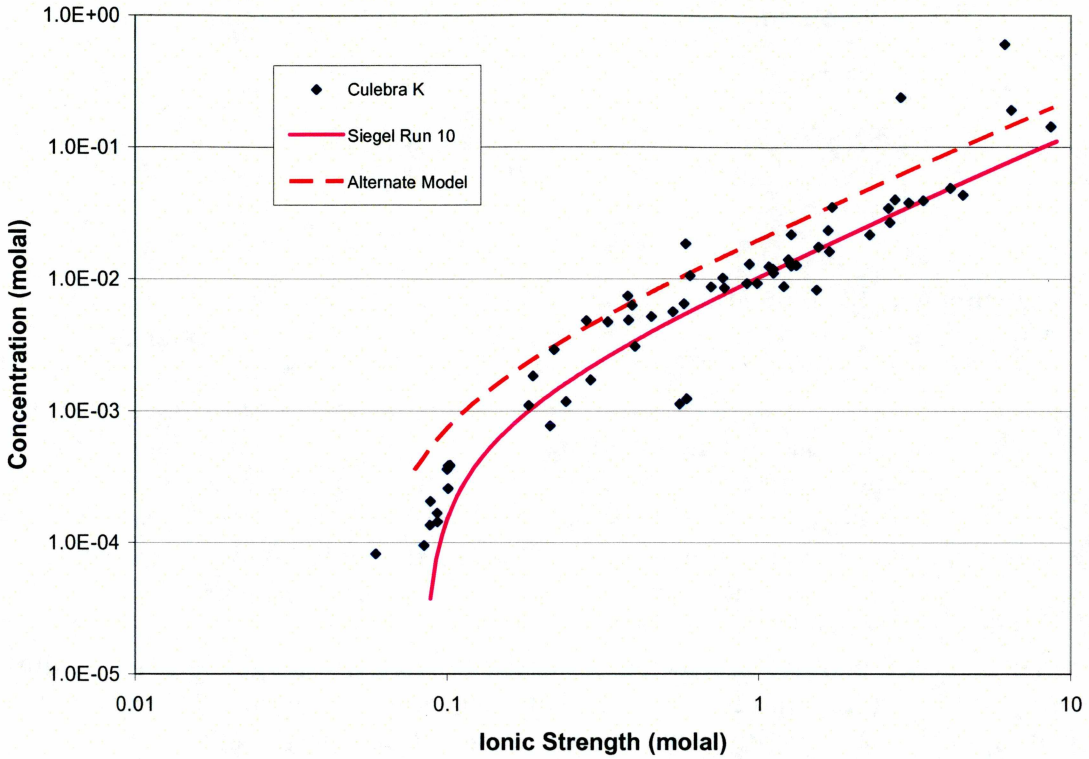

Figure 33. Measured and simulated potassium concentration versus ionic strength.

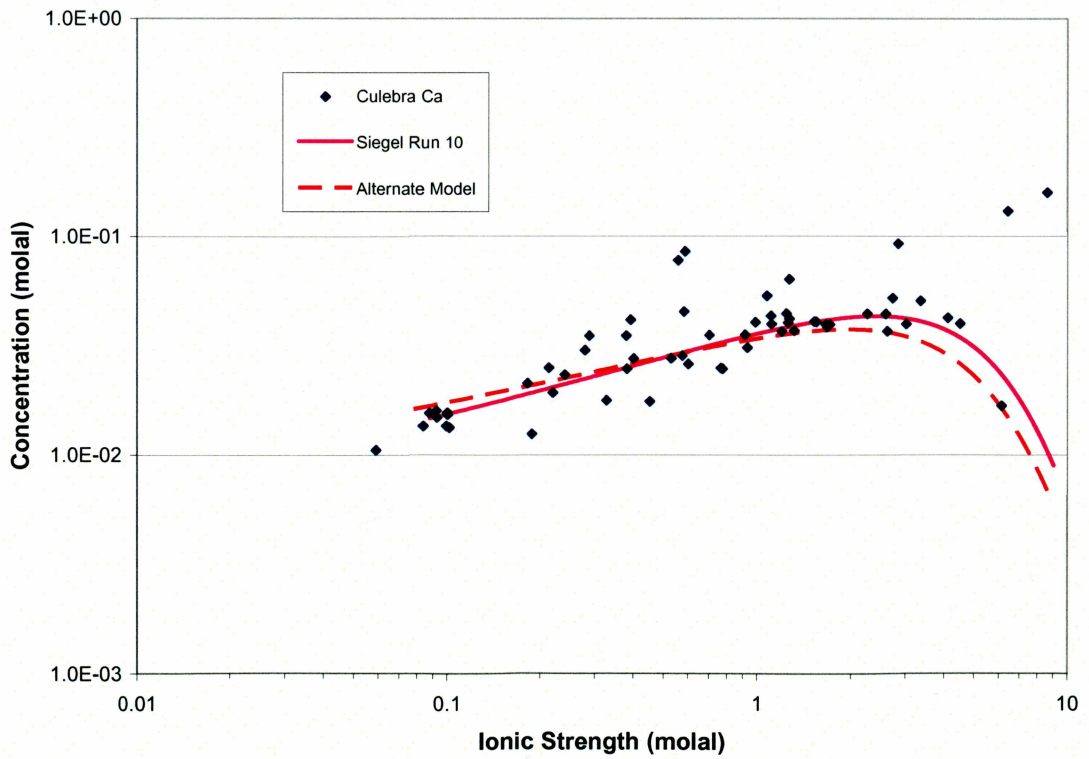

Figure 34. Measured and simulated calcium concentration versus ionic strength.

Information Only

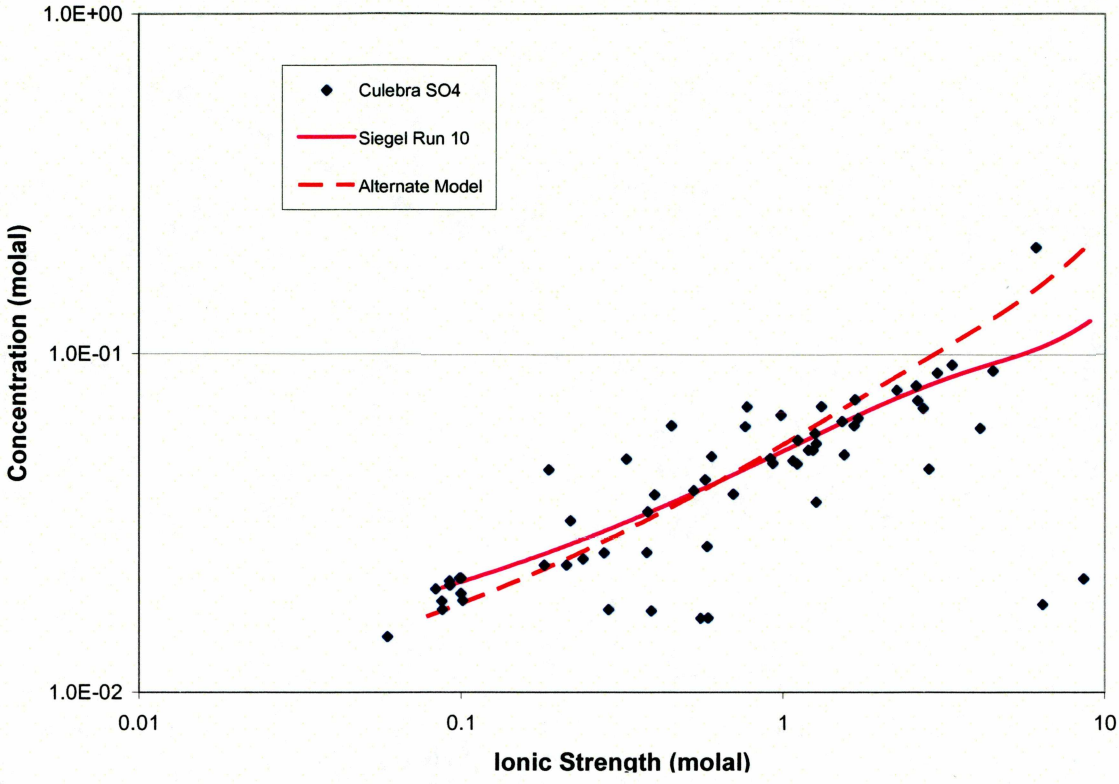

Figure 35. Measured and simulated sulfate concentration versus ionic strength.

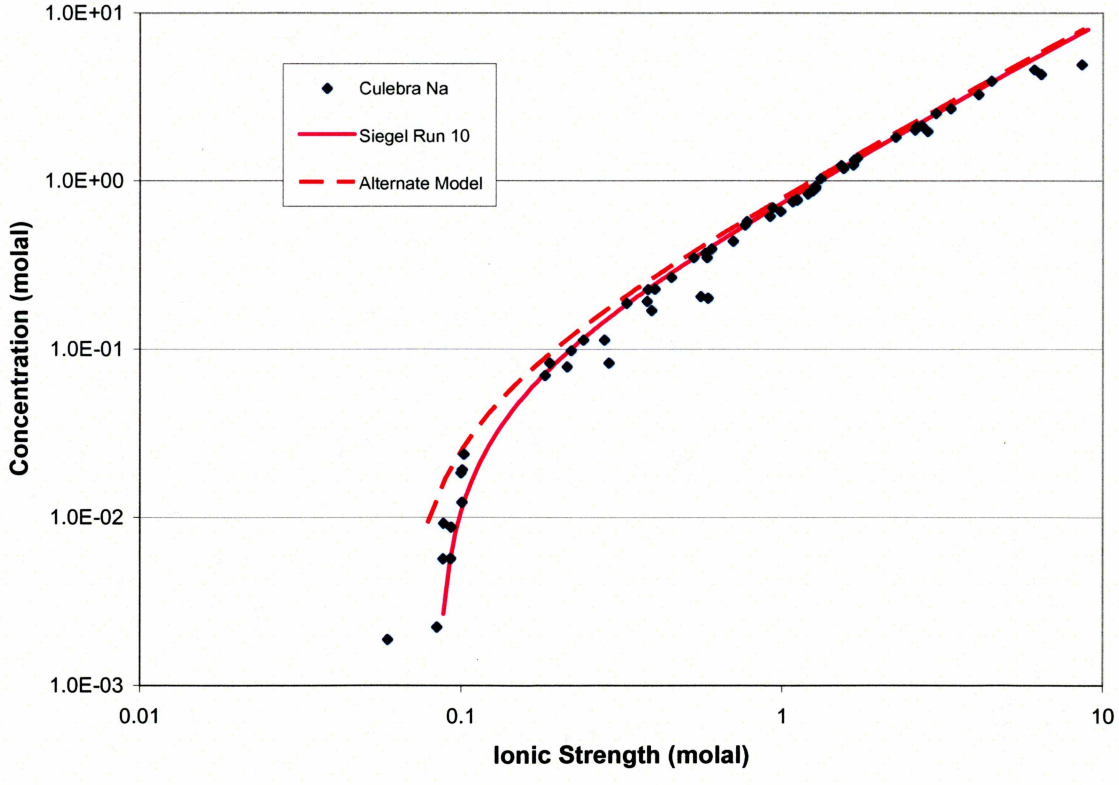

Figure 36. Measured and simulated sodium concentration versus ionic strength.

Information Only

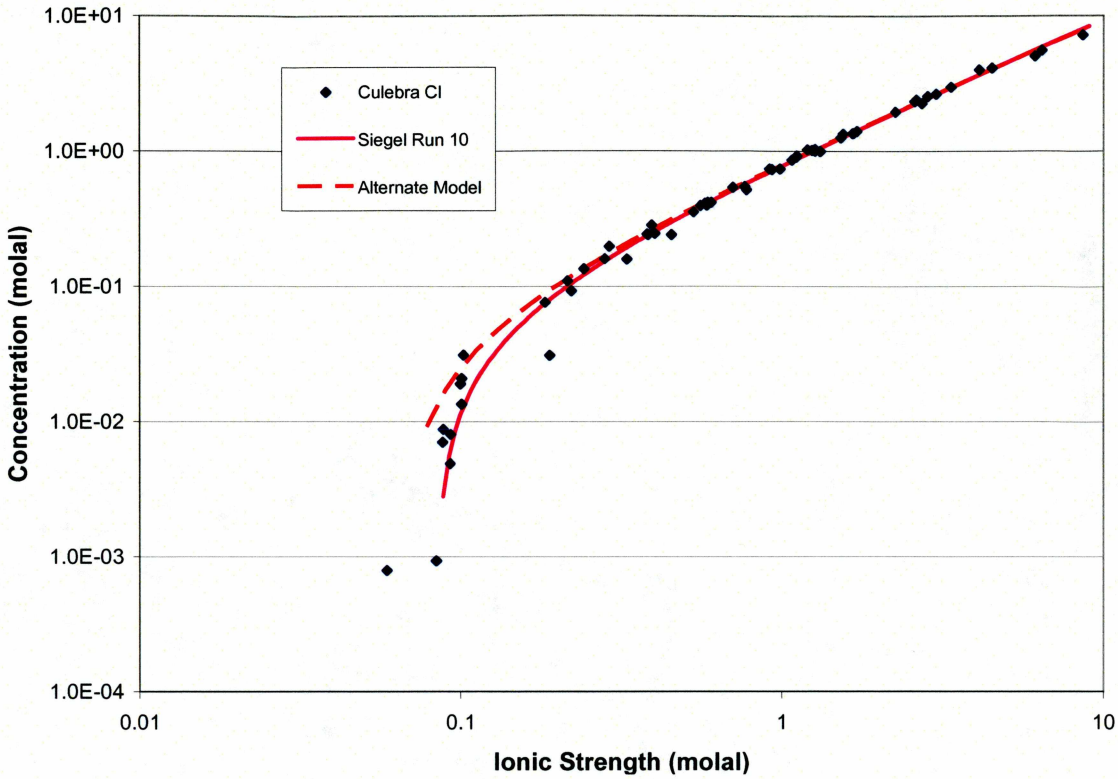

Figure 37. Measured and simulated chloride concentration versus ionic strength.

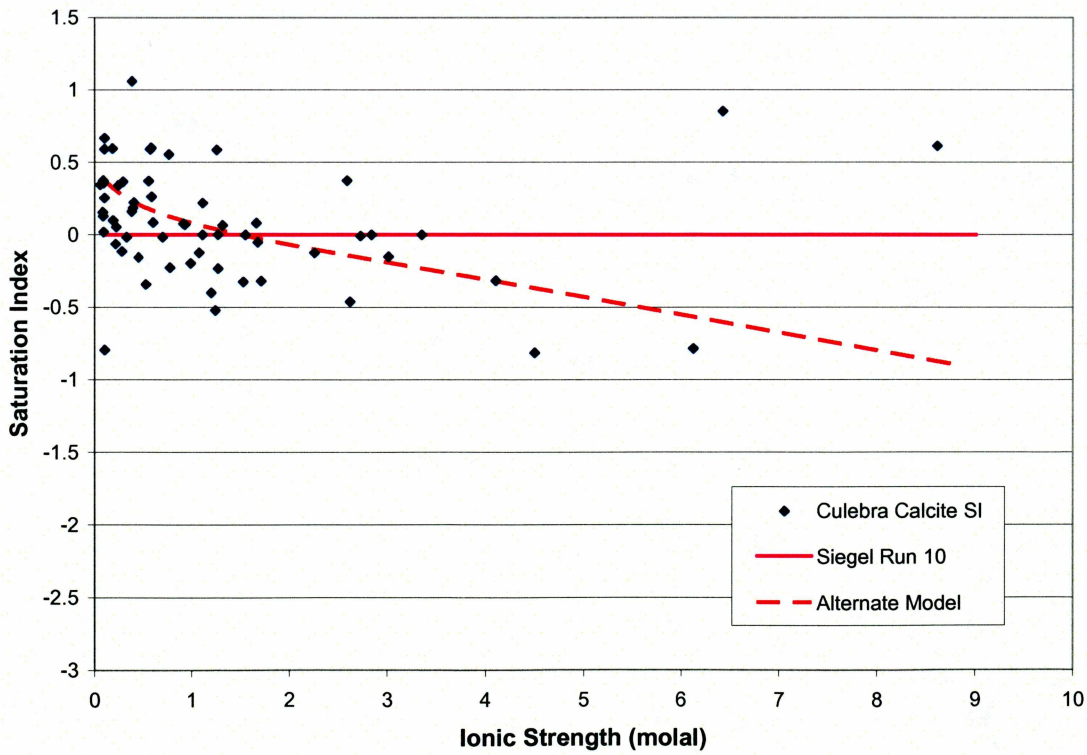

Figure 38. Measured and simulated calcite saturation versus ionic strength.

Information Only

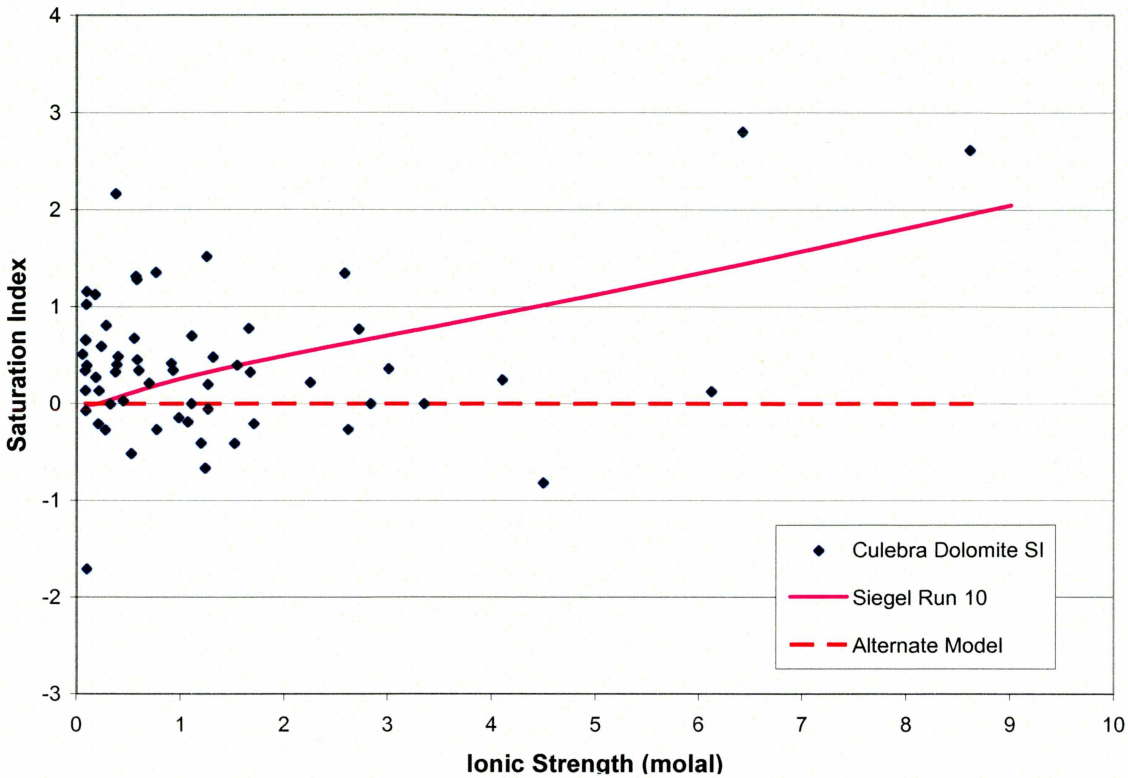

Figure 39. Measured and simulated dolomite saturation versus ionic strength.

The absence of documented carnallite in the Rustler Formation and the instability of sylvite are two arguments against the use of carnallite in modeling the evolution of the Culebra water chemistry. With the elimination of carnallite as a contributor to the solute budget, and the inability of the alternate model to fit the magnesium data, the question as to the source of the excess magnesium in the Culebra waters needs to be explored.

Siegel et al. (1991b) and Siegel and Anderholm (1994) discuss the possibility of dissolution of the clay mineral corrensite ($(Ca,Na,K)(Mg,Fe,Al)_9(Si,Al)_8O_{20}(OH)_{10}\cdot n(H_2O)$) and concomitant precipitation of sodium smectite as a reaction that could liberate magnesium. Corrensite is well documented in the Culebra (Sewards et al., 1991a; 1991b) where it can comprise up to 50% of the clay minerals present. Sewards et al. (1991a; 1991b) described the transformation of dioctahedral smectite to corrensite during the deposition of the Culebra: as the magnesium activity of the brines increased, the magnesium replaced aluminum in the octahedral smectite layers, and the aluminum replaced silicon in the tetrahedral smectite layers, transforming smectite to corrensite with the resulting phase being a mixed-layer chlorite/smectite. Given enough time in a solution with low magnesium activity, the corrensite reaction could retrograde to smectite and release magnesium. This would be a difficult problem to model because of the lack of high quality silica and aluminum data for the Culebra waters, the absence of thermodynamic data for silica and aluminum species in the PHREEQCI Pitzer database, and lack of thermodynamic data for the solid solution between smectite and corrensite. However, it is a hypothesis worth investigating in the future.

Information Only

The downturn in the simulated calcium data (Figure 34) for both models was caused by the ionic strength effect. Because calcium in solution is controlled by gypsum equilibrium, when the calcium activity coefficient increases above its initial value (~0.33) as a function of increasing ionic strength, the total amount of calcium in solution decreases. This downturn in concentration is not observed for the simulated magnesium concentrations because magnesium is being added to the solution through a non-equilibrium reaction of leonite for Run 10, and by polyhalite for the alternate model. The observation that many of the Culebra waters have calcium concentrations that are greater than the simulated values suggests processes that are not accounted for by either model.

The use of leonite as a surrogate for polyhalite in the Run 10 model was an unnecessary step; polyhalite could have been used without altering the simulated fluid composition. In Section 4.2, it was established that the Culebra waters were all saturated with respect to gypsum, and in both models, gypsum saturation is maintained where gypsum may dissolve or precipitate as the reaction progresses. Therefore, in a system at equilibrium with gypsum, dissolution of polyhalite will result in gypsum precipitation to maintain gypsum equilibrium. Like carnallite and sylvite, polyhalite and gypsum behave in a similar manner -- if the system is below gypsum saturation, then polyhalite will dissolve congruently, and if the system is above gypsum saturation, then polyhalite will dissolve incongruently.

Figure 35 displays the measured and simulated sulfate concentration as a function of ionic strength. Both the Run 10 model and alternate model do an adequate job of fitting the measured data. The source of sulfate ions in both simulations is from maintaining gypsum saturation and from the addition of polyhalite.

Figures 36 and 37 show the measured and simulated sodium and chloride concentrations, respectively, plotted versus ionic strength. Both models are based on the primary assumption that halite dissolution is the driving force in the dissolution of the other solute-contributing phases and, as such, both models fit the measured data well.

As was demonstrated in Section 4.2, all of the Culebra waters are saturated or very close to saturation with respect to dolomite and calcite. The Run 10 model assumes that as the Culebra waters evolve, they maintain equilibrium with calcite (Figure 38), while in the alternate model dolomite equilibrium is assumed (Figure 39). The question as to which is more correct is difficult to resolve since both models do a relatively good job of matching the observed calcium concentrations. Based on the occurrence of dolomite in Culebra core samples, Siegel et al. (1991b) report that it ranges from a few percent up to 99% of the rock mass, with the majority of samples having 80% or more dolomite. In terms of calcite, Siegel et al. (1991b) report that calcite is abundant near the top of the Culebra in the WIPP-29 core, where it may have been deposited as part of dedolomitization of the Culebra dolomite as calcium-sulfate-rich waters entered from the overlying strata. Sewards et al. (1991a) render the same analysis for calcite occurring at the top of the Culebra in core from WIPP-19, and label calcite as a phase present in trace quantities. Based on their modes of occurrence, dolomite would be the logical phase of choice over calcite for fluid-mineral equilibria in the Culebra.

Information Only

In summary, both the Siegel et al. (1991b) Run 10 model and the alternate model presented here do an adequate job of simulating some of the processes responsible for the evolution of the observed Culebra chemistries. The dominant process in the evolution of the Culebra groundwater chemistry is the dissolution of halite. Halite dissolution is a driving force that functions to increase the equilibrium saturation concentration of gypsum, calcite, and dolomite. Based on its occurrence in the Rustler Formation and how it functioned in the models, polyhalite appears to be an important accessory phase in the evolution of the Culebra chemistry. The question of the source of magnesium in excess of dolomite equilibrium and potential polyhalite dissolution still needs to be addressed, but as was previously discussed, it may be from the retrograde reaction of corrensite to smectite. The reaction-path models do not provide any information on the role of mixing of concentrated waters with dilute waters in the Culebra; the models are simple static models meant to explore possible reaction scenarios in the evolution of the groundwater.

4.4 Large-Scale Groundwater Mixing

To gain a better understanding of the role of mixing on the observed Culebra water chemistries, some end-member water compositions were chosen and PHREEQCI was used to perform mixing calculations. The only constraints on the PHREEQCI mixing model were the inclusion of gypsum and calcite as phases which could precipitate should they become saturated (SI>0). The output compositions of the PHREEQCI runs were used as input for SNORM for ready comparison to the salt norm types presented in Section 3.

4.4.1 Mixing of SNL-16 and H-8 Waters

The waters from well SNL-16 and well H-8 were chosen for mixing because they both originate in areas where the neighboring wells have characteristic normative signatures, "diagenetic" for the SNL-16 area, and "sulfatic weathering" for the area surrounding H-8b, and between these two types a third normative type, "sulfatic weathering with a marine component," exists. Thus, the purpose of the mixing model was to test the hypothesis that mixtures of these two types (diagenetic and sulfatic weathering) could result in the third type -- sulfatic weathering with a marine component.

Figure 40 is a plot of the normative minerals which result from mixing SNL-16 with H-8b water. Between about 5% SNL-16 water up to nearly 50% SNL-16 water, the sulfatic weathering with a marine component salt norm type was generated. The salt norm of H-7b1 is included on the plot (Figure 40), and reveals a greater abundance of normative anhydrite compared with the simulated mixing compositions. Whereas the mixing simulation represents an ideal mixture of two water types without consideration of the actual flowpath, the excess anhydrite in the H-7b1 salt norm is probably due to dissolution of additional sulfate phases somewhere along the flowpath to the well. Thus, the mixing calculations demonstrated that mixing of a dilute diagenetic water (SNL-16) with sulfatic weathering water (H-8) resulted in an intermediate type with the same salt norm as sulfatic weathering with a marine component. The calculations confirmed the hypothesis that diagenetic waters present along Nash Draw such as that from wells SNL-16, WIPP-26, and IMC-461, when mixed with waters such as that from the southern facies B wells (USGS-1, H-9b, Engle, H-8b, and Poker Trap) can result in waters of intermediate composition like the waters from the northern facies B wells (Mobley, USGS-4, H-7b1, SNL-12,

Information Only

and SNL-17A) (see Figure 12). These results imply that water may flow along a NW – SE vector in this area and create a broad mixing zone

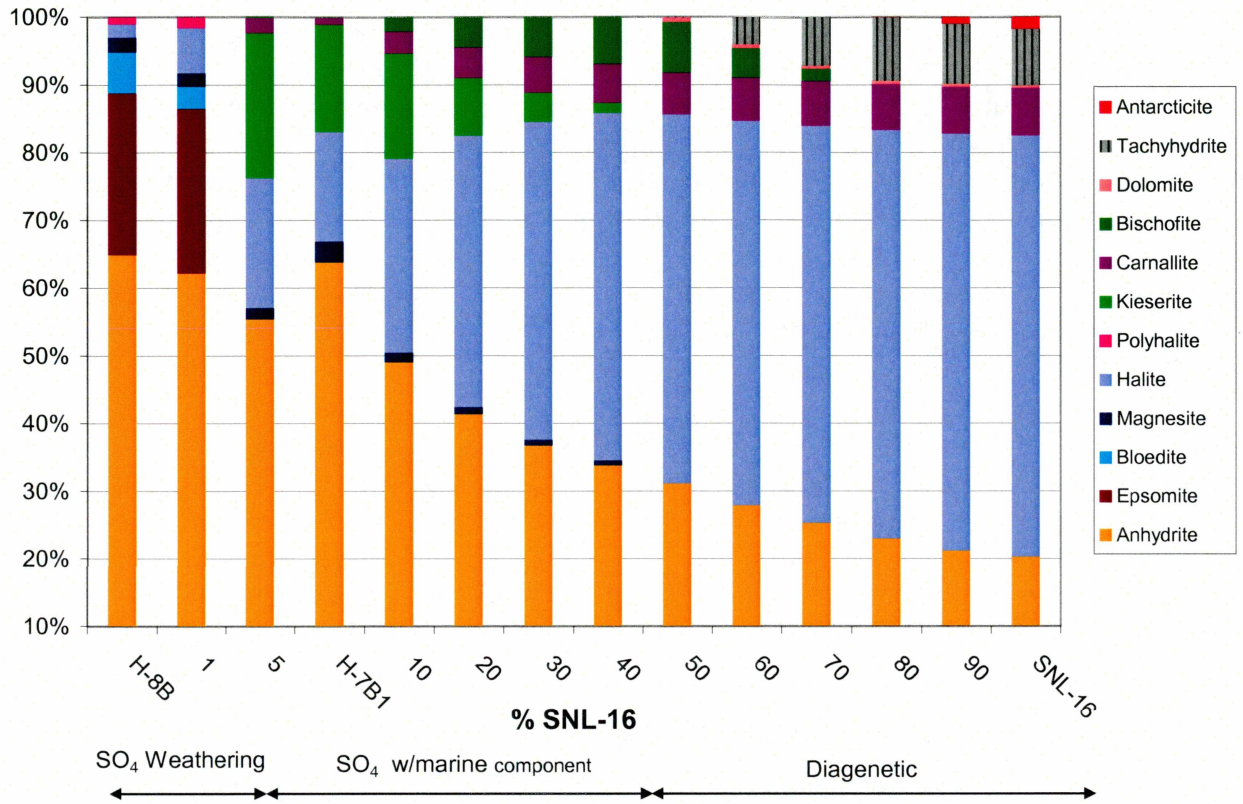

Figure 40. Normative phases resulting from mixing SNL-16 and H-8b waters. Also plotted is the H-7b1 salt norm.

4.4.2 Mixing of SNL-15 and WQSP-4 Waters

The waters from wells SNL-6 and SNL-15 clearly represent an end-member composition for the Culebra. Therefore, if water of this composition is diffusing or otherwise being released into the higher transmissivity area west of the M2-H2 margin, then it will mix with waters west of the margin and intermediate types should exist in the Culebra. To test this hypothesis, SNL-15 water (primitive diagenetic) was mixed with WQSP-4 water (sulfatic weathering solution with a marine component) to see if any of the mixed compositions were similar to the DOE-1 composition (marine). These wells were chosen based on their different salt norm types and their relatively close proximity to one another (Figure 12).

The results of the mixing model are plotted in Figure 41 and show that when between about 5 to 10 percent SNL-15 water is added to WQSP-4 water, a marine-type salt norm is observed. The phase eliminated from the WQSP-4 norm is polyhalite, and with the absence of tachyhydrite, characteristic of the SNL-15 norm, a new normative assemblage typical of a marine norm, such as DOE-1, exists. The salt norm of DOE-1 is included on the plot (Figure 41), and reveals a greater abundance of normative halite compared with the simulated mixing compositions. The excess halite in the DOE-1 salt norm is probably due to dissolution of halite along the M2-H2 margin. Of interest is that only a small amount, 5-10%, of the primitive diagenetic SNL-15

Information Only

water was necessary to create this marine normative assemblage. This result provides further support that the origin of the dilute diagenetic waters (non-SNL-6 and SNL-15) was not as vestigial primitive brines that were somehow preserved or isolated in low transmissivity regions of the Culebra only to be sampled in the wells where they have been identified, because their diagenetic signature would have been wiped out upon mixing with waters as dilute as the dilute diagenetic waters tend to be.

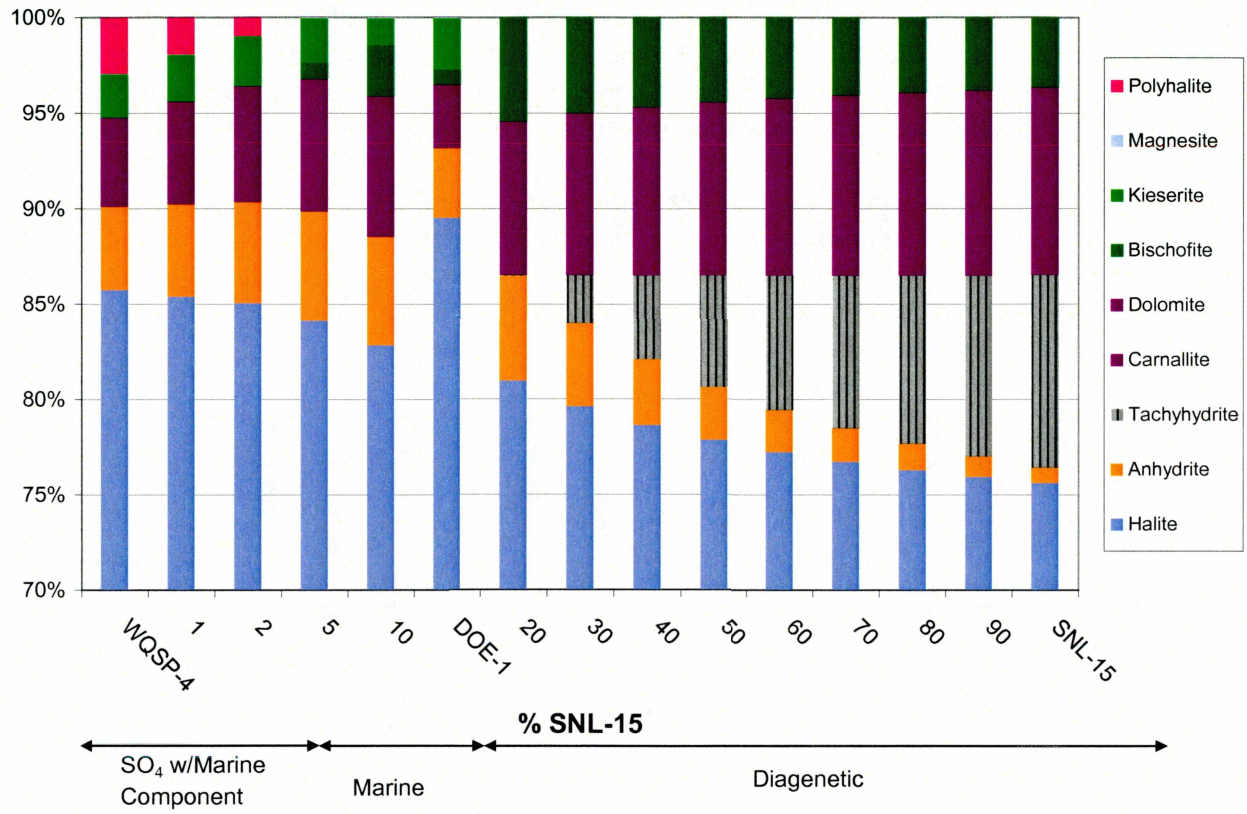

Figure 41. Normative phases resulting from mixing SNL-15 and WQSP-4 waters. Also plotted is the DOE-1 salt norm.

These calculations have shown how the mixing of a sulfatic weathering with a marine component type water (WQSP-4) with a primitive diagenetic water (SNL-15) resulted in a water with a marine type signature, such as that of DOE-1. This is a mixing scenario that we would expect to be occurring in the area near the M2-H2 margin where the concentrations of the waters are high (ionic strength > 2 molal). Wells that probably represent the waters like those used in this mixing calculation were discussed in Section 3.3 and include H-5c, WQSP-3, H-15, DOE-1, H-17, SNL-8, WQSP-4, H-19b0, H-11b3, SNL-14, P-17, H-12, and H-10b.

4.4.3 Mixing of H-2c and H-3b2 Waters

Another large group of wells is found within and to the north and northwest of the WIPP site that have somewhat more dilute waters compared to the waters discussed in Section 4.4.2, and yet the waters still retain either a marine salt norm signature or a sulfatic weathering with a marine component signature. This group includes wells SNL-1, SNL-18, SNL-19, WIPP-28, WIPP-30,

Information Only

SNL-3, SNL-2, WIPP-11, DOE-2, WIPP-13, H-18, WQSP-1, WQSP-2, and WIPP-19. The presence of waters of lower ionic strength with marine or sulfatic weathering with a marine component signatures appears somewhat anomalous in these locations where either dilute diagenetic type waters or sulfatic weathering type waters might be expected. In an effort to understand the occurrence of these waters, a mixing calculation was performed using a dilute diagenetic composition water (H-3b2) and a sulfatic weathering solution type water (H-2c). The difference between this mixing calculation and that described in Section 4.4.1, where waters of the same types were mixed, is that, as was discussed in Section 3.2.1, the sulfatic weathering solutions located within the WIPP site, i.e., the "northern cluster" wells, have higher ionic strengths, greater normative halite, and lower normative anhydrite than the southern cluster of sulfatic weathering solutions, like H-8b, used in Section 4.4.1.

The results of the mixing calculation are plotted in Figure 42 and show that in mixing a northern cluster sulfatic weathering solution with a dilute diagenetic water, two intermediate compositions result. At low percentages (5-20%) of dilute diagenetic water, a water with a mixed sulfate-marine norm is observed. At higher percentages (30-60%) of dilute diagenetic water, a marine norm persists, and above 70%, the diagenetic type is observed.

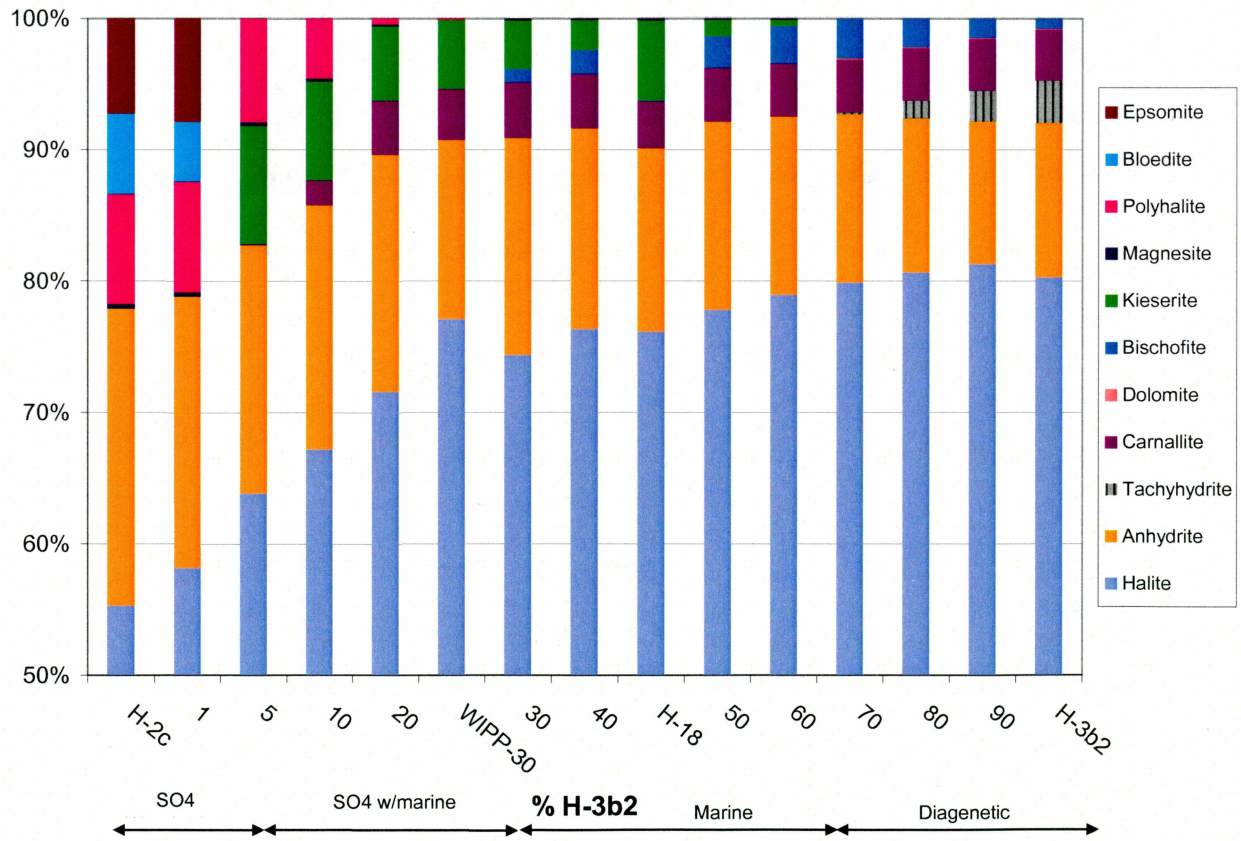

Figure 42. Normative phases resulting from mixing H-2c and H-3b2 waters. Also plotted are the WIPP-30 and H-18 salt norms.

Information Only

The salt norms for WIPP-30, a sulfatic weathering with a marine component type water, and H-18, a marine type water, are plotted on Figure 42 for comparison to the modeled compositions. This mixing scenario provides a possible explanation for the existence of the more dilute marine and sulfatic weathering with a marine component type waters within the WIPP site and to the north and northwest of the site. Waters with dilute diagenetic and sulfatic weathering signatures may well be present and mixing in these areas, and thereby be responsible for the occurrence of all the observed water types.

4.4.4 Conclusions from Mixing Calculations

The results of the mixing calculations suggest that broad-scale mixing of waters in the Culebra is an important process in defining the distribution of solutes. The mixing calculations demonstrate that the marine and sulfatic weathering with a marine component type waters may be derived from combinations of the sulfatic weathering, dilute diagenetic, and primitive diagenetic type waters, with the dilute diagenetic type being the common water type. From the mixing model results, we conclude that the dilute diagenetic and primitive diagenetic waters have independent origins. Thus, discounting the potash-contaminated waters, the Culebra appears to have three end-member water compositions: sulfatic weathering, dilute diagenetic, and primitive diagenetic.

Information Only

5. Summary

The groundwater chemistry from 59 wells screened in the Culebra Dolomite Member of the Rustler Formation was analyzed and examined for the purpose of gaining a better understanding of how the chemistry relates to geologic conditions and to provide insight into the hydrodynamics of the Culebra flow system. This information will be used in the development of a conceptual groundwater model for the Culebra.

These goals were accomplished by classifying the water types, identifying trends in the chemistry, correlating the observed chemistry with geologic, hydrogeologic and geomorphic features, and through the use of computer models to simulate the observed trends in the chemistry.

Since the publication of Siegel et al. (1991a), many new wells have been completed in the Culebra, and water quality sampling is an ongoing process. Included in this report are the analyses from 59 Culebra well locations, in comparison to 22 Culebra well locations considered in Siegel et al. (1991b). These new data provide increased data density over a wider area of the WIPP site and surrounding area.

The Culebra waters were classified using three methods: 1) the hydrochemical facies designations of Siegel et al. (1991b) were employed and expanded upon; 2) the normative salt assemblages, first employed by Bodine and Jones (1990), were calculated for the Culebra waters; and 3) weight percentages of excess halite and anhydrite from the salt norm outputs were used to classify the waters to show the large-scale differences in the two primary anions, sulfate and chloride, present in the Culebra waters.

The excess normative halite and anhydrite classification provided a broad picture of calcium-sulfate-rich waters predominating on the western side of the study area, which grade into waters with increasing amounts of chloride (halite) on the eastern margin of the study area. Broadly interpreted, this trend suggests a greater component of vertical flow on the western margins of the study area where the Culebra is closer to the surface and flow paths from the surface and through the overlying sulfate-bearing units are shorter than further to the east where the Culebra is deeper. However, it was shown in Section 3.3 that more dilute calcium-sulfate-rich waters may still enter the Culebra from overlying strata on the eastern reaches of the study area, where these waters mix with high-salinity waters to produce waters with both excess halite and excess anhydrite.

The hydrochemical facies, or zones, provide a more detailed, albeit more complex, view of the distribution of water types within the Culebra. The most dilute facies, facies B, is unique to a wide area in the southwestern portion of the study area. The high sulfate content and low ionic strength of these waters set them apart from other Culebra waters and suggest a stable hydrogeologic and geochemical regime for this region. The estimated transmissivity values for the wells in this area are among the highest for the Culebra, which correlates with the observed low concentration as solutes would tend to be flushed from the system faster than in a low-transmissivity region.

Information Only

The most concentrated facies, facies E, exists only east of the M2-H2 margin where the cores from boreholes SNL-6 and SNL-15 showed that halite is present as cement and fracture fillings. The highly concentrated chemistry of the water from these locations is in perfect agreement with the geology and the hydrogeology, in that the transmissivity is extremely low, preventing flushing of the solutes from the Culebra.

The intermediate concentration facies, B/C, C, A/C, and A, form a series of increasing concentration, with the high-salinity facies A occurring along the M2-H2 margin where halite is found below the Culebra. The other facies, A/C, C, and B/C, become progressively more dilute in an east to west direction, with Nash Draw on the western margin forming a prominent geomorphic feature where recharge is likely entering the subsurface (Powers, 2006).

Of all the classification schemes, the normative mineral assemblage, or salt norm type, provides the most geochemical information about the potential source of the solutes in water samples. As such, the salt norm type classification provides a level of sensitivity to subtle changes in chemistry that were undetected by the other classifications. Five salt norm types were identified: marine, diagenetic, sulfatic weathering, sulfatic weathering with a marine component, and potash.

Plotting the salt norm types on a map (Figure 12) shows a degree of chemical heterogeneity not seen with the other classification schemes. The facies B waters were subdivided into two salt norm types – sulfatic weathering and sulfatic weathering with a marine component. The facies C and B/C waters along the margin of Nash Draw were combined into a single salt norm type – dilute diagenetic. The facies E waters east of the M2-H2 margin compose the primitive diagenetic type. The wells in the west-central portion of the WIPP site (AIS, SNL-10, H-2c, and WQSP-6) with a less evolved (low ionic strength) sulfatic weathering type water are surrounded by more evolved waters. From a chemical perspective, these waters would have had to arrive at their location via a different, perhaps shorter flow path than the waters in the surrounding wells. Thus, the advantage of the salt norm approach is that it provides more detailed information than the other classification schemes, and suggests the processes responsible for the chemistries that are observed.

As was shown by the PHREEQCI mixing simulations in Section 4.4, all of the salt norm types can be derived from mixing of the sulfatic weathering solution, primitive diagenetic, and dilute diagenetic water types. The sulfatic weathering solutions appear to have a clear origin in recharge reaching the Rustler sulfate units directly, and then traveling to the Culebra. The primitive diagenetic water represents a syndepositional brine present in the Culebra since the Permian. The origin of the dilute diagenetic water is the most poorly understood. This water probably flows into the WIPP site area from the north along long flowpaths where it has encountered a variety of minerals and mixing conditions.

The reaction-path model for the evolution of the Culebra waters demonstrated that it was possible to start with a dilute calcium-sulfate water and, via reactions with halite and

Information Only

polyhalite and equilibrium with gypsum and dolomite, obtain a continuum of compositions that closely resembled the compositions of the Culebra waters. However, considering the geologic and hydrogeologic data for the entire region, we know that the chemistry of the Culebra waters did not evolve as a continuum. Rather, the water chemistry has evolved heterogeneously, i.e., local areas of more or less constant composition, which are correlated to the local geologic and hydrologic conditions. Then these different composition waters create the continuum of compositions that are observed in the Culebra through mixing, and possibly chemical diffusion. This model of geochemical evolution stands in contrast to the evolution of water in a typical clastic basin, where water may proceed along a flowpath from dilute oxidizing, carbonate-dominant waters to sulfate-rich waters to reducing concentrated chloride-dominant waters.

Future studies may include examination of the groundwater chemistry data from wells completed to the Magenta Dolomite Member of the Rustler, which is stratigraphically higher than the Culebra, to investigate possible correlations between the chemistry of the waters of the two dolomites. Examination of the retrograde reaction of corrensite transforming to smectite and the role of this reaction on the magnesium budget of the Culebra fluids might also be investigated in future studies. Additional PHREEQCI mixing calculations may be performed to test more combinations of Culebra waters which may aid in elucidating other mixing zones in the Culebra.

Information Only

6. References

Beauheim, R.L., and R.M. Holt. 1990. "Hydrogeology of the WIPP Site," *Geological and Hydrological Studies of Evaporites in the Northern Delaware Basin for the Waste Isolation Pilot Plant (WIPP), New Mexico, GSA Field Trip #14 Guidebook.* Dallas, TX: Dallas Geological Society. 131-179. ISBN 1-879325-12-8.

Bodine, M.W., and B.F. Jones. 1986. *The Salt Norm: A Quantitative Chemical Mineralogical Characterization of Natural Waters.* Water Resources Investigation Report 86-4086. Reston, VA: U.S. Geological Survey.

Bodine, M.W., Jr., and B.F. Jones. 1990. "Normative Analysis of Groundwaters from the Rustler Formation Associated with the Waste Isolation Pilot Plant (WIPP), Southeastern New Mexico," *in* R.J. Spencer and I-Ming Chou, eds., Fluid-Mineral Interactions: A Tribute to H.P. Eugster, *Geochemical Society Special Publication No. 2*, 213-269.

Bodine, M.W., Jr., B.F. Jones, and S.J. Lambert. 1991. "Normative Analysis of Groundwaters from the Rustler Formation Associated with the Waste Isolation Pilot Plant, Southeastern New Mexico," *in* M.D. Siegel, S.J. Lambert, and K.L. Robinson, eds., *Hydrogeochemical Studies of the Rustler Formation and Related Rocks in the Waste Isolation Pilot Plant Area, Southeastern New Mexico.* SAND88-0196. Albuquerque, NM: Sandia National Laboratories.

Bowman, D.O., and R.M. Roberts. 2008. Analysis Report for AP-070, Analysis of Hydraulic Tests Performed in Wells IMC-461, SNL-6, H-11b2, H-15, and C-2737. ERMS Package # 539221. Carlsbad, NM: Sandia National Laboratories, WIPP Records Center.

Brookins, D.G., and S.J. Lambert. 1988. "WIPP Site Studies: Secondary Selenite Veins in the Rustler Formation and Dewey Lake Red Beds," *Materials Research Society Symposium Proceedings*. 112:233-241.

Chapman, J.B. 1988. *Chemical and Radiochemical Characteristics of Groundwater in the Culebra Dolomite, Southeastern New Mexico.* EEG-39. Albuquerque, NM: New Mexico Environmental Evaluation Group.

Corbet, T.F. 1998. "Integration of Hydrogeology and Geochemistry of the Culebra Member of the Rustler Formation in the Vicinity of the Waste Isolation Pilot Plant (USA)," *Use of Hydrogeochemical Information in Testing Groundwater Flow Models, Workshop Proceedings, Borgholm, Sweden, 1-3 September 1997.* Paris, France: OECD NEA. 135-149.

Corbet, T.F., and P.M. Knupp. 1996. *The Role of Regional Groundwater Flow in the Hydrogeology of the Culebra Member of the Rustler Formation at the Waste Isolation*

Information Only

Pilot Plant (WIPP), Southeastern New Mexico. SAND96-2133. Albuquerque, NM: Sandia National Laboratories.

Domski, P.S., and R.L. Beauheim. 2005. *Analysis Plan for the Evaluation of Culebra Brine Compositions, AP-125.* ERMS# 540680. Carlsbad, NM: Sandia National Laboratories, WIPP Records Center.

Hillesheim, M.B., L.A. Hillesheim, and N.J. Toll. 2007. "Mapping of Pressure-Head Responses of a Fractured Rock Aquifer to Rainfall Events," *Proceedings of the 2007 U.S. EPA/NGWA Fractured Rock Conference.* Westerville, OH: National Ground Water Association. 522-536.

Holt, R.M., and D.W. Powers. 1988. *Facies Variability and Post-Depositional Alteration Within the Rustler Formation in the Vicinity of the Waste Isolation Pilot Plant, Southeastern New Mexico.* DOE/WIPP 88-004. Carlsbad, NM: U.S. Department of Energy.

Holt, R.M., R.L. Beauheim, and D.W. Powers. 2005. "Predicting Fractured Zones in the Culebra Dolomite," *in* B. Faybishenko, P. Witherspoon, and J. Gale, eds. *Dynamics of Fluids and Transport in Fractured Rock.* Geophysical Monograph Series, Volume 162. Washington, DC: American Geophysical Union. 103-116.

Kröhn, K.P., and K. Schelkes. 1996. "Modelling of Regional Variable Density Groundwater Flow in an Area of New Mexico: Importance of Influencing Parameters and Processes," *Calibration and Reliability in Groundwater Modelling, Proceedings of the ModelCARE 96 Conference, Golden Colorado.* IAHS Publ. no. 237.

Lambert, S.J. 1987. *Feasibility Study: Applicability of Geochronologic Methods Involving Radiocarbon and Other Nuclides to the Groundwater Hydrology of the Rustler Formation, Southeastern New Mexico.* SAND86-1054. Albuquerque, NM: Sandia National Laboratories.

Lambert, S.J. 1991. "Isotopic Constraints on the Rustler and Dewey Lake Groundwater Systems," *in* M.D. Siegel, S.J. Lambert, and K.L. Robinson, eds., *Hydrogeochemical Studies of the Rustler Formation and Related Rocks in the Waste Isolation Pilot Plant Area, Southeastern New Mexico.* SAND88-0196. Albuquerque, NM: Sandia National Laboratories.

Lambert, S.J., and J.A. Carter. 1987. *Uranium Isotope Systematics in Groundwaters of the Rustler Formation, Northern Delaware Basin, Southeastern New Mexico, I: Principles and Preliminary Results.* SAND87-0388. Albuquerque, NM: Sandia National Laboratories.

Levy, Y. 1977. "The Origin and Evolution of Brine in Coastal Sabkhas, Northern Sinai," *Journal of Sedimentary Petrology.* 47(1): 451-462.

Myers, J., P. Drez, and P. James. 1991. "The Redox State and the Occurrence and Influence of Organics in the Culebra," *in* M.D. Siegel, S.J. Lambert, and K.L. Robinson,

Information Only

eds., *Hydrogeochemical Studies of the Rustler Formation and Related Rocks in the Waste Isolation Pilot Plant Area, Southeastern New Mexico*. SAND88-0196. Albuquerque, NM: Sandia National Laboratories.

Parkhurst, D.L., and C.A.J. Appelo. 1999. *User's Guide to PHREEQCI (Version 2)--A Computer Program for Speciation, Batch-Reaction, One-Dimensional Transport, and Inverse Geochemical Calculations*: U.S. Geological Survey Water- Resources Investigations Report 99-4259, 312 p.

Piper, A.M. 1944. "A Graphic Procedure in the Geochemical Interpretation of Water-Analyses," *Transactions, American Geophysical Union*. 25(6):914-923.

Powers, D.W. 2006. Analysis Report, Task 1B of AP-114, Identify Possible Area of Recharge to the Culebra West and South of WIPP. ERMS# 543094. Carlsbad, NM: Sandia National Laboratories, WIPP Records Center.

Powers, D.W. 2007. Analysis Report for Task 1A of AP-114: Refinement of Rustler Halite Margins Within the Culebra Modeling Domain. ERMS# 547559. Carlsbad, NM: Sandia National Laboratories, WIPP Records Center.

Powers, D.W., and R.M. Holt. 2000. "The Salt that Wasn't There: Mudflat Facies Equivalents to Halite of the Permian Rustler Formation, Southeastern New Mexico," *Journal of Sedimentary Research*. 70(1):29-36.

Powers, D.W., R.M. Holt, R.L. Beauheim, and R.G. Richardson. 2006. "Advances in Depositional Models of the Permian Rustler Formation, Southeastern New Mexico," in L. Land, V.W. Lueth, W. Raatz, P. Boston, and D.L. Love, eds., *Caves and Karst of Southeastern New Mexico*. New Mexico Geological Society, 57th Annual Fall Field Conference Guidebook. 267-276.

Ramey, D.S. 1985. *Chemistry of Rustler Fluids*. EEG-31. Albuquerque, NM: New Mexico Environmental Evaluation Group.

Roberts, R.M. 2007. Analysis Report for AP-070, Analysis of Culebra Hydraulic Tests Performed Between June 2006 and September 2007. ERMS# 547418. Carlsbad, NM: Sandia National Laboratories, WIPP Records Center.

Sewards, T., R. Glenn, and K. Keil. 1991a. *Mineralogy of the Rustler Formation in the WIPP-19 Core*. SAND87-7036. Albuquerque, NM: Sandia National Laboratories.

Sewards, T., M.L. Williams, and K. Keil. 1991b. *Mineralogy of the Culebra Dolomite Member of the Rustler Formation*. SAND90-7008. Albuquerque, NM: Sandia National Laboratories.

Siegel, M.D., and S. Anderholm. 1994. "Geochemical Evolution of Groundwater in the Culebra Dolomite Near the Waste Isolation Pilot Plant, Southeastern New Mexico, USA," *Geochimica et Cosmochimica Acta*, 58(10):2299-2323.

Information Only

Siegel, M.D., and S.J. Lambert. 1991. "Summary of Hydrogeochemical Constraints on Groundwater Flow and Evolution In the Rustler Formation," *in* M.D. Siegel, S.J. Lambert, and K.L. Robinson, eds., *Hydrogeochemical studies of the Rustler Formation and Related Rocks in the Waste Isolation Pilot Plant Area, Southeastern New Mexico.* SAND88-0196. Albuquerque, NM: Sandia National Laboratories.

Siegel, M.D. S.J. Lambert, and K.L. Robinson, eds. 1991a. *Hydrogeochemical Studies of the Rustler Formation and Related Rocks in the Waste Isolation Pilot Plant Area, Southeastern New Mexico.* SAND88-0196. Albuquerque, NM: Sandia National Laboratories.

Siegel, M.D., K.L. Robinson, and J. Myers. 1991b. "Solute Relationships in Groundwaters from the Culebra Dolomite and Related Rocks in the Waste Isolation Pilot Plant Area, Southeastern New Mexico," *in* M.D. Siegel, S.J. Lambert, and K.L. Robinson, eds., *Hydrogeochemical Studies of the Rustler Formation and Related Rocks in the Waste Isolation Pilot Plant Area, Southeastern New Mexico.* SAND88-0196. Albuquerque, NM: Sandia National Laboratories.

Wolery, T.J. 1992. *EQ3/6: Software Package for Geochemical Modeling of Aqueous Systems: Package Overview and Installation Guide (Version 7.0).* UCRL-MA-110662 PT I. Livermore, CA: Lawrence Livermore National Laboratory.

Information Only

Appendix 1 – Computer Files

File Key:

Table A1: File names and purpose from the PHREEQCI directory and Section-labeled subdirectory.

File(s) Names	Purpose
pitzer.dat	PHREEQCI thermodynamic database
All_Culebra.pqi & .pqo	PHC I/O Culebra water analyses
Culebra_Data.xls	PHC user specified output files
H-10B_halite.pqi & .pqo	PHC I/O Section 3.3
Mix_SNL15_WQSP4.pqi, .pqo, & .xls	PHC I/O & user specified output, Section 4.3
Mix_SNL16-H8.pqi, .pqo, & .xls	PHC I/O & user specified output, Section 4.3
Mix_WIPP25_DOE1.pqi, .pqo, & .xls	PHC I/O & user specified output, Section 4.3
polyhalite_RXN.pqi & .pqo	PHC I/O, Section 4.2
poly_rxn.xls	PHC user specified output files
polyhalite_RXN_Mg.pqi & .pqo	PHC I/O, Section 4.2
poly_rxn_Mg.xls	PHC user specified output files
Run_10.pqi & .pqo	PHC I/O, Section 4.2
Run10.xls	PHC user specified output files
PHC = PHREEQCI	
I/O = input/output	

Table A2 contains the file information for the SNORM subdirectory.

Table A2: File names and purpose from the SNORM directory and Section-labeled subdirectory.

File(s) Names	Purpose
CUL_?	Culebra SNORM input files, ? = 1-13
CUL_?.OUT	Culebra SNORM output files, ? = 1-13
CUL_?.SS	Culebra SNORM simple salt files, ? = 1-13
MIX_?	Culebra mixing SNORM input files, ? = 1, 6, or 7
MIX_?.OUT	Culebra mixing SNORM output files, ? = 1, 6, or 7
MIX_?.SS	Culebra mixing SNORM simple salt files, ? = 1, 6, or 7
H-10B	H-10b SNORM input file, Section 3.3
H-10B.OUT	H-10b SNORM output file, Section 3.3
H-10B.SS	H-10b SNORM simple salt file, Section 3.3

Information Only

Table A3 contains the file information for the XLS subdirectory.

Table A3: File names and purpose from the XLS directory and Section-labeled subdirectory.

File(s) Names	Purpose	Use
Culebra_Hydrochemical_Data.xls	Master spreadsheet contains all classification data	Table 2, 5, 13 tab "report tables" 6, 7, 8, 9, 10 tab "Sorted by SNORM type" Figures 13,15,16,19,21,23,25,27,29
Gamma.xls	Data for ionic strength discussion, Section 4.1	Figures 17 & 18
PHRQC_CBE.xls	Data for uncertainty discussion, Section 1.4	Section 1.4
PHRQC_CBE_frozen.xls	Section 1.4, same as PHRQC_CBE.xls, but all formulas converted to values	Section 1.4, Table 3 Figures 5, 6, 7, 8
Charge balance.xls	Balanced analyses, Section 1.4	Section 1.4
Simulation_results.xls	Data from reaction path models, Section 4.3	Section 4.3, Figures 30-39
SNORM_MIX.xls	Data from mixing models, Section 4.4	Section 4.4, Figures 40-42
SI_Ions.xls	Saturation Index plots, Section 4.3	Section 4.3, Figures, 20,22,24,26,28

Directory of files

```
D:\Hydrochem\Culebra>dir /s
 Volume in drive D is 080730_1018
 Volume Serial Number is 6C25-B8A9

 Directory of D:\Hydrochem\Culebra

07/30/2008  09:29 AM    <DIR>          .
07/26/2008  12:12 PM    <DIR>          ..
07/30/2008  10:54 AM         2,027,004 AP-125 Analysis Report.pdf
07/25/2008  01:26 PM    <DIR>          final files
               1 File(s)      2,027,983 bytes

 Directory of D:\Hydrochem\Culebra\final files

07/25/2008  01:26 PM    <DIR>          .
07/30/2008  09:29 AM    <DIR>          ..
07/25/2008  01:26 PM    <DIR>          PHREEQCI
07/25/2008  01:26 PM    <DIR>          SNORM
07/29/2008  01:30 PM    <DIR>          xls
               0 File(s)              0 bytes
```


Information Only

Directory of D:\Hydrochem\Culebra\final files\PHREEQCI

07/25/2008 01:26 PM <DIR> .
07/25/2008 01:26 PM <DIR> ..
07/25/2008 08:46 AM 6,871 All_Culebra.pqi
07/25/2008 08:46 AM 336,193 All_Culebra.pqo
07/25/2008 01:01 PM 60,416 Culebra_Data.xls
09/23/2005 09:02 AM 24,561 pitzer.dat
07/25/2008 01:26 PM <DIR> Section 3.3
07/25/2008 01:26 PM <DIR> Section 4.3
07/25/2008 01:26 PM <DIR> Section 4.4
4 File(s) 428,041 bytes

Directory of D:\Hydrochem\Culebra\final files\PHREEQCI\Section 3.3

07/25/2008 01:26 PM <DIR> .
07/25/2008 01:26 PM <DIR> ..
06/25/2008 10:32 AM 407 H-10B_halite.pqi
06/25/2008 10:39 AM 13,032 H-10B_halite.pqo
2 File(s) 13,439 bytes

Directory of D:\Hydrochem\Culebra\final files\PHREEQCI\Section 4.3

07/25/2008 01:26 PM <DIR> .
07/25/2008 01:26 PM <DIR> ..
07/07/2008 08:26 AM 1,173 polyhalite_RXN.pqi
07/07/2008 08:23 AM 6,671,639 polyhalite_RXN.pqo
07/03/2008 02:17 PM 340,342 poly_rxn.xls
07/25/2008 09:23 AM 1,257,115 Run10.xls
07/25/2008 09:23 AM 1,463 Run_10.pqi
07/25/2008 09:23 AM 20,142,177 Run_10.pqo
6 File(s) 28,413,909 bytes

Directory of D:\Hydrochem\Culebra\final files\PHREEQCI\Section 4.4

07/25/2008 01:26 PM <DIR> .
07/25/2008 01:26 PM <DIR> ..
07/08/2008 09:26 AM 2,408 Mix_SNL15_WQSP4.pqi
07/08/2008 09:26 AM 93,259 Mix_SNL15_WQSP4.pqo
07/08/2008 09:26 AM 2,175 Mix_SNL15_WQSP4.xls
07/09/2008 11:17 AM 2,329 Mix_SNL16-H8.pqi
07/09/2008 11:18 AM 86,576 Mix_SNL16-H8.pqo
07/09/2008 11:18 AM 2,030 Mix_SNL16-H8.xls
07/07/2008 04:14 PM 2,328 Mix_WIPP25_DOE1.pqi
07/07/2008 04:14 PM 86,584 Mix_WIPP25_DOE1.pqo

Information Only

```
07/07/2008  04:14 PM         2,030 Mix_WIPP25_DOE1.xls
          9 File(s)      279,719 bytes

 Directory of D:\Hydrochem\Culebra\final files\SNORM

07/25/2008  01:26 PM   <DIR>        .
07/25/2008  01:26 PM   <DIR>        ..
07/25/2008  01:26 PM   <DIR>        Section 1.4
07/25/2008  01:26 PM   <DIR>        Section 3.2
07/25/2008  01:26 PM   <DIR>        Section 3.3
07/25/2008  01:26 PM   <DIR>        Section 4.4
          0 File(s)          0 bytes

 Directory of D:\Hydrochem\Culebra\final files\SNORM\Section 1.4

07/25/2008  01:26 PM   <DIR>        .
07/25/2008  01:26 PM   <DIR>        ..
03/27/2008  01:23 PM           569 DOE-1
03/27/2008  01:23 PM         9,363 DOE-1.OUT
03/27/2008  01:23 PM           738 DOE-1.SS
03/28/2008  10:45 AM           569 H-17
03/28/2008  10:45 AM         9,625 H-17.OUT
03/28/2008  10:45 AM           738 H-17.SS
03/28/2008  08:57 AM           360 SNL-10
03/28/2008  08:57 AM         4,708 SNL-10.OUT
03/28/2008  08:57 AM           410 SNL-10.SS
03/27/2008  01:12 PM           569 SNL-8
03/27/2008  01:12 PM         9,363 SNL-8.OUT
03/27/2008  01:12 PM           738 SNL-8.SS
03/27/2008  02:24 PM           569 USGS-1
03/27/2008  02:24 PM         9,494 USGS-1.OUT
03/27/2008  02:24 PM           738 USGS-1.SS
03/27/2008  02:35 PM           569 USGS-4
03/27/2008  02:35 PM         9,103 USGS-4.OUT
03/27/2008  02:35 PM           738 USGS-4.SS
03/28/2008  11:23 AM           569 WQSP-6
03/28/2008  11:23 AM         9,363 WQSP-6.OUT
03/28/2008  11:23 AM           738 WQSP-6.SS
         21 File(s)      69,631 bytes

 Directory of D:\Hydrochem\Culebra\final files\SNORM\Section 3.2

07/25/2008  01:26 PM   <DIR>        .
07/25/2008  01:26 PM   <DIR>        ..
07/24/2008  06:16 PM        12,487 culebra
07/24/2008  06:17 PM       271,257 CULEBRA.OUT
```


Information Only

```
07/24/2008  06:04 PM         20,746 CULEBRA.SS
               3 File(s)      304,490 bytes

 Directory of D:\Hydrochem\Culebra\final files\SNORM\Section 3.3

07/25/2008  01:26 PM    <DIR>          .
07/25/2008  01:26 PM    <DIR>          ..
06/25/2008  10:22 AM               360 H-10B
06/25/2008  10:22 AM             4,817 H-10B.OUT
06/25/2008  10:22 AM               410 H-10B.SS
               3 File(s)          5,587 bytes

 Directory of D:\Hydrochem\Culebra\final files\SNORM\Section 4.4

07/25/2008  01:26 PM    <DIR>          .
07/25/2008  01:26 PM    <DIR>          ..
04/07/2008  02:27 PM             2,450 MIX_1
04/07/2008  02:27 PM            51,526 MIX_1.OUT
04/04/2008  12:34 PM             3,690 MIX_1.SS
07/08/2008  09:30 AM             2,659 MIX_2
07/08/2008  09:30 AM            56,805 MIX_2.OUT
07/08/2008  08:44 AM             4,018 MIX_2.SS
07/07/2008  04:40 PM             2,450 MIX_3
07/07/2008  04:40 PM            52,252 MIX_3.OUT
07/07/2008  04:40 PM             3,690 MIX_3.SS
               9 File(s)        179,540 bytes

 Directory of D:\Hydrochem\Culebra\final files\xls

07/29/2008  01:30 PM    <DIR>          .
07/25/2008  01:26 PM    <DIR>          ..
07/29/2008  01:30 PM           566,784 Culebra_Hydrochemical_Data.xls
07/25/2008  01:26 PM    <DIR>          Section 1.4
07/25/2008  01:26 PM    <DIR>          Section 4:1
07/25/2008  01:26 PM    <DIR>          Section 4.3
07/25/2008  01:26 PM    <DIR>          Section 4.4
               1 File(s)        566,784 bytes

 Directory of D:\Hydrochem\Culebra\final files\xls\Section 1.4

07/25/2008  01:26 PM    <DIR>          .
07/29/2008  01:30 PM    <DIR>          ..
07/24/2008  05:36 PM            89,600 Charge balance.xls
07/25/2008  10:02 AM           443,392 PHRQC_CBE.xls
07/25/2008  10:18 AM           434,176 PHRQC_CBE_frozen.xls
               3 File(s)        967,168 bytes
```


Information Only

Directory of D:\Hydrochem\Culebra\final files\xls\Section 4.1

07/25/2008 01:26 PM <DIR> .
07/29/2008 01:30 PM <DIR> ..
07/25/2008 09:00 AM 132,608 Gamma.xls
1 File(s) 132,608 bytes

Directory of D:\Hydrochem\Culebra\final files\xls\Section 4.3

07/25/2008 01:26 PM <DIR> .
07/29/2008 01:30 PM <DIR> ..
07/28/2008 03:25 PM 2,768,896 Simulation_results.xls
07/25/2008 11:22 AM 79,872 SI_Ions.xls
2 File(s) 2,848,768 bytes

Directory of D:\Hydrochem\Culebra\final files\xls\Section 4.4

07/25/2008 01:26 PM <DIR> .
07/29/2008 01:30 PM <DIR> ..
07/25/2008 10:48 AM 72,192 SNORM_MIX.xls
1 File(s) 72,192 bytes

Total Files Listed:
66 File(s) 36,309,859 bytes
47 Dir(s) 0 bytes free

Information Only